UNIVERSITY OF NAPLES "FEDERICO II"

University of Naples "Federico II"

Department of Chemical Sciences

Ph.D School in Chemical Sciences–Cycle XXXI

Design, formulation and characterization of anhydrous highly concentrated surfactant mixtures

Ph.D student:

Antonio Fabozzi

UNIVERSITY OF NAPLES "FEDERICO II"

Ph.D School in Chemical Sciences–Cycle XXXI

Design, formulation and characterization of anhydrous highly concentrated surfactant mixtures

Ph.D student

Antonio Fabozzi

Tutors: Examiner:

Gerardino D'Errico   Alessandro Vergara

Christopher Jones

Index

Preface

Surfactants are among the chemical compounds more exploited in industry. They are used in the more different fields, ranging from the production of inks, paints and varnishes to pharmaceutics, from processes of extraction/recovery of oil to detergency. Indeed, surfactants are the basic ingredients of all detergent formulations. Therefore, it should not surprise that research aiming at understand surfactant behavior as well as developing new surfactants has always been very rich and lively, in spite of the fact that surfactant catalogs already list hundreds if not thousands of molecules of all types: anionic, cationic, and nonionic, including zwitterionic.

The world production of surfactants is probably close to million tons per year and is worth is very high. Any new surfactant with novel properties or improved performances or capable of improving the economics of a given process would translate into savings of millions of dollars. In addition, new surfactants with lower toxicity or environmental friendly features have a promising future, since the widespread sensibility to environmental issues is resulting in new regulations requiring the surfactants used in formulations to have lower toxicity and less impact on environment, and to be more easily produced by processes with a low environmental impact and degraded by aerobic and anaerobic processes.

In the last decade, highly concentrated liquid detergent formulations have gained a prominent role in the market of detergents [1,2], as highlighted by the increasing number of patents [3-5]. The low water content reduces the ecological footprint of the product, as less plastic packaging is used, and significantly decreases the transport costs [6]. However, the formulations based on concentrated surfactant mixtures have shown serious issues related to the high viscosity that hampers their processability during production and kinetically limits their water dissolution during use [7]. This drives the researchers towards the molecular design of surfactants able to form highly concentrated liquid mixtures with relatively low viscosity.

A possible strategy to tune the surfactant aggregation properties is the introduction of alkyl chain branching in the molecular architecture. Tail branching affects the surfactant-water as well as the surfactant-surfactant interactions [8], thus leading to the formation of self-aggregates different from those formed by the linear analogues [9-13]. The features of branched surfactants depend on both the length of the branched chain and its position along the main hydrocarbon chain [9,10,14-17]. In most cases, it is found that branches disfavour surfactant self-aggregation by disrupting the packing of hydrophobic tails [18-21] and reducing the attractive tail-tail interactions [16,22,23]. In concentrated surfactant mixtures, the stability of hydrated solid crystals is reduced, while lyotropic liquid crystalline (LLC) phases form, low-viscosity lamellar structures predominating over high-viscosity hexagonal arrangements [10,14-16]. From this perspective, branched surfactants appear as

suitable components of highly concentrated formulations. However, some opposite results have been also reported, indicating the stabilization of more compact aggregates with increased size [8,24]. These discrepancies suggest that a fine interplay among possible inter- and intramolecular interactions has to be considered in these mixtures. As an example, the head group nature determines the effect of tail branching on packing and ordering of the molecules at the aggregate interfaces [25]. Further research is needed to fully elucidate these points, in order to build a reliable scientific basis for the rational molecular design of new surfactants.

Currently, in home fabric and personal care formulations, because of the ease and low cost of synthesis and their low environmental impact, amine oxide and alkyl ethoxysulfate surfactants have become the most used. Specifically, amine oxide surfactants control the foaming and cleaning properties of the final product, while ethoxysulfate ones control the emulsifiability and the wettability properties. Both classes of surfactants have been, and are still, widely studied.

Among N-oxide surfactants, N,N-dimethylalkylamine oxides ($CH_3(CH_2)_{n-1}N^+(CH_3)_2O^-$) are the most common. In aqueous mixtures, these surfactants present an equilibrium between the protonated and the non-protonated form.

$$CH_3(CH_2)_{n-1}N^+(CH_3)_2O^- + H^+ = CH_3(CH_2)_{n-1}N^+(CH_3)_2OH.$$
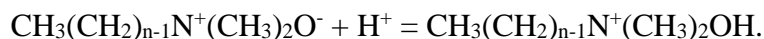
At pH lower than the surfactant pKa, they are protonated and behave as cationic surfactants, while in mixtures with a pH value higher than their pKa, they are in the non-protonated form and behave as amphoteric surfactants.

Unfortunately, the presence of extended stability regions for highly viscous liquid lyotropic crystalline phases, which form already at low surfactant content (0.32 w/w), in the case of amino oxide surfactants with either a long alkyl chain or a short chain, tend to limit the functionality of their detergent formulations, including those of *N,N*-dimethyldodecyl-1-amine oxide (C$_{12}$DAO-linear), at the moment the most investigated and used among amine oxide surfactants, because of its very low cost production.

For this reason, the interest of formulation scientists, in both academic and industrial contexts, is moving towards the class of branched amine oxide surfactants, which have been proposed, for their superior properties and special performances, in formulating more effective products for wetting, solubilizing, foam-boosting, drug delivery and other industrial uses. Indeed, branched amine oxide surfactants present several advantages with respect to their linear counterpart: 1) they have a higher critical micelle concentration (cmc); 2) they are more effective at increasing the surface tension of water and interfacial area at the air-water interface; 3) their aqueous solutions may present new interesting rheological features, at the same concentration of linear analogues; 4) their structure may result in formation of unexpected micellar shapes.

The present Ph.D. project, born by a collaboration between the University of Naples "Federico II" and the Procter and Gamble (P&G) company, falls in this context and aims at designing a new branched amine oxide surfactant able to overcome

limitations of the currently used $C_{12}DAO$-linear, by forming, because of steric hindrance, isotropic micellar aggregates in a wide range of conditions, and especially of surfactant concentration, at the expenses of lyotropic liquid crystalline arrangements. The brand-new branched amine oxide surfactant reported in Figure 1, *N,N*-dimethyl-2-propylheptan-1-amine oxide, bearing a tail branched at position 2 and hereafter named $C_{10}DAO$-branched, has been synthesized and thoroughly characterized.
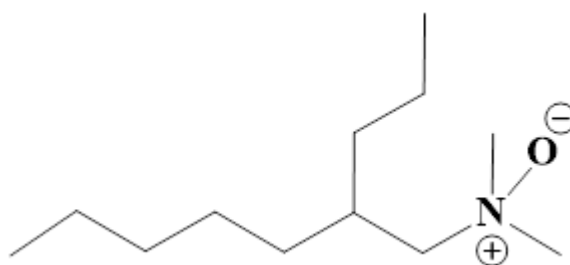
Figure 1: *N,N*-dimethyl-2-propylheptan-1-amine oxide ($C_{10}DAO$-branched)

An investigation on the structural and dynamical properties of its highly concentrated aqueous mixtures is presented. Moreover its aggregation and physico-chemical properties have been compared with those of its linear isomer *N,N*-dimethyldecyl-1-amine oxide named ($C_{10}DAO$-linear). Polarized Optical Microscopy (POM), Small Angle Neutron and X-ray Scattering (SANS and SAXS, respectively) experiments are used to investigate the structure of the supramolecular aggregates. The results are confirmed by Humidity Scan Quartz Crystal Microbalance Dissipation (HS QCM-D) measurements, which have been recently proposed as a reliable approach for a

rapid scrutiny of surfactant phase behavior [26]. Rheology is used to investigate the viscosity of the mixtures. Analysis of the results offers the opportunity to highlight differences and similarities between supramolecular organization of the branched and linear amine oxide isomers, opening new perspectives for their exploitation in formulative chemistry.

Upon synthesis and characterization of this molecule, we focus on formulation and characterization of innovative surfactant mixtures, based on co-formulation of the new branched amino oxide surfactant and a very commonly employed anionic alkyl ethoxy sulfate surfactant, sodium lauryl ether sulfate or SLES, characterized by higher active concentration, still maintaining the feature to be ship-able, flow-able and stable.

Thus, in the framework of the fast-growing field of formulation science and technology, this study represents a precious example, in which a detailed physical-chemical investigation gives a reliable basis to link the functional behavior of a surfactant-based formulation to its microstructure and dynamics.

1) Introduction

The largest market for surfactant use is that of home, fabric and personal care cleaning, such as household and industrial laundry detergents, dishwashing products, cleaners for hard surfaces, hand and body soaps, shampoos, etc. Because of their importance, these products have been and continue to be the focus of research and development aiming at achieving improved performances, reduced production costs and lower environmental impact in production, consumption and disposal phases. Particularly, in the last decade, both economic and environmental reasons have driven the producer and consumer preference for concentrated liquid detergent formulations [27,28], as well highlighted by the increasing number of patents concerning these formulations [29-31]. Indeed, a low water content reduces the ecological footprint of the product, as less plastic packaging is needed, and economically it is convenient because of the reduced transport costs [32]. However, formulations based on concentrated surfactant mixtures have shown serious issues related to their high viscosity, which hampers their processability during the production phase and kinetically limits their water dissolution when used [8]. These drawbacks have wakened a research line devoted to the design of new surfactants and formulations able to form highly concentrated liquid mixtures with relatively low viscosity.

1.1) Anionic Surfactant

Surfactants are molecules consisting of a water soluble polar head, which can be positively (cationic surfactants) or negatively (anionic surfactants) charged or even uncharged (nonionic surfactants), and a hydrophobic hydrocarbon tails [33] and are designed to have mainly cleaning or solubilizing properties [34].

Among surfactants, anionic ones represent a heterogeneous group of chemicals that are currently used in a wide set of commercial products. In the last 30 years, anionic surfactants have been extensively used as detergents for hard surfaces, particularly for domestic uses [35], household cleaning and personal care products, such as laundry and liquid dishwashing detergents, shampoos, hair conditioners and liquid soap. They are also successfully employed in pharmaceutical, agricultural, pesticide formulations, oil recovery, etc. It has been estimated that anionic surfactants are about 60% of worldwide surfactant production [36].

Anionic surfactants are constituted by a predominantly linear aliphatic hydrocarbon chain, whose length ranges between 8 and 18 carbon atoms, and the polar negative head neutralized by a counter ion, such as Na^+, K^+, NH_4^+, or by an alkanolamine cation [37, 38].

The variety of anionic surfactant available arises primarily from the many types of hydrophobic groups that can be modified by the addition of the proper anionic species. With respect to the polar head, the main subgroups are alkyl carboxylates or soaps, sulfates, sulfonates and, to a lesser degree, phosphates. Alkyl ethoxy sulfates

(AES) represent the second class of anionic surfactants in terms of application fields [39-42]. They are composed of several homologues, in which the composition and length of both the hydrocarbon and the ethoxy tails can differ.

One of the most important parameter that determines the behavior of surfactants is the Hydrophilic-Lipophilic Balance (HLB). The HLB is an empirical expression of the equilibrium of dimensions and resistance of the hydrophobic part and the hydrophilic part of an emulsifier and is useful to identify the solubility of the surfactant, i.e. if it will create an oil emulsion in water (O/W) or a water emulsion in oil (W/O). The HLB value can be calculated with the following formula:

$$HLB = \frac{20 * M_h}{M} \tag{1}$$

where M_h is the molecular mass of the hydrophilic portion and M is the molecular mass of the whole molecule.

A surfactant that is characterized by lipophilic character will have a low value of HLB whereas a hydrophilic one a high HLB value. The following table shows the correlation between the HLB factor and the emulsifier properties (Table 1)[43].

HLB	Emulsifying properties
4-6	Emulsifier W/O
7-9	Wetting agent
8-18	Emulsifier O/W
13-15	Detergent

Table 1. Correlation of HLB factor and emulsifying properties.

Molecules that fall at the extreme of the range are the most effective detergent.

1.1.1) Sodium lauryl ethoxy sulphate

One of the most widespread alkyl ethoxy sulfates, is sodium lauryl ethoxy sulphate, SLES, (Figure 2) which consists of a linear carbon chain (C_{12} to C_{14}) and a number n of oxyethylene units varying between 2 and 3[44]. SLES has an HLB~15, indicating it is a strong detergent, and SLES is indeed one of the most used and ductile surfactants. It is present in the formulation of many commercial detergents and personal care products [45].
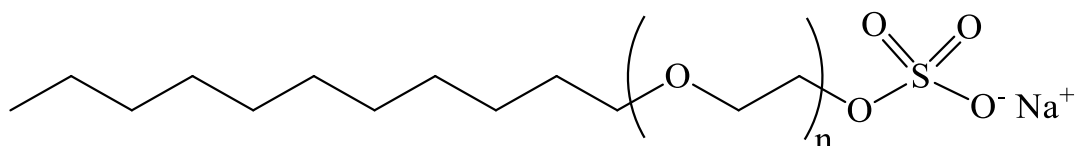
Figure 2. Sodium lauryl ethoxy sulphate structure.

SLES can be more easily biodegraded compared to other surfactants [46], both in aerobic [47, 48] and anaerobic conditions[49]. Aerobic degradation of linear AES, and SLES in particular, may occur by ether or ester cleavage. The former mechanism [50-51], proceeds with the formation of an intermediate that it is further degraded with release of the sulfate group (Scheme 1). According to the ester cleavage mechanism, the sulfate group is directly split off with formation of the intermediate, followed by degradation of the carbon tail [52]. Thus, the presence of sulfate can be used as an indication of SLES degradation in both cases.

R⎯/\/\/\(⎯O⎯)$_n$⎯O⎯SO_3^- Na^+

Ether cleavage   Ester Cleavage

Intermediate Compounds   Intermediate Compounds + SO_4^{2-}

ß-oxidation

$CO_2 + H_2O$ + biomass + SO_4^{2-} $CO_2 + H_2O$ + biomass

Scheme 1. Scheme of possible SLES cleavage mechanisms for complete degradation to CO_2 and biomass formation. The general molecular structure of SLES is shown, where n is the mean of

ethoxy units (2<n<3 in commercial products), and R is the alkyl group (the linear alkyl chain of AES surfactants can have 12 to 18 carbons) [53].

1.2) Amphoteric surfactants

The family of surfactants commonly referred to as "amphotheres" are surface-active materials that contain, or have the potential to form, both a positive and a negative functional group under specified conditions [54, 55]. Their definition as a separate class of surfactants has been somewhat controversial historically, since they may be electrically neutral and their general properties under many conditions make them functionally similar to some nonionic surfactants [56, 57].

Although amphoteres represent only a small portion of the total worldwide surfactant production, their market position is increasing significantly, because of the unique properties that such molecules can impart to a formulation [58, 59]; for example, they often show considerable synergism when employed with other classes of surfactants [60-63]. Coformulation of amphoteric and anionic surfactants has supplanted cationic surfactants in several fields, such as home and personal care detergents to increase the viscosity of washing products [64]. Moreover, amphoteric surfactants are commonly used for home-fabric and personal care formulations [65, 66], and because of their amphoteric nature, that makes their behavior pH-dependent, have been proved especially useful in personal care formulation, such as shampoos [67, 68].

Amphoteric surfactant systems show a pH-dependent behavior related to the pKa values of their substituent groups [69-71]: at pH lower than the pKa, they behave as cationic surfactants, while at pH higher than the pKa the net charge is zero and they behave as pure non-ionic surfactants [72-74]. Thus properties of amphoteric surfactants strongly depend on the pH and pH sensitivity varies according to the specific structure of the molecule [75-77]. In particular, the CMC, whose typical values are 10^{-5}–10^{-1} M for amphoteric surfactants at room temperature, significantly change with the pH [78-82], as well as the aggregate size and morphology, a consequence of the change of the ionization degree induced by pH variation [83-90].

Although a rather large group of organic functionalities with the potential for producing amphoteric surfactants exists, only four classes of materials are most often encountered: i) imidazoline derivatives, ii) betaines and sulfobetaines, iii) amino acid derivatives, and iv) lecithin and related phosphatides [91-93]. Beyond organic amphoteres, also charge-separated compounds, such as amine-oxides and sulfoxides, could be easily included among amphoteric surfactants [94, 95]. Particularly, in the last decades, amine oxide-based surfactants have been increasingly exploited in a variety of applications, e.g., as cleaning, emulsifying, antistatic and/or antibacterial agents [96-99].
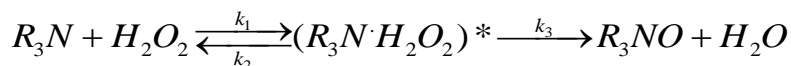
1.2.1) Linear amine oxide surfactants.

Amine-oxide surfactants are characterized by a polar head with a nitrogen-oxygen group where the net charge is zero, but the strong dipolar moment existing between the two atoms almost leads to a positive charge on the nitrogen and a negative one on the oxygen atom. At low pH, the oxygen atom protonates and the surfactant behaves as a cationic one [100-102].

In recent years, amine-oxide surfactants have found increasing uses in different fields, thanks to their low toxicity and ready biodegradability under both aerobic and anaerobic conditions [103-106]. As a general feature, amine-oxide surfactants are excellent foam-boosters and foam-stabilizer in blends including other anionic or amphoteric surfactants and are extensively used in highly concentrated hand washing-up liquids, detergents and antistatic preparations [98, 99]. However, it is well known that surfactant properties strongly depend on the molecular structure, and even small modifications of the polar head or of the alkyl chain may result in completely different aggregation properties, in terms of either critical concentrations or architecture of supramolecular assemblies. These changes in turn affect the physical-chemical, rheological and functional properties of the surfactant mixtures, finally reflecting in their potential applications. So, field of application of amino-oxide surfactants depends also on their molecular structure and in particular on the length of the alkyl chain and on the substituents on the nitrogen atom of the head [107, 108]. Various linear alkyl substituents of nitrogen have been tested and the

frequency by which some substituents are employed depends on the application field. The most effective and versatile combination found in detergency field is two methyl groups plus one long alkyl chain [109, 110].

1.2.2) Synthesis of Amine Oxide Surfactants

The most frequent synthetic approach for production of amino oxides is based on the oxidation of a tertiary amine [111-113] and well apply to production of amino oxide surfactants too. Hydrogen peroxide is generally used as oxidant and ammonium peroxide forms as the reaction intermediate, in a reversible step, followed by formation of the desired amino-oxide by splitting off of water [114]. The proposed reaction mechanism is reported below:

$$R_3N + H_2O_2 \underset{k_2}{\overset{k_1}{\rightleftarrows}} (R_3N^{\cdot}H_2O_2)^* \xrightarrow{k_3} R_3NO + H_2O$$

The rate of formation of the amine-oxide surfactant can be derived by the "steady-state approximation":

$$\gamma_{(R_3N^{\cdot}H_2O_2)} = k_3[R_3N^{\cdot}H_2O_2]^* \qquad\qquad (1)$$

then

$$\gamma_{(R_3N^{\cdot}H_2O_2)^*} = k_1[R_3N^{\cdot}H_2O_2] - k_2[R_3N^{\cdot}H_2O_2]^* - k_3[R_3N^{\cdot}H_2O_2]^* \qquad (2)$$

and assuming $\gamma_{(R_3N^{\cdot}H_2O_2)^*} = 0$ \hfill (3)

we obtain combining equations (1), (2), and (3)

$$\gamma_{(R_3N)} = \frac{k_1 k_3 [R_3N][H_2O_2]}{k_2 + k_3}$$

Or

$$\gamma_{(R_3N)} = k[R_3N][H_2O_2] \qquad\qquad (4)$$

Where k is the overall rate constant

$$k = \frac{k_1 k_3}{(k_2 + k_3)}$$

From equation (4) it clearly emerges that the overall order of reaction for amine oxide formation is 2, in complete agreement with experimental data [115].

For what concerns the degree of conversion of tertiary amines to the corresponding amine-oxide, it has been observed that it depends on the purity of the starting amine. With freshly redistilled tertiary amine, and with 10% molar excess hydrogen peroxide, the yield reaches 99% [115].

Several successful examples of synthesis of amine oxide surfactants through oxidation of the corresponding tertiary ammine are reported in the literature, slightly differing for experimental conditions. For example 2-Alkoxy-*N,N*-dimethylethylamine N-Oxides [116] is synthesized at room temperature, while aromatic amine oxides in mild conditions at 65° C [117].

An alternative interesting method for synthesis of linear amine oxide was developed by Rathman and Kust. They investigated the synthesis of *N,N*-dimethyldodecyl-1-amine oxide in aqueous solutions by micellar autocatalysis [118]. The lipophilic reactant, *N,N*-dimethyldodecyl-1-amine was initially solubilized in micellar solutions of the amine oxide surfactant, resulting in substantially higher reaction rates with a conversions of 90-100% within 2h at 70° C.

This method is important for two main reasons: i) micellar auto catalysis provides a method for synthesizing surfactants without employing volatile organic solvents in the reaction medium, with potential economic and environmental benefits; ii) deep knowledge of micellar auto catalytic reactions may refine and extend the understanding of other types of reactions in aqueous surfactant solutions.

1.2.3) Physical-chemical and aggregation properties of amine oxide surfactants

Many authors have reported studies on the physical-chemistry properties of amine oxide surfactants, such as critical micelle concentration, aggregate size, morphology and supramolecular organization, [118] and have pointed out how these properties are affected by both physical-chemical (pH, temperature, ionic strength) and molecular (length of the alkyl chain, substituents on the polar head) parameters.

The effect pH has on the amino oxide surfactant aggregation properties is one of the most studied. In aqueous mixtures, an equilibrium between the protonated and the non-protonated form exists; at pH lower than the surfactant pKa, the oxygen atom protonates and amine oxide surfactants behave as a cationic surfactant; at pH higher

than the pKa, they are non-protonated and behave as nonionic, more precisely, zwitterionic, surfactants [54, 101, 102, 119]. When the amine oxide surfactant become positively charged (pH<pKa), repulsive electrostatic interactions between interfacial head groups become significant with a resulting increase of the CMC. On the contrary, when the surfactant is a pure zwitterion (pH>pKa), repulsive interactions between polar heads, only due to dipole moments, are lower and the interaction between the hydrophobic tails favors the micellization process [120]. Thus, the critical micelle concentration is always higher in the case of the protonated form than in the case of the zwitterionic form, independently of molecular features, such as the length of the alkyl chain. This behavior is due to the positively charged hydrophilic head that on the one hand favors the monomer solubilization in water while on the other disfavors close packing of molecules in micellar aggregates because of electrostatic repulsion [121, 122].

Similar considerations stand for micelle size. A net charge on an ionic micelle induces formation of small aggregates, so micelle size at pH<pKa, when the surfactant is cationic, is definitely smaller than that at pH>pKa. [123]. Moreover, formation of hydrogen bonds involving the oxygen of the head group may favor self-aggregation in micelles with a wide set of different morphologies [124].

Solution pH, and consequently protonation of surfactant heads, do not affect only formation and features of isotropic micellar phases, but also those of liquid lyotropic crystalline (LLC) phases, in dependence on molecular features of the surfactant. For

example, when protonated these surfactants tend to form concentrated isotropic micellar phases more effectively than in zwitterionic form. This is due mainly to the strong repulsive electrostatic interactions between their hydrophilic heads of surfactants and secondly to their interaction with the water in the hydration process. As in the case of general aggregation processes, even in the case of LLC formation, the repulsive interaction between heads group disfavors efficient packing and supramolecular organization, thus phase diagrams of cationic surfactants, and similarly phase diagram of amphoteric surfactants in protonated form, are composed of large isotropic micellar stability regions. On the contrary, formation of supramolecular structures is more favored for amine oxide when they are in zwitterionic form.

Since the electrostatic repulsion between charged head groups is a main limiting factor in both micelle formation and supramolecular aggregation, an increase of ionic strength has a shielding effect that favors aggregation, both in the non-ionic and cationic form.

Another important physical-chemical parameter, capable of altering the interactions between the molecules and, consequently, their aggregation and supramolecular organization is the temperature. Especially as regards surfactants the temperature effects are well-highlighted by built-up and analysis of phase diagrams. Depending on their structural features and surfactant-surfactant interactions, several organized supramolecular structures may be thermodynamically stable in a certain temperature

range and form a mesophase. The mesophases obtained by heating a crystalline solid, or cooling an isotropic liquid, are called thermotropic, as the phase transition is induced by temperature. What happens is that by increasing the temperature, the normal crystal order changes, the thermal motion of the molecules within the lattice increases until vibrations become so intense they destroy the previous arrangement, thus giving rise to a completely disordered phase. The temperature at which this occurs is called melting temperature, however in thermotropic liquid crystals, the melting process occurs through one or more intermediate phases, thus giving rise to further phase transitions [125]. This totally general argument also apply to amino oxide surfactants, for example the *N,N*-dimethyldodecil-1-amine oxide (C_{12}DAO-linear or DDAO) phase diagram, built by means of sorption calorimetric and DSC by Kocherbitov *et al.*[126], is reported in figure 3well highlights stability regions of the different mesophases and transition temperatures.
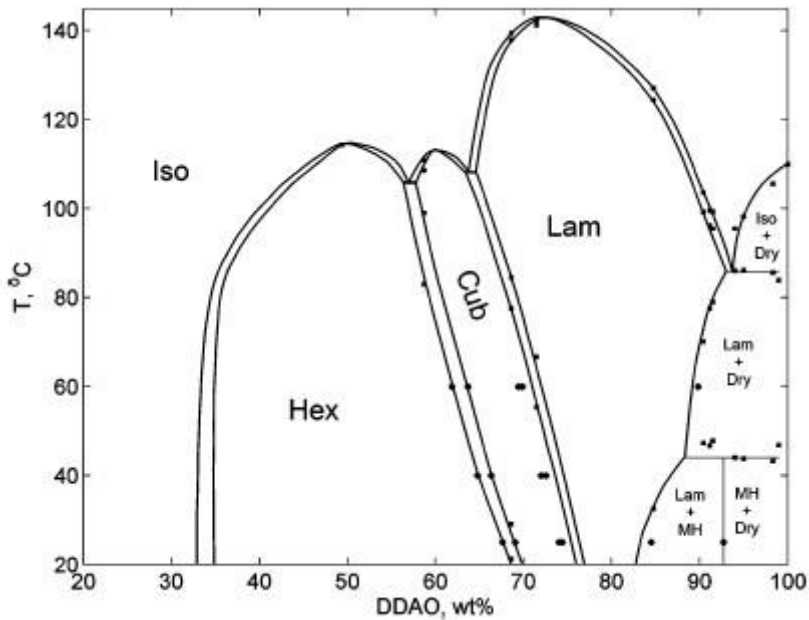
Figure 3. *N,N*-dimethyldodecyl-1-amine oxide water phase diagram

Aggregation properties of amine oxide surfactants depend strongly on their molecular structure: even small modifications of the polar head or of the alkyl chain length may result in completely different critical micelle concentrations or architecture of supramolecular assemblies. In particular, longer aliphatic tails result in higher tendency toward micelle formation. In other words, the longer the chain the lower the CMC (figure 4) [127].
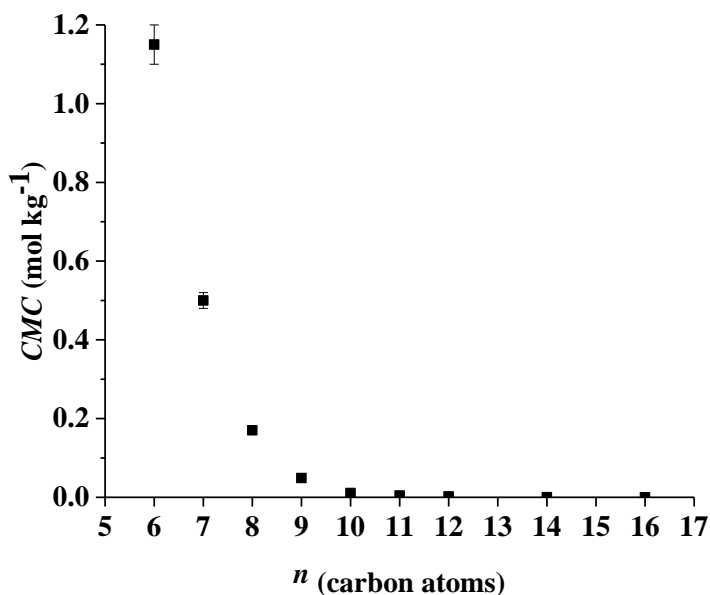
Figure 4. CMC versus alkyl chain length of *N,N*-dimethylalkylamine oxides.

The chain length also affects the molecular arrangement within the aggregates and consequently their morphology. For example, amine oxide surfactants with short chains (C_8-C_{10}) [128] form spherical micelles, whereas in the case of those with longer tails (C_{12}-C_{16}) either rod-like or ellipsoidal morphologies are preferred over spherical ones [108, 129].

The presence of insaturations along the alkyl chain also affects the morphologies of supramolecular aggregates formed by amino oxide surfactants. For example, in the case of alkyldimethylamine oxides with saturated hydrocarbon chains (C_nDMAO, chain length: n=4, 16, and 18), the phase sequence of lyotropic liquid crystals is hardly affected by the protonation. Only in the case of the half-ionized C_{14}DMAO,

i.e. when a mixture of non-ionic and protonated amino oxide surfactant is present, it is observed an elongation of the cylinders of the hexagonal phase. On the other hand, the phase diagram of half-ionized oleyl-*N,N*-dimethylamine oxide (OlDMAO) [(Z)-*N,N*-dimethyloctadec-9-en-1-amine oxide] looks quite similar to those of double-chained ionic surfactants, with a marked preference for bilayer structures over other LLC, which has been was interpreted in terms of dimers stabilized by hydrogen bonds between the nonionic and the protonated surfactants. It can be inferred that the predominant bilayer formation by the half-ionized OlDMAO is due to the combined effect of the hydrogen-bonded dimer formation and the cis-double-bond configuration of the alkyl chain [130, 131].

Various linear alkyl substituents of nitrogen have been tested and used to tune the functional properties of amino oxide surfactants, because of their effects on physical-chemical properties of these systems [109, 119, 132]. The introduction of hydrophilic head substituent alters the repulsion interactions between the polar heads and consequently the interactions between the hydrophobic tails.

Finally, a crucial parameter underlying all surfactant aggregation properties is hydration, or more generally, interaction of these amphiphilic molecules with the solvent. When water is added to a system, two general processes may occur: i) water uptake by a single phase where the phase gradually swells as a result of the incorporation of water molecules and ii) water uptake involving a phase change where the addition of water molecules causes a transition from one phase to another.

During both types of hydration processes, several properties of the system may change, such as structural parameters, molecular mobility, viscosity, density, reactivity, permeability, and so forth. For surfactant-based systems, used in, for example, industrial applications, it is mandatory to characterize and understand hydration-induced phase transitions to enable control of the phase structure required for successful application. Hydration-induced phase transitions have been extensively characterized in the case, for example, of *N,N*-dimethyldodecyl-1-amine oxide, both in bulk and in thin films and a good agreement between results was obtained, with main transitions (reported in Table 2) occurring at almost the same water activity with only slight effects on the transition kinetics.

Phase	Water activity
Liquid micellar phase	~1
Hexagonal phase	~0.8-1
Cubic phase	~0.7-0.8
Lamellar phase	~0.2-0.7
Solid phases	~0-0.2

Table 2. Phase transition of *N,N*-dimethyldodecyl-1-amine oxide induced by hydration process.

1.2.4) Safety of the amine oxide surfactants

Amine oxides surfactants are nonvolatile compounds that show low bioaccumulation in aquatic tissues and, as a consequence, bio-concentration in terrestrial organisms.

All available information on amine oxides demonstrates they have low-to-moderate level of toxicity in water [133].

Amine oxides surfactants are generally readily biodegradable under both aerobic and anaerobic conditions; however, in anaerobic conditions, they are less biodegradable than in aerobic ones. In particular, in the case of aerobic biodegradation, a relationship between pH/biodegradability exists: at neutral pH amine oxide surfactants are readily biodegradable. The main biodegradation pathway consists of ω-oxidation of the terminal methyl group to obtain an ω-amino fatty acid, followed by deamination, providing an amine and an ω-oxo fatty acid. Conversely, their biodegradability is much lower at acid pH, because protonation affects the first step of ω-oxidation [134].

1.2.5) Applications of amine oxide surfactants

Amine oxide surfactants find use in a wide and various range of fields, from detergency to personal care, from antimicrobial to pharmaceutical applications, depending on the length of the main alkyl chain and the substituents on the nitrogen atom.

For example, the *N,N*-dimethylamidoalkyl amine oxide serve as a very effective foam boosters in light duty detergents and shampoos[135], while the higher stearyl amine oxides can be used as hair conditioners [136]. By simply changing the length of the hydrophobic tail, Tomah company of Milton, WI developed a whole series of

amine *N,N*-diethanol-1-amine oxide surfactants with decreasing efficiency as foam boasters, namely C_9DEHAO-branched, C_{10}DEHAO-branched, C_{11}DEHAO-branched and C_{12}DEHAO-branched, having property of high foaming, moderate foaming, low foaming and extremely low foaming respectively, getting application in various types of cleaners.

Interestingly, alkyldimethyl amine oxides have been shown to exert pronounced anti-microbial activity when used individually or in combination with alkyl betaines. Although several studies have been performed with these compounds in combinations, only equimolar concentrations of the C_{12}/C_{12} and C_{16}/C_{14} chain lengths for the betaine and the amine oxide, respectively, have been investigated.

Birnie *et al*. investigated the anti-microbial activity of a wide range of chain lengths (C_8 to C_{18}) for both the amine oxide and the betaine and also attempted to correlate their micelle-forming capabilities with their biological activity [127]. Anti-microbial activity was found to increase with increasing chain length for both homologous series up to a point, exhibiting a cut off effect at chain lengths of approximately 14 for amine oxide and 16 for betaine. Additionally, the C_{18} oleyl derivative of both compounds exhibited activity in the same range as the peak alkyl compounds. Like most other surfactants, they are believed to be membrane perturbants, disrupting the cell membrane of the microorganism.

1.2.6) Amine oxide surfactants used in home care formulations.

Amine oxide surfactants have already been described as components of certain formulations, comprising detergents, dishwashing liquids, antistatic preparations, shampoos, hair conditioners and shaving foams [137-139]. Particularly, they are effective mild multifunctional surfactants, for their low cost, they are used also in mixtures for very specific requirements, such as hard-surface cleaners, laundry and dish detergents and other washing product. Because of their efficiency and chemical versatility, amine oxide surfactants are the most used in liquid detergents formulation.

The amine oxide surfactant most used in home-care formulations is the *N,N*-dimethyldodecyl-1-amine oxide (C_{12}DAO-linear) because of it presents a low cmc and low chemical instability up at high temperature, has low production cost, and low toxicity. In Figure 5 the phase behavior of C_{12}DAO-linear in water by POM and SAXS is reported.
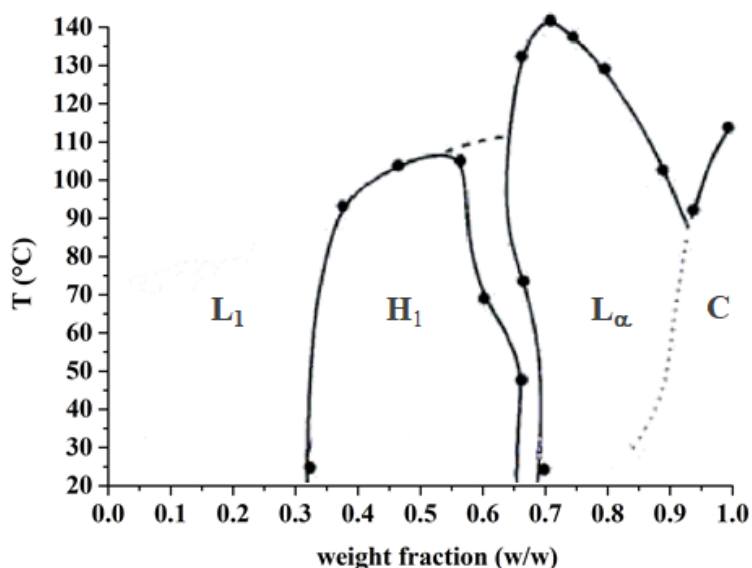
Figure 5. Phase diagram (weight fraction versus temperature) of C_{12}DAO-linear/water system. The following notation is used for the various region: L_1=isotropic phase, H_1=hexagonal LLC phase, L_α=lamellar LLC phase, C=crystalline phase.

The phase diagram shows an extended micellar phase; however, liquid lyotropic crystalline phases are stable above around 0.3 mole fraction. The presence of these phases already at relatively low surfactant concentration has the detrimental effect of limiting the functionality of detergent formulations, because of their low processability. For this reason, during formulate production, a large amount of water must be added to assure mixture flowability and processability.

A very effective modification aimed at tuning the surfactant behavior is either the shortening or the insertion of branches in the alkyl chain. Indeed, branching is likely

to disrupt tail-tail interaction and their effective packing, affecting aggregation tendency as well as supramolecular organization of surfactants.

1.3) Branched surfactants

Many of the surfactants used in new home fabric and personal care formulations have branched hydrocarbon tails [140, 141], irrespective of their polar head. Branched surfactants have the capability to modify the interactions between both the hydrophobic tails and the hydrophilic heads, thus modifying the physical-chemical properties of their systems with respect to those of their linear analogues.

1.3.1) Physical-Chemical properties of branched surfactants

Branched surfactants are classified by Wormuth *et. al*. as: i) methyl branched, ii) double tailed, iii) highly branched.

i)   Methyl-branched surfactants consist of a single hydrocarbon chain with one or more small pendant groups (methyl or ethyl groups) attached at any position along the main chain.

ii)   Double-tail surfactants consist of a main hydrocarbon chain with one pendant chain. The pendant chain was unbranched, contains three or more carbon atoms, and is attached at or near the hydrophilic group (at the α or β carbon).

iii)   Highly branched surfactants consist of a hydrocarbon chain with more pendant chains. The pedant chains are one or two carbon atoms long, are

branched and are attached either close or far away from the hydrophilic group.

A general examples of methyl branched, double tail and highly branched zwitterionic surfactants are reported in the figure 6.
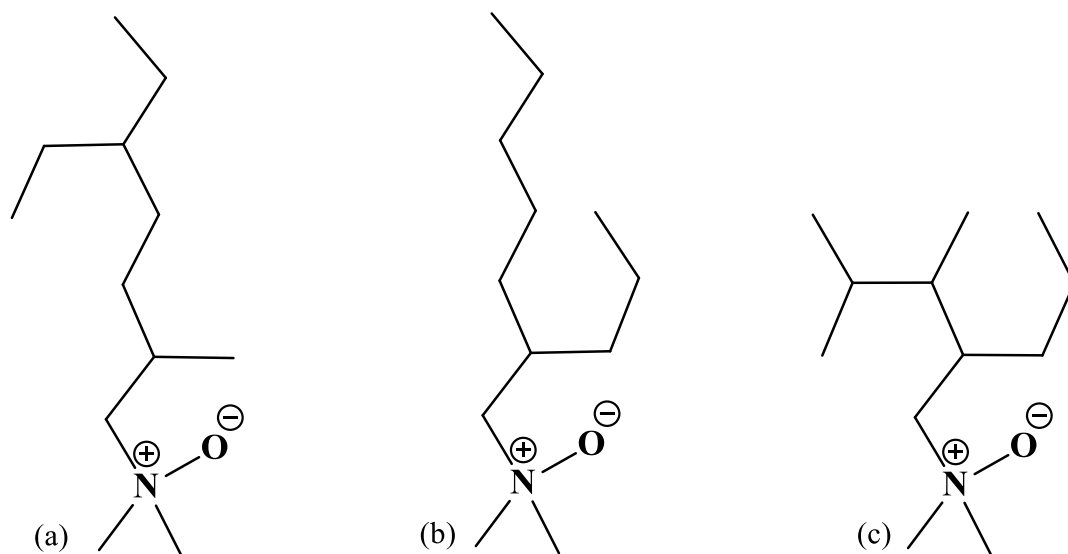

Figure 6. (a) The methyl-branched 5-ethyl-*N,N*-2-trimethylheptan-1-amine oxide; (b) The double-tail surfactants *N,N*-dimethyl-2-propylheptan-1-amine oxide; (c) The highly branched surfactants *N,N*-3,4-tetramethyl-2-propylpentan-1-amine oxide).

Most of the branched surfactants analyzed in the literature belong to the double-tail group.

By moving the attachment point of the hydrophilic group incrementally along a linear hydrocarbon chain, a series of surfactant isomers of constant carbon number

is created, in which the surfactant evolves from single-tail (hydrophilic group at the end of the hydrocarbon chain), to double tails of unequal length (hydrophilic group between the end and the center of the hydrocarbon chain), to double tails of equal length (hydrophilic group at the center of the hydrocarbon chain) [20]. An example for amino oxide surfactants is reported in the figure 7.
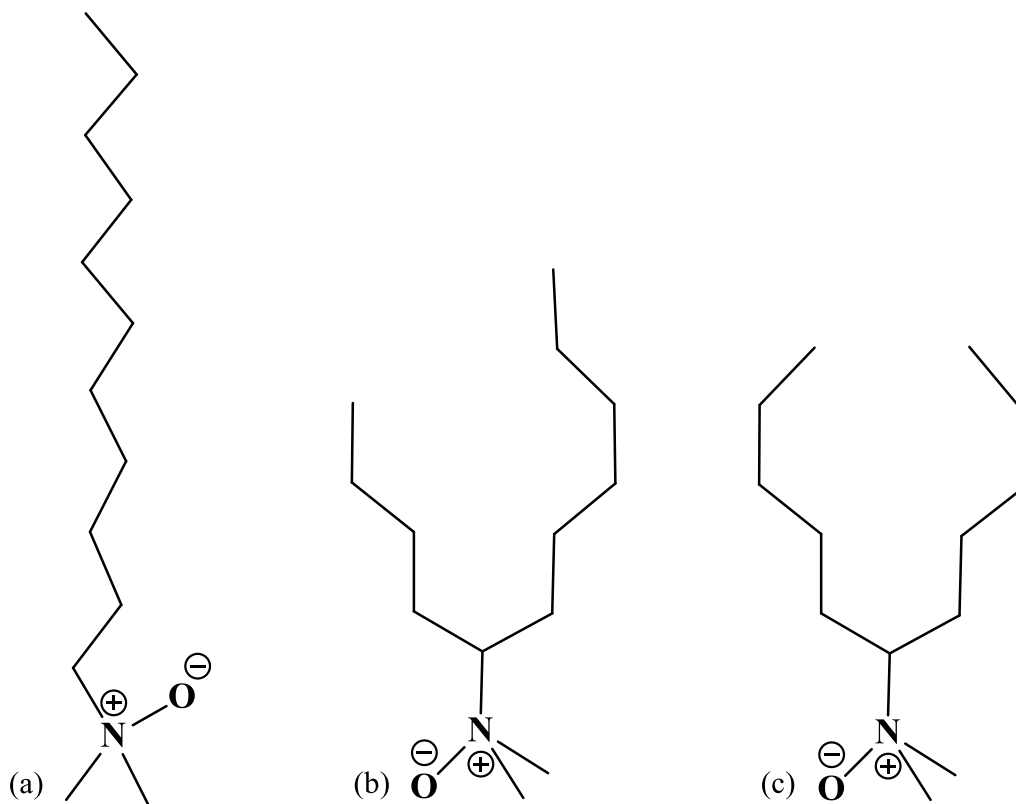

Figure 7. (a) Linear amine oxide surfactant (*N,N*-dimethylundecan-1-amine oxide); (b) Branched amine oxide surfactant (*N,N*-dimethylundecan-5-amine oxide); (c) Symmetrical branched amine oxide surfactant (*N,N*-dimethylundecan-6-amine oxide).

As the surfactant tails become equal in length, the Kraft point decreases [142] the critical micelle concentration increases [143], the surfactant becomes more effective

at reducing the air-water surface tension [144] and stability domains of its LLC phases change [145].

One of the most interesting effects of insertion of branching on the linear hydrocarbon chain of surfactants is the modification of their micellization processes. In particular, these effects arise from both a different disposal of molecules at the water-air interface with respect to linear analogues (surface effects) and a different capability to assemble in discrete aggregates in solution (bulk effects).

For amphiphiles with a single straight-chain aliphatic tail, the polar or electrostatic repulsion between head groups overcomes the hydrophobic interactions between aliphatic tails that should pull molecules together, hindering a surfactant disposal with hydrophobic tails perpendicular to the water surface, even at concentrations higher than the interfacial saturation adsorption. As a consequence of the tilted surfactant orientation on the water surface, the terminal CH_3 groups are not able to cover the solution surface sufficiently, leaving part of CH_2 groups (with higher free energy than CH_3) and polar water molecules partially exposed to the air. In contrast, in the presence of branching along the surfactant aliphatic tail, the density of hydrocarbon chains on the solution surface increases, as a result of a more tightly packed arrangement of hydrophobic tails, held together perpendicularly to the surface by a stronger hydrophobic interaction (figure 8), thus creating a liquid hydrocarbon surface.
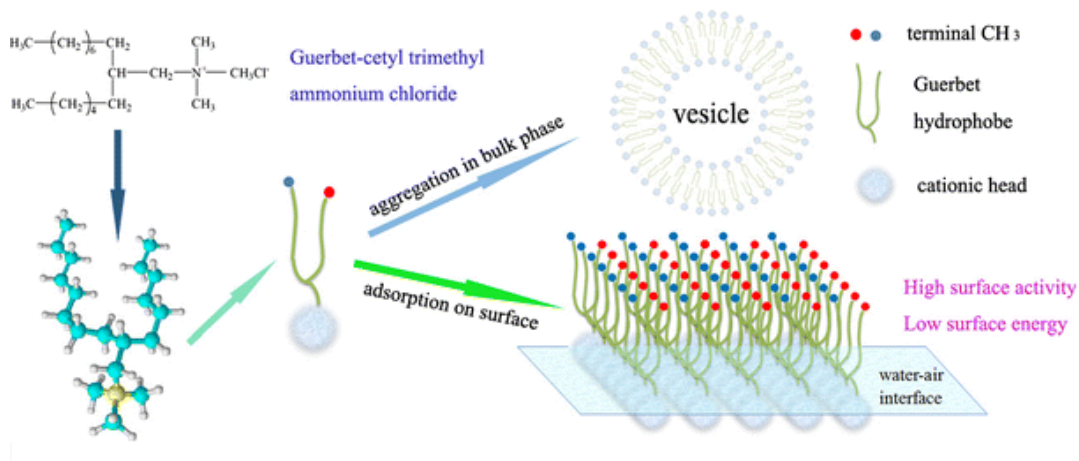
Figure 8. Schematic illustration of aggregation pattern of branched cationic surfactant molecules in solution–air interface and bulk phase.

This justifies why branched surfactants are more effective at decreasing surface tension that their linear counterparts. So surface effects of branching include a lower γ_{cmc} while bulk effects a higher CMC value, i.e. adsorption on aqueous solution surface is enhanced, while micellization in bulk phase is hindered because of steric hindrance, respectively. Analysis of interfacial tension of branched surfactants systems indicated that critical micelle concentration increases with the branching degree, in the order highly branched > double tail > methyl branched > linear, while surface tension at the cmc decreases with the same trend [146].

All branched surfactants are much more "hydrophobic" than corresponding linear (single-tail) surfactants [11, 13, 15, 22].

Surfactant aggregation properties are determined by a fine balance between their hydrophobic and hydrophilic regions, thus any structural modification, such as the

insertion of one or more branches in the hydrophobic tail, can alter their supramolecular aggregation and liquid lyotropic crystalline phase formation, with consequences in their possible applications. This depends on both different intramolecular (surfactant-surfactant) and intermolecular (surfactant-water) interactions. [19].

Relative length of the branch and the main chain affects formation of LLC phases: branches that are longer than the main hydrophobic chain reduce stability regions of liquid lyotropic crystalline phases, in particular of the hexagonal one; on the other hand, symmetric (same length) branches and alkyl tails, determine a phase behavior of the branched surfactant very similar to that of the linear analogue [24].

1.3.1) Biodegradability of branched surfactants

Biodegradability of branched surfactants with respect to their linear analogues depends on the class of surfactants. Nonetheless, some general trend exists: i) their biodegradability in both aerobic and anaerobic conditions depends on the number of branches on the main surfactant hydrocarbon chain, as well as on their length [147]; ii) the lower the number of branches and carbon atoms that make up the branch, the more the surfactant is biodegradable, with the most biodegradable surfactants being those bearing only one methyl long branch, irrespective of the surfactant class [148].

A thorough comparison of biodegradability of linear and branched non-ionic surfactants well proves the second point, in particular showing how surfactants with

only one methyl branch are as biodegradable as their linear analogues in both aerobic and anaerobic conditions.

Biodegradability of cationic surfactants both in aerobic and anaerobic has been studied. In particular, the branching effect has been investigated on the biodegradation process of cationic surfactants. Even in the case of cationic surfactants their biodegradability has been evaluated in relation to the ω-oxidation reaction. This reaction involves a reaction of the C-N bond (deamination which in the case of cationic surfactants) is more facilitated as there is the presence of a positively charged nitrogen atom [149, 150].

Biodegradability of anionic surfactants has been thoroughly analyzed both in aerobic and anaerobic aquatic environments and branching has been found to cause a lower biodegradability in both conditions. In particular, in the case of sulfonate surfactants the last step of the biodegradation mechanism is a desulphonation reaction, which requires a large amount of both water and heat to take place with subsequent production of sulfuric acid, and this step is mostly affected by branching making branched sulfonate surfactants the less biodegradable surfactants [151].

1.3.2) Application of branched surfactants

In the last ten years, the number of patents and papers related to the employment of branched surfactants in home, fabric and personal-care formulations is doubled, approximately.

As already anticipated, phase behavior of branched surfactants depends on the number of branches, their length and their position on the main hydrocarbon chain, since branching affects the interactions between both hydrophobic tails and hydrophilic heads of surfactant, but mainly modifies the surfactant-water interactions. Thus, branching can completely change features of surfactant mixtures, leading to formulations characterized by higher performances, including cleaning, foaming, wetting and other properties that last over time, and active concentrations, two aims strongly pursued by formulative industry.

However, many authors have shown that the complete substitution of linear surfactants with branched ones does not always lead to better performances, which have been shown can be obtained using mixtures of linear and branched surfactants. In this way, the performances of the final formulations can be improved up to 50% [152].

Detergent performances of home-fabrics and personal care formulations can be improved by tuning the number of branches and the water content. As regards the branches, highly branched surfactants usually present higher foaming propensity, but, as seen above, are less biodegradable and additionally are likely to by poor wetting agents [153]. For these reasons, double-tail surfactants, which present well balanced synthesis ease, significant biodegradability and high performances, are the most used branched surfactants.

In the last ten years, branched surfactants have been also widely used in oil recovery [40], because of their higher effectiveness in reducing interfacial tension, which is the principle at the basis of Enhanced Oil Recovery (EOR) with chemicals, already at low concentrations and without requiring addition of alkaline agents or co-surfactants with respect to linear ones. Indeed. EOR involves the use of surfactants dispersed in water (*surfactant flooding*), in order to reduce the interfacial tension of the oil at values of the order of 10^{-5}-10^{-4} N/m^2, in such a way to zero the capillary pressure value and favor the escape of the oil from the pores of the rock, behind the thrust of water [154].

1.4) New branched amine oxide surfactant

In this context, we present the synthesis and characterization of a new amine-oxide surfactant, *N,N*-dimethyl-2-propylheptan-1-amine oxide, bearing a C10 tail branched at position 2 and hereafter named C$_{10}$DAO-branched. The protonation equilibrium in dilute solution was monitored using potentiometry. Due to the peculiar features of the polar head of this class of surfactants, we analyzed the surfactant behavior under both acidic and basic conditions, by means of tensiometric titration and dynamic light scattering (DLS) measurements. The same techniques were used to investigate the aggregation behavior of the C$_{10}$DAO-linear analog, *N,N*-dimethyldecyl-1-amine oxide. Finally, we tested and compared the foamability of the two surfactants.

Hereafter, the phase behavior of C_{10}DAO-branched in water is studied as a function of both concentration and temperature and compared with that of C_{10}DAO-linear, which is also investigated as a reference. Polarized Optical Microscopy (POM), Small Angle Neutron and X-ray Scattering (SANS and SAXS, respectively) experiments are used to investigate the structure of the supramolecular aggregates. The results are confirmed by Humidity Scan Quartz Crystal Microbalance Dissipation (HS QCM-D) measurements, which have been recently proposed as a reliable approach for a rapid scrutiny of surfactant phase behavior [155]. Rheology is used to investigate the viscosity of the mixtures. The phase behavior of the ternary systems of C_{10}DAO-branched/AES/water and C_{10}DAO-branched/AES/water system were built by using the same procedure adopted for the binary phase diagrams

Analysis of the results offers the opportunity to highlight differences and similarities between supramolecular organization of the branched and linear amine oxide isomers, first in water and then in co-formulation with one of the most used anionic surfactants (SLES), opening new perspectives in their exploitation in formulative chemistry.

2) Materials and methods

Hydrobromic acid (48 % v/v), sulfuric acid (purity 96 %), ethanol (96 %) and starch paper iodide were purchased from Carlo Erba (Italy). *N,N*-dimethylamine (40 % w/w aqueous solution), hydrogen peroxide (50 % w/w), sodium sulfate anhydrous, chloroform (99 %), toluene (99.8 %), diethyl ether (99.8 %), $CDCl_3$ (99 %), active carbon (DARCO®, 4-12 mesh particle size, granular) D_2O (isotropic enrichment >99.8%) and lithium cloride (99.99%) were purchased from Sigma Aldrich (Milan, Italy). 2-propylheptan-1-ol was kindly supplied by Procter and Gamble (Belgium). All aqueous solutions were prepared by using double distilled water. Sodium lauryl ethoxy sulphate kindly furnished by Procter and Gamble (Batch 16-155-1), Brussels, Belgium.

2.1) N,N-dimethyl-2-propylheptan-1-amine oxide synthesis

N,N-dimethyl-2-propylheptan-1-amine oxide ($C_{10}DAO$-branched) was synthetized through a synthetic approach [156] including three steps, as reported in Scheme 2: 1) bimolecular nucleophilic substitution (S_N2) converting 2-propylheptan-1-ol in 4-(bromomethyl)nonane; 2) unimolecular nucleophilic substitution (S_N1) on 4-(bromomethyl)nonane leading to *N,N*-dimethyl-2-propylheptan-1-amine; 3) final oxidation of *N,N*-dimethyl-2-propylheptan-1-amine in *N,N*-dimethyl-2-propylheptan-1-amine oxide ($C_{10}DAO$-branched).
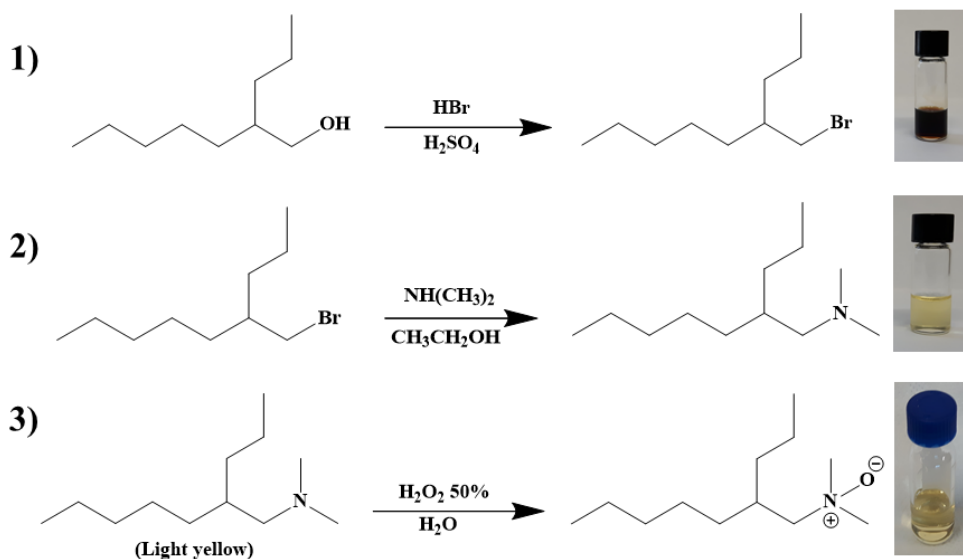
Scheme 2. Reaction scheme for the synthesis of C_{10}DAO-branched.

The product of each synthetic step was characterized by ^{1}H NMR in CDCl$_3$ solution. NMR spectra were collected on a Bruker DRX-400 instrument (Rheinstetten, Germany; ^{1}H: 400 MHz) at 298 K. Heteronuclear single quantum correlation-distortionless enhancement by polarization transfer (HSQC-DEPT) experiments were measured in the ^{1}H-detected mode via single quantum coherence with proton decoupling in the ^{13}C domain. In the case of the newly synthesized C_{10}DAO-branched surfactant, a further characterization was performed by means of HSQC-DEPT 2D-NMR, using a Bruker DRX-600 (^{1}H: 600 MHz) spectrometer.

In the first reaction step, 2-propylheptan-1-ol reacted with an excess of hydrobromic acid (1:7.22 molar ratio) and sulfuric acid (1:1.65 molar ratio) at 383 K under reflux conditions [156]. After 3.5 h the reaction was quenched by cooling the mixture to room temperature. Then it was washed with diethyl ether and water in order to remove hydrobromic acid excess. The organic phase was purified from water traces using anhydrous sodium sulfate that was filtered afterwards. The resulting solution was further purified with active carbon and then vacuum-dried, in order to remove diethyl ether, so obtaining 4-(bromomethyl)nonane [157, 158], as a brown viscous liquid (see inset of Scheme 2) with yield ≥ 95 %. The obtainment of 4-(bromomethyl)nonane was confirmed by analysis of ^{1}H-NMR spectrum (see supplementary material). In particular, the diagnostic peaks are a triplet at δ 1.60 due the proton of the ternary carbon (C$\underline{H}$), and a doublet at δ 3.45 due to the deshielded protons of the ((C$\underline{H}_2$)Br) group.

The second reaction step between 4-bromomethylnonane and *N,N*-dimethylamine (1:7.31 molar ratio) was carried out at 353 K in ethanol under reflux conditions [159]. After 24 hours the reaction was quenched by cooling to room temperature, the reaction mixture was washed with chloroform and water to remove excess *N,N*-dimethylamine, and the organic phase dehydrated with anhydrous sodium sulfate and filtered. The liquid mixture was vacuum-dried to remove chloroform, so obtaining *N,N*-dimethyl-2-propylheptan-1-amine, which after purification with active carbon appeared as a light yellow viscous liquid (inset of Scheme 2). The yield of the second reaction step was ≥ 95%, and the chemical identity of the product was confirmed by

^{1}H-NMR analysis (see supplementary material), in particular by the presence of a diagnostic triplet at δ 1.48, due to the (C$\underline{H}$) group, together with a doublet at δ 2.01 and a singlet at δ 2.12, due to ((C$\underline{H_2}$)N(CH$_3$)$_2$ and ((CH$_2$)N(C$\underline{H_3}$)$_2$, respectively.

Finally, oxidation of *N,N*-dimethyl-2-propylheptan-1-amine was carried out with hydrogen peroxide (1:5.2 molar ratio) at 343 K in water for 3.5 hours under reflux conditions in a jacketed glass reactor. Then the reaction was quenched by cooling to room temperature, the absence of residual traces of H_2O_2 was checked with starch paper iodide, and the resulting mixture was concentrated by co-evaporation with toluene (three times). The product (C$_{10}$DAO-branched) was obtained as a light yellow viscous liquid (inset of Scheme 2), with a yield≥95 %. The NMR spectrum shows the presence of a triplet at δ 1.97, due to the (C$\underline{H}$) proton, much more deshielded than the corresponding atom in intermediate products, a doublet at δ 3.22, due to ((C$\underline{H_2}$)N$^+$O$^-$) and a singlet at δ 3.24 ((C$\underline{H_3}$)$_2$N$^+$O$^-$), which confirm the presence of the N$^+$O$^-$ group.

2.2) Mass Spectrometry measurements

C$_{10}$DAO-branched and C$_{10}$DAO-linear were analyzed by means of electrospray mass spectrometry (ESI-MS) in the positive ion mode, using an Agilent 6230 TOF mass spectrometer coupled to an Agilent HPLC system (1260 Series) with a reverse-phase C18 column (Poroshell 120 EC-C18, 2.1 x 100 mm, 2.7 μm; Agilent Life Sciences, Santa Clara, CA, USA). The ESI-MS source operated with capillary voltage of 3000 V, gas temperature of 598 K, dry gas (N$_2$) flow of 5 L min^{-1} and nebulizer at 35 psi.

MS spectra were acquired in a range of 150-1000 m/z with a rate of 1 spectrum s^{-1}, time of 1000 ms per spectrum and transient per spectrum of 9961 ms.

2.3) Potentiometric measurements

The protonation constant of $C_{10}DAO$-branched in monomeric (unmicellized) form was conducted at 298 K at various NaCl concentrations (I), by measuring [H$^+$] in a series of surfactant solutions. The measurements were carried out as potentiometric titrations where the hydrogen ion concentration was determined by the e.m.f. of cell (A) [160]:

$$(-) \text{ RE/Test Solution/GE } (+) \tag{A}$$

in which GE symbolizes the glass electrode and RE is the reference half−cell: R =I M NaCl// I M NaCl /AgCl(s) /Ag(s). Surfactant concentration was varied in the range 3×10^{-3} - 1×10^{-2} M, i.e. well below the CMC (see below). During the measurements, the cell assembly, automatic burette, and gas washing bottles were placed in an air thermostat kept at (25.0 ± 0.02) °C. Glass electrodes manufactured by Metrohm Ltd. (Switzerland) were employed. Potentiometric titrations were carried out with a programmable computer-controlled data acquisition unit 34970A, Agilent Technologies (USA).

2.4) Tensiometric titration

The surface tension, γ, of the $C_{10}DAO$-branched or $C_{10}DAO$-linear aqueous mixtures in both acidic and basic conditions was measured with a Sigma 70 tensiometer (KSV,

Stockholm, Sweden) using the Du Noüy ring method as described elsewhere [161]. γ was correlated to the force required to raise the ring from the surface of the air/liquid interface. Successive aliquots of a stock surfactant mixture, freshly prepared in Millipore water and previously filtered with a 0.22 µm filter, were added to the vessel with a known volume of water. After each addition the sample was mixed using a magnetic stirrer and three minutes were waited to attain equilibrium; γ was then measured.

2.5) Dynamic Light Scattering (DLS)

DLS measurements were performed with a home-made instrument composed of a Photocor compact goniometer, a SMD 6000 Laser Quantum 50 mW light source operating at 5325 Å, a photomultiplier (PMT-120-OP/B) and a correlator (Flex02-01D) from Correlator.com. The experiments were carried out at room temperature at a scattering angle $\theta=90°$. The scattered intensity correlation function was analyzed using a regularization algorithm [162, 163]. The diffusion coefficient of each population of diffusing particles was calculated as the z-average of the diffusion coefficients of the corresponding distributions [164]. Considering that the mixtures are diluted, the Stokes–Einstein equation has been used to evaluate the hydrodynamic radius, R_H, of the aggregates from their translation diffusion coefficient, D.

2.6) Foaming properties

Foaming assay was performed with a custom-made foam preparation apparatus described elsewhere [165]. The apparatus consisted of a 500 mL graduated cylinder (4.8 cm i.d.). Decarbonated air was pumped (flux of 100 mL/min for 5 min) into 250 mL of sample solution (1 % w/w) through a gas diffuser positioned at the cylinder bottom at 25 °C. The foam height was measured soon after the pump stop and monitored over a time course of 10 min.

2.7) Sample preparation of the binary systems

Samples for phase diagram determination, POM, SAXS, QCM-D and rheology measurements were prepared by weighing appropriate amounts of $C_{10}DAO$-branched or $C_{10}DAO$-linear and doubly distilled and degassed water in screw-cap glass vials, followed by a Vortex mixing. Samples for SANS measurements were prepared using D_2O as solvent. Liquid crystalline samples were mixed by repeated centrifugation for 3 days. Thoroughly mixed samples were kept at 25 °C for 2 weeks and checked at regular intervals by ocular inspection with the help of cross-polarizers. No variation was observed after this equilibration period.

2.8) Phase diagram determination

In order to build the phase diagrams of the systems ($C_{10}DAO$-branched)-water and ($C_{10}DAO$-linear)-water, 20-25 samples were prepared for each of them, spanning the whole concentration range (Figures S_1 a-b). Preliminarily, a visual inspection of all samples through cross-polarizers was carried out, checking for homogeneity and birefringency. Ocular inspection was first done at 25 °C; the temperature was then raised up to 70 °C, for $C_{10}DAO$-branched, and to 110 °C, in the case of $C_{10}DAO$-linear, by steps of 5 °C through a thermostat. Birefringent samples, containing optically anisotropic LLCs, were further analyzed by POM in order to discriminate

the different surfactant supramolecular arrangements. Confirmation of LLCs morphology was obtained by SAXS diffraction patterns, which also furnished a wealth of structural details. Isotropic (no birefringent) samples were analyzed by SANS measurements.

The surfactants' phase diagrams were also investigated by an alternative approach, based on HS QCM-D, which allows a fast screening of LLC phase transitions as a function of the water content in the mixtures.

2.9) Sample preparation of the ternary system

Samples for phase diagram determination, POM, SAXS, QCM-D and rheology measurements were prepared by weighing appropriate amounts of C_{10}DAO-branched or C_{10}DAO-linear, AES and doubly distilled and degassed water in screw-cap glass vials, followed by a Vortex mixing. Liquid crystalline samples were mixed by repeated centrifugation for 3 days. Thoroughly mixed samples were kept at 25 °C for 2 weeks and checked at regular intervals by ocular inspection with the help of cross-polarizers. No variation was observed after this equilibration period.

2.10) Phase diagram determination of the ternary system

In order to build the phase diagrams of the systems (C_{10}DAO-branched)-AES-water and (C_{10}DAO-linear)-AES-water at 25 °C, 100-150 samples were prepared for each of them, exploring the whole concentration range (Figures S_9 a-b). Preliminarily, a visual inspection of all samples through cross-polarizers was carried out, checking for homogeneity and birefringency. Afterwards, birefringent samples, containing optically anisotropic LLCs, were analyzed by POM in order to discriminate the different surfactant supramolecular organizations. Confirmation of LLCs morphology was obtained by SAXS diffraction patterns, which also provided a quantitative structural characterization of the surfactants' supramolecular aggregates. The phase diagrams were also investigated by an alternative approach,

based on HS QCM-D, which allows a fast screening of LLC phase transitions as a function of the water content in the mixtures. In particular, the samples with and equal weight fraction of $C_{10}DAO$-branched (or $C_{10}DAO$-linear) and AES ($w_{C_{10}DAO} = w_{AES} = 0.50$) were investigated.

2.11) Polarized Optical Microscopy

The polarized optical microscopy images were collected using a Laser Scanning Confocal Microscope (LSM) 5 Pascal (Carl Zeiss Advanced Imaging Microscopy, Jena, Germany). The instrument is equipped with an Axiovert 200 M light microscope coupled with an AxioCam HRm high resolution digital camera (Carl Zeiss Light Microscopy, Göttingen, Germany). The microscope is also equipped with a home-made incubator capable of keeping the sample temperature at (25.0 ± 0.1) °C.

2.12) Small-angle X-ray scattering

Small-angle X-ray scattering patterns were recorded with a S3-MICRO SWAXS camera system (HECUS X-ray Systems, Graz, Austria) employing Cu Kα radiation of wavelength 1.542 Å provided by a GeniX X-ray generator, operating at 50 kV and 1 mA. The scattered X-rays in the small-angle region were detected by a 1D-PSD-50 M system containing 1024 channels of width 54.0 μm. The working q-range (Å^{-1}) was $0.02 \leq q \leq 0.4$, where $q = 4\pi\sin(\theta)\lambda^{-1}$ is the modulus of the scattering wave vector. A stainless steel sample holder with thin polymeric sheet (Kapton X-ray film roll TF-475, FluXana GmbH & Co. KG, Bedburg-Hau, Germany) was used. I(q) was denoted as the intensity of scattering. Silver Behenate, $CH_3\text{-}(CH_2)_{20}\text{-}COOAg$, was used as a standard for the calibration of the angular scale.

Structural parameters of lamellar and hexagonal phases were calculated according to the following equations:

$$a_{lam} = d \cdot h$$

$$(1a)$$

$$d_W = a(1 - \phi)$$

$$(1b)$$

$$d_L = a - d_W$$

$$(1c)$$

$$a_{hex} = d \cdot \frac{2}{\sqrt{3}} \cdot \sqrt{(h^2 + k^2 + hk)}$$

$$(2)$$

where $d = 2\pi/q$, a is the lattice parameter, d_W is the water layer thickness, d_L is the bilayer thickness, h and k are the Miller indices. In equation 1b ϕ is the surfactant volume fraction, calculated as follows:

$$\phi = \frac{\frac{w_{surf}}{\rho_{surf}}}{\frac{w_{surf}}{\rho_{surf}} + \frac{w_W}{\rho_W}} \qquad (3)$$

where w_{surf}, ρ_{surf}, w_W, and ρ_W are weight and density of, respectively, the surfactant and the water. Errors on the lattice parameters were always less than 2% (standard deviation).

2.13) Small-angle neutron scattering

Small angle neutron scattering measurements were performed at the KWS2 instrument located at the FRJ-2 reactor of the Forschungszentrum Jülich, Germany, and at the LOQ instrument sited at the ISIS facility of the Rutherford Appleton Laboratory of Chilton, United Kingdom. In the first case, neutrons with an average wavelength (λ) of 7 Å and a wavelength spread of $\Delta\lambda/\lambda \leq 0.2$ were used. A two dimensional area detector at three different sample-to-detector distances (2, 8, and 20 m) measured neutrons scattered from the samples. These configurations allowed the collection of scattering cross sections in an interval of transferred momentum q $= 4\pi/\lambda \sin(\theta/2)$ between 0.002 Å^{-1} and 0.45 Å^{-1}, where 2θ is the scattering angle. The

samples were contained in a closed quartz cell, in order toprevent the solvent evaporation, and all measurements were per-formed at 25 °C. Each measurement lasted for a period sufficient to obtain ~1.5 million counts. The raw data were corrected for background and empty cell scattering. Detector efficiency correction, radial average and transformation to absolute scattering cross sections ($d\sigma/d\Omega$) were made with a secondary plexiglass standard [166, 167]. Scattering profile were collected for $C_{10}DAO$-linear w_s=0.15 at Forschungszentrum Jülich, Germany.

At the ISIS pulsed neutron source, the LOQ instrument uses neutrons of wavelengths ranging between 2.2 and 10 Å detected by a time-of-flight analysis on a 64 cm^2 two-dimensional detector placed 4 m from the sample giving a q range of 0.008-0.279 Å^{-1}. The raw data were corrected for background and empty cell scattering, and detector efficiency and then put into absolute scattering cross sections ($d\sigma/d\Omega$) by comparison with scattering from a partially deuterated polystyrene standard. Scattering profile were collected for $C_{10}DAO$-branched w_s=0.15 and w_s=0.40 at ISIS pulsed neutron source, Didcot (UK).

The cross-section ($d\sigma/d\Omega$) were plotted as function of scattering vector (q). The dependence of ($d\sigma/d\Omega$) from the scattering vector was analyzed according to Eq. (4):

$$\frac{d\sigma}{d\Omega} = n_P P(q)S(q) + \left(\frac{d\sigma}{d\Omega}\right)_{fract} + \left(\frac{d\sigma}{d\Omega}\right)_{inch} \tag{4}$$

where n_P is the number density of crystallites, $P(q)$ is the form factore, $S(q)$ is the interparticle structure factor of the equivalent sphere that can be calculated by solving the Ornstein-Zernike equation [168] using the closure relation given by the rescaled mean spherical approximation (RMSA)[169-171] and $(d\sigma/d\Omega)_{inch}$ is the incoherent contribution to the scattering cross section.

2.14) Humidity Scanning (HS) Quartz Crystal Microbalance Dissipation (QCM-D)

A q-sense QCM-D E4 instrument equipped with humidity module QHM 401 and AT-cut SiO_2 sensors (QSX 303, 5 MHz) from Biolin Scientific AB (Västra Frölunda, Sweden) was used. New sensors were washed with water and ethanol before use. Reused sensors were cleaned by the procedures described in the q-sense guidelines manual (cleaning protocol B for QSX 303).

The QCM-D is an ultrasensitive method for the mass determination of materials adsorbed on a piezoelectric quartz sensor. The QCM-D technique monitors the frequency of the oscillating shear motion of the quartz sensor, which is stimulated by an applied potential. The mass of the adsorbed materials can be calculated using the Sauerbrey equation [172], which describes the linear relationship between mass addition and frequency shift

$$\frac{\Delta f}{n} = \frac{2f_0^2 m_f}{Z_q}$$ (5)

where $\Delta f/n$ is the frequency change normalized to the overtone number n, $Z_q = 8.8 \times 10^6$ kg m^{-2} s^{-1} is the acoustic or mechanical impedance of quartz, f_0 is the fundamental frequency (5 MHz), and m_f is the mass in kg m^{-2}. In addition to the frequency change, the QCM-D technique also monitors the dissipation D, which is related to the decay time of the oscillating resonator when the alternating potential is turned off. The decay time is related to the viscoelastic properties of the film that coats the sensor. Thus, the dissipation in combination with the frequecy gives a whole information on phase transitions during the hydration process [172]

2.15) Rheology

Rheology measurements were performed with a DHR-3 rheometer (TA instruments, New Castle, DE, USA). A cone-plate sensor was used, with a diameter of 40 mm and the cone angle of 2°. The measuring temperature was maintained at 25.0 ± 0.1

°C. Each sample was gently inserted onto the top of the cone-plate. The excess sample squeezed out from the sensor system was gently removed. To allow for the stress relaxation, measurements were carried out after 10 min.

3) Results and discussion

3.1) Synthesis of N,N-dimethyl-2-propylheptan-1-amine oxide (C₁₀DAO-branched)

The synthesis proposed in this work was inspired by that employed for production of the analogue linear surfactant [173] because it can be easily scaled up to large volumes, and was purposely modified in order to avoid expensive reactants and/or procedures, as well as toxic and/or dangerous chemicals. The starting reactant was the alcohol 2-propylheptan-1-ol, which was converted to the corresponding bromide through a S_N2 reaction, thus obtaining 4-bromomethylnonane. Bromide was preferred to other halides, because of its higher selectivity [174]. Differently from previously reported procedures [11], we employed a diluted hydrobromic acid solution, which is handled more easily and safely. With the aim at retaining high reaction conversion, despite the lower HBr concentration, we performed the first step of the reaction at 110 °C under reflux conditions. The same considerations prompted us to use a 40 % dimethylamine in water solution in the second step of reaction and to perform the substitution reaction of bromide at 80 °C under reflux conditions, obtaining *N,N*-dimethyl-2-propylheptan-1-amine [159]. The final oxidation step aimed at producing *N,N*-dimethyl-2-propylheptan-1-amine oxide (C₁₀DAO-branched) was performed with a stoichiometric amount of H_2O_2, with no need of expensive catalysts [175]. Residual water was removed by the formation of a minimum azeotrope with toluene at 30 °C, thus avoiding dehydration in oven at high temperature, conditions in which the amine oxides could degrade to form the alkene [176] or the recrystallization with acetone, which also needs high temperature for complete solvent removal [116].

The bi-dimensional HSQC-DEPT NMR spectrum of the final product was acquired (Figure 9) in order to definitely assess the molecular structure of the synthesized compound, and highlight possible contaminations, thanks to the high resolution of the technique [177]. In the 2D-NMR HSQC-DEPT spectra ^{1}H signals are reported on the abscissa while ^{13}C ones on the ordinate axis.

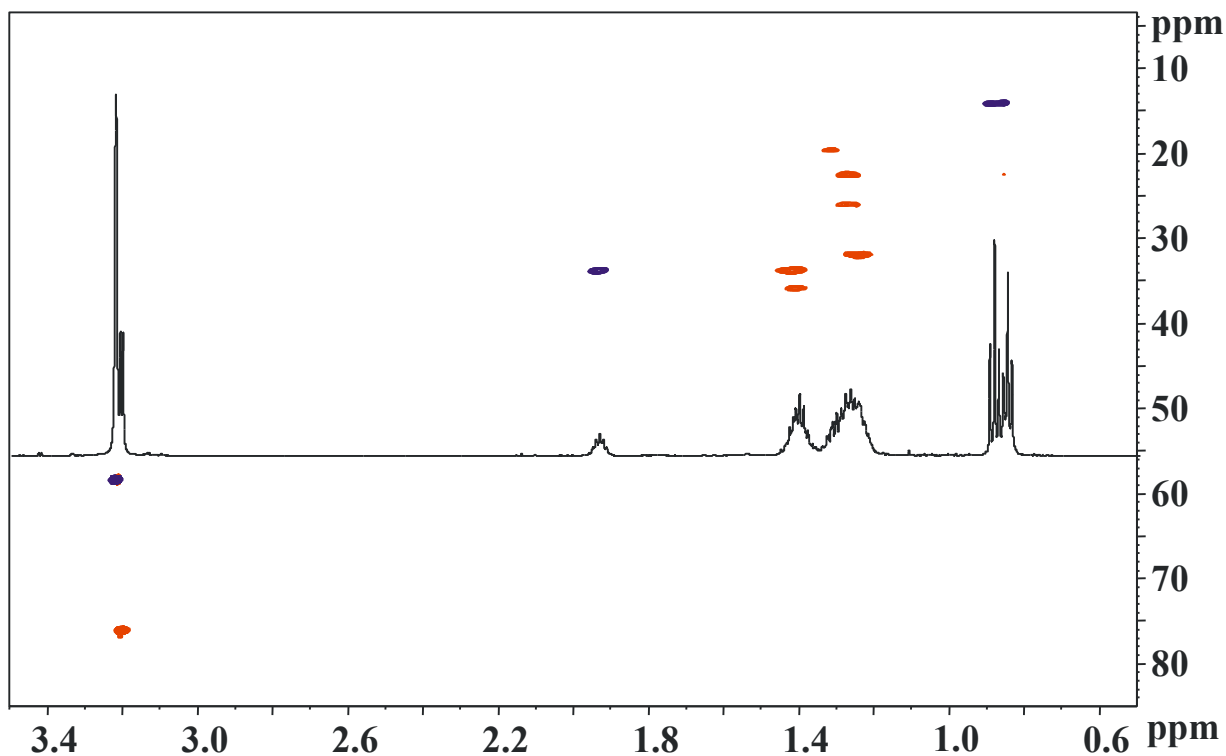Figure 9. 2D NMR HSQC-DEPT spectrum of $C_{10}DAO$ -branched in $CDCl_3$

In the figure, methyl and methine group are reported in blue while ethyl groups are in red. In particular, at δ_C 14.2 the $\underline{C}H_3$ terminal groups generate a single signal because the carbons are equivalents and correspond to two triplets at δ_H 0.84-0.90 on the ^{1}H axis. At δ_C 18.1-35.8 the typical signals of $\underline{C}H_2$ groups of both the main alkyl chain and the branch are visible, corresponding to multiplets at δ_H 1.25-1.42 on the ^{1}H axis. It is possible to highlight the diagnostic signal for $C_{10}DAO$-branched at δ_C 33.8 in the typical region of $\underline{C}H$ in β with respect to the N^+O^- group, corresponding

to a triplet at δ_H 1.94 on the ^{1}H axis; at δ_C 76.1 the typical signal of $\underline{C}$H$_2$ in α with respect to N$^+$O$^-$ is present, corresponding to a doublet at δ_H 3.20; at δ_C 58.7 the typical signal of $\underline{C}$H$_3$ group in α with respect to N$^+$O$^-$ is detected due to the presence of the two equivalent carbons bonded to N$^+$O$^-$, corresponding to six equivalent protons at δ_H 3.22 on the ^{1}H axis. Thus, the 2D NMR HSQC-DEPT confirms the exclusive presence of C$_{10}$DAO-branched in the final product, ruling out the presence of unreacted tertiary amine or undesired by-products.

Finally, both C$_{10}$DAO-branched and C$_{10}$DAO-linear have been analyzed by ESI-MS. MS spectra of the two surfactants are similar (Figure 10), showing a main signal at m/z 202.2, due to the mono-protonated surfactant, and a second one at m/z 403.4, an artefact probably due to non-covalent dimeric species easily formed by amino-oxide surfactants at the liquid-gas interface [178], like the extended one of the aerosol generated in the ESI source.
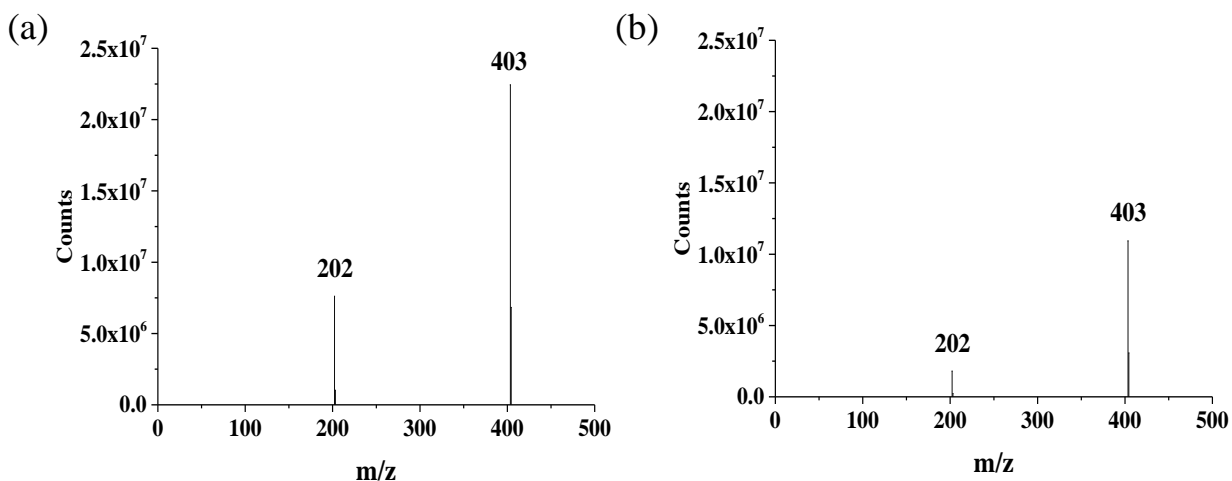
(a)

(b)

Figure 10. ESI-MS spectra of C$_{10}$DAO-branched (A) and C$_{10}$DAO-linear (B)

Remarkably, MS spectra of the newly synthesized C$_{10}$DAO-branched are fully comparable to those of the C$_{10}$DAO-linear, which is a 99% purity grade commercial

product, thus confirming that the final product of our synthesis presents high purity levels.

3.2) Acid-base properties of C₁₀DAO-branched

The determination of acidity constant of $C_{10}DAO$-branched was carried out by potentiometric titration in dilute solutions, in which only monomers are present. The surfactant was considered as a simple base [179] and the logarithm of acidity constant (pK_a) of the monomer was evaluated by:

$$pK_a = pH + \log(\alpha_0/(1-\alpha_0))$$

where α_0 represents the protonated fraction of the surfactant. pK_a values determined in NaCl ionic medium at various concentration (I) are reported in Figure 11. The presence of an inert electrolyte (the ionic medium method) of sufficiently high concentration (0.1 to 3 M) ensures that activity coefficients of the reacting species remain reasonably invariable.
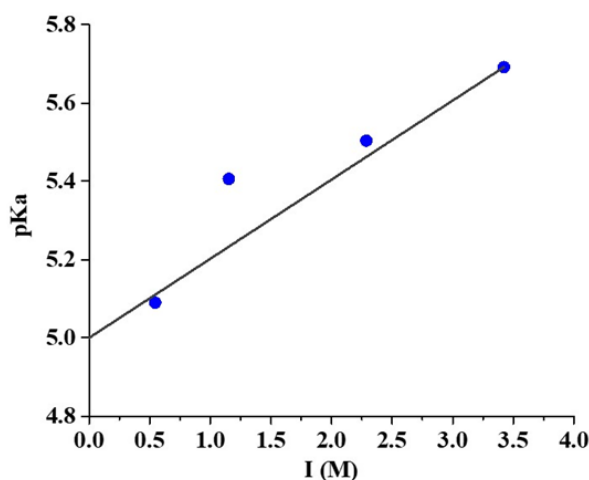

Figure 11. The dependence of pKa of *N,N*-dimethyl-2-propylheptan-1-amine oxide on NaCl

concentration (I).

The constants at known ionic strengths are equally valid as thermodynamic equilibrium constants provided that the background salt solution is defined as the standard state. The extrapolated value at infinite dilution is $pK_a°=5.0±0.1$ that is comparable with $pK_a=4.9±0.1$ reported in the literature for $C_{10}DAO$-linear [122].

3.3) Aggregation behavior of C$_{10}$DAO-branched and C$_{10}$DAO-linear in water

At acid pH amine-oxide surfactants are fully protonated and behave as cationic surfactants, while at basic pH they are non-protonated and behave as non-ionic (zwitterionic, actually) surfactants[100, 122, 180]. We studied the aggregation behavior of $C_{10}DAO$-branched and $C_{10}DAO$-linear at pH=3 and pH=8. The pH value was carefully adjusted by adding proper amounts of either HCl or NaOH, respectively, to the surfactant aqueous solutions. This procedure was preferred to the use of buffers to avoid undesired effects of added salts.

We employed tensiometric titration experiments to determine the CMC. Surface tension measurements for $C_{10}DAO$-branched and $C_{10}DAO$-linear at both considered pH values are reported in Figure 12.
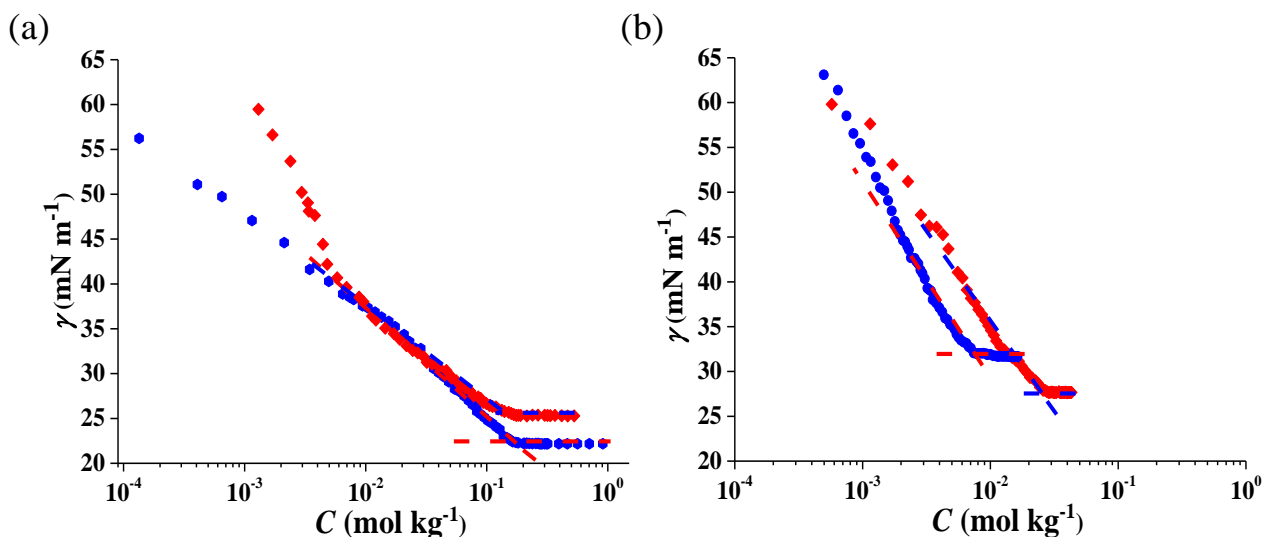
(a)   (b)

Figure 12. Surface tension vs. total surfactant concentration for $C_{10}DAO$ -branched (a) and

$C_{10}DAO$-linear (b) at pH 3 (red diamonds, ◆) and pH 8 (blue circles, ●)

In all cases, γ decreases with increasing surfactant concentration up to a critical value above which its value remains nearly constant. The abrupt slope change corresponds to the micellization onset. CMC values, evaluated as the concentrations corresponding at the intersection between two straight lines fitting the data in the premicellar and micellar concentration range, respectively, are reported in Table 3.

	CMC (mol kg^{-1})		γ_{mic} (mN m^{-1})		A_{min} (Å^2)		R_H (nm)	
	pH 3	pH 8	pH 3	pH 8	pH 3	pH 8	pH 3	pH 8
C$_{10}$DAO-branched	0.17±0.02	0.15±0.02	25.3±0.2	22.2±0.2	180±12	77±3	2.0±0.5 17±1	2.0±0.5
C$_{10}$DAO-linear	0.029±0.005	0.009±0.003	27.7±0.2	31.6±0.3	126±6	32±3	3.0±0.5	2.0±0.5

Table 3. Aggregation properties of C$_{10}$DAO-branched and C$_{10}$DAO-linear at pH 3 and 8

Inspection of table shows that at both pH=3 and pH=8 C$_{10}$DAO-branched is characterized by a higher CMC with respect to C$_{10}$DAO-linear, indicating that tail branching effectively hampers surfactant aggregation. In the case of C$_{10}$DAO-linear when the pH decreases from pH=8 to pH=3, the CMC shows a three-fold increase due to the positively charged hydrophilic head that favors the monomer solubilization in water and, at the same time, disfavors close packing of molecules in micellar aggregates, because of electrostatic repulsion. Interestingly, this effect is much less marked for C$_{10}$DAO-branched, for which the CMC only slightly changes.

The plot of the surface tension versus the logarithm of the surfactant concentration also allows the area per adsorbed surfactant molecule at the solution-air interface (A_{min}) to be calculated. A_{min} was calculated by means of the Gibbs isotherm

$$A_{min} = -\frac{1}{N_A}\left[\frac{1}{nRT}\left(\frac{\partial \gamma}{\partial \ln c}\right)\right]^{-1} \tag{5}$$

where N_A is Avogadro number, R is the gas constant, T is the absolute temperature and $\frac{\partial \gamma}{\partial \ln C}$ is the slope of the γ trend in the premicellar area, close to the CMC. n is the coefficient taking into account the dissociation of ionic surfactants; its value, which is 2 for completely dissociated species, decreases in the presence of added salts, going down to 1 which is the value expected for nonionic surfactants [181]. We used $n=1$ at pH 8 and $n=2$ at pH 3. Indeed, A_{min} values computed for our surfactants using $n=2$ are likely to be upper estimates, considering the high CMC values and the consequent high ionic strength of the solutions due to surfactant monomers.

Resulting values are reported in Table 3, in which the constant γ values observed above the CMC in all the considered systems, γ_{mic}, are also collected. It clearly emerges that the branched surfactant occupies a larger area per molecule compared to the linear analogue, because of the steric hindrance between the bulkier hydrophobic moieties and their lower tendency to cooperatively align perpendicular to the air/water interface. As reported for other branched surfactants, this result in a more disordered monolayer [182]. $C_{10}DAO$-branched also presents a lower γ_{mic}, since the higher CMC increases adsorption at the air/water interface. These results are in good agreement with those reported in the literature for branched nonionic ethoxylated surfactants [22].

Our data show that for both surfactants A_{min} is sensitive to the pH value, in that it increases at acidic pH, while the opposite trend is observed for γ_{mic}. These evidences indicate that the surfactants form a more compact monolayer in the zwitterionic form. The percent variation is much lower for the branched surfactant than for the

linear isomer. Moreover, similarly to what observed for the CMC and A_{min}, the γ_{mic} variations are much less evident for $C_{10}DAO$-branched than for $C_{10}DAO$-linear.

$C_{10}DAO$-branched and $C_{10}DAO$-linear samples with surfactant concentrations ten times above the CMC value were monitored at room temperature by means of DLS (Figure 13).
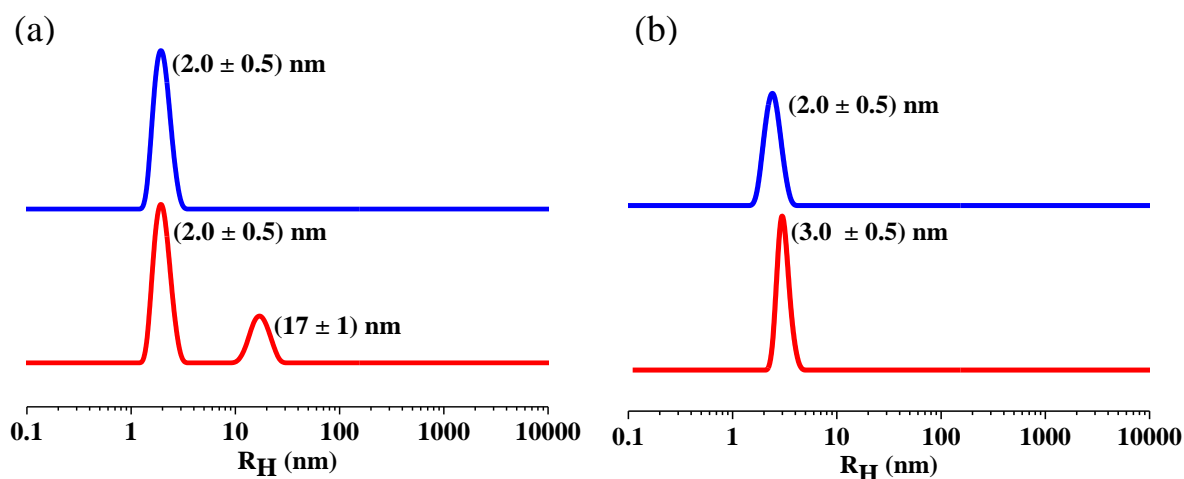

Figure 13. Intensity weighed hydrodynamic radius distributions of $C_{10}DAO$-branched (a) and $C_{10}DAO$-linear (b) at pH 3 (in red) and pH 8 (in blue) at surfactant concentration 10 times the CMC.

DLS analysis shows that at pH=3, $C_{10}DAO$-branched present two populations centered at R_H =2 and 17 nm, possibly related to the co-existence of small micelles with larger aggregates. In the case of $C_{10}DAO$-linear there is one micelle population centered at R_H = 2 nm. At pH=8, only one population at 3 nm is observed for $C_{10}DAO$-branched, while no significant difference is observed for $C_{10}DAO$-linear with respect to pH=3. Thus, chain branching results in the tendency to form larger aggregates, the effect being more evident in acidic pH.

3.4) Foamability and foam stability of $C_{10}DAO$-branched and $C_{10}DAO$-linear aqueous solution

The foam volumes obtained from the $C_{10}DAO$-branched and, as a comparison, from $C_{10}DAO$-linear aqueous solution at pH=3 and pH=8 are shown in Fig. 6. At both pH values $C_{10}DAO$-branched produces a higher foam volume than the linear analogue. This results are in contrast with those recently reported by Wang et al. concerning anionic sulfonate surfactants [183], thus highlighting that the effect of tail branches on surfactant foamability is hardly predictable from the molecular structure, being determined by a complex interplay of intermolecular interactions. On the other hand, from a phenomenological viewpoint, a lower surface tension is expected to increase the foamability of a solution from the perspective of surface energy [184]. This is fully confirmed by our data: the increased foamability $C_{10}DAO$-branched positively correlates with its higher effectiveness in reducing the surface tension (see the γ_{mic} values). This holds even when data collected at different pH are compared: $C_{10}DAO$-branched foamability significantly increases at basic pH, i.e., in the conditions in which the lowest γ_{mic} has been observed.

Inspection of Figure 14 shows that, while the foam formed by the zwitterionic form of the branched surfactant occupies a larger volume, its stability is poorer.
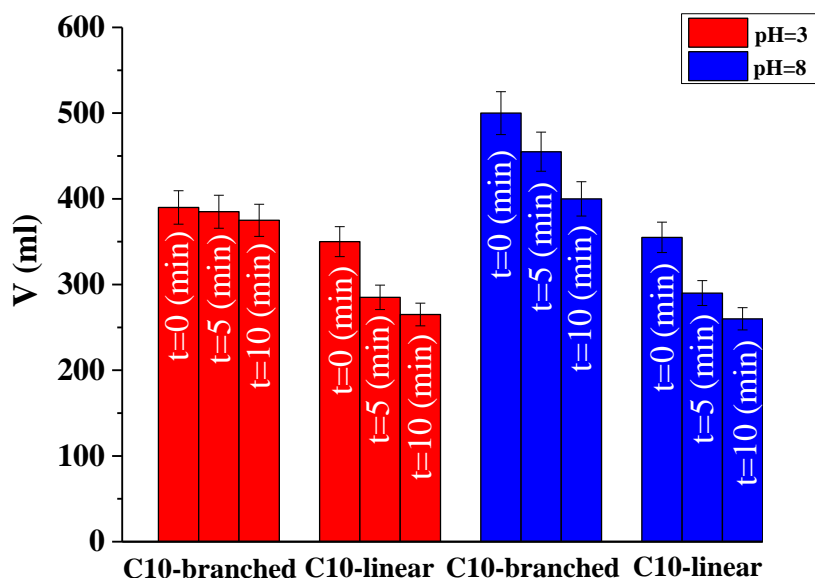
Figure 14. Foaming properties of C_{10}DAO-branched and C_{10}DAO-linear at pH 3 and 8.

This is in line with the results reported for other branched surfactants [184], and is interpreted in terms of weaker intermolecular cohesive forces at the air/water interface among branched tails with respect to linear ones. Interestingly, data collected at pH=3 show longer foam stability for the branched surfactant, which suggests a synergy between hydrophobic and electrostatic interactions in stabilizing the surfactant monolayer.

3.5) Phase behavior: POM and SAXS

The phase behaviour C_{10}DAO-branched and C_{10}DAO-linear in aqueous mixtures was initially identified by visual inspection, POM, and SAXS, across the entire composition range. Particularly, the phase behaviour of C_{10}DAO-branched was investigated in a temperature range between 25 and 70 °C, while for the linear isomer the investigation was extended up to 110 °C. Above these thresholds both surfactants are chemically unstable, a typical feature of amine oxide surfactants. Thus, C_{10}DAO-branched degrades at a temperature lower than C_{10}DAO-linear [176]. The branching in position 2 promotes the thermal decomposition since, upon the β−elimination of *N,N*-dimethylhydroxylamine, a disubstituted alkene is obtained (Scheme S_2 Figure

^{1}H NMR S$_2$), which is more stable than the mono-substituted one obtained from the linear surfactant.

The phase diagram of the (C$_{10}$DAO-branched)-water binary system is shown in Figure 15.
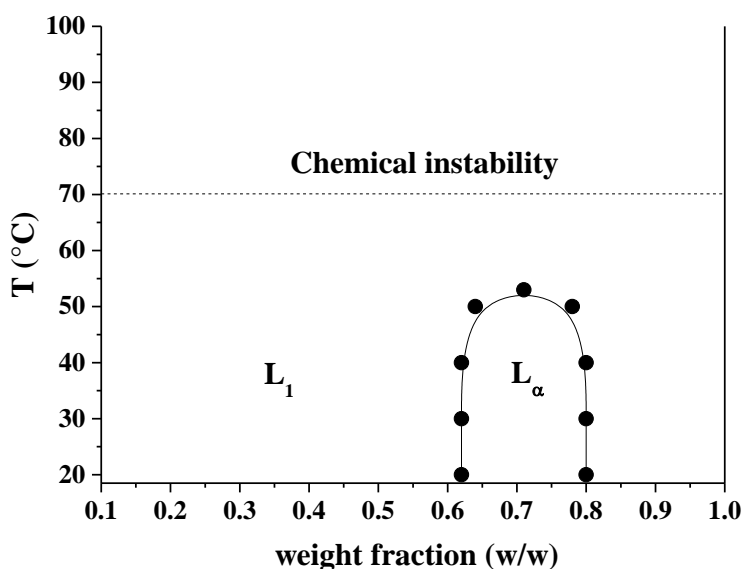

Figure 15. Phase diagram (weight fraction versus temperature) of C$_{10}$DAO-branched/water system. The following notation is used for the various region: L$_1$=isotropic phase, L$_\alpha$=lamellar LLC phase.

Samples prepared in the w_s range 0.62-0.80 at 25 °C were found very viscous (as judged by naked eyes) and birefringent (when seen through polarized glasses). Moreover, under the polarized optical microscope, these samples showed the texture dominated by Maltese crosses characteristic of a lamellar LLC phase (L$_\alpha$, Figure 16 a). The L$_\alpha$ arrangement of the surfactant molecules was found to be stable below 53 °C. At C$_{10}$DAO-branched weight percent lower than 0.62 and higher than 0.80, and at a temperature higher than 53 °C, isotropic mixtures formed, which easily flowed under their own weight.
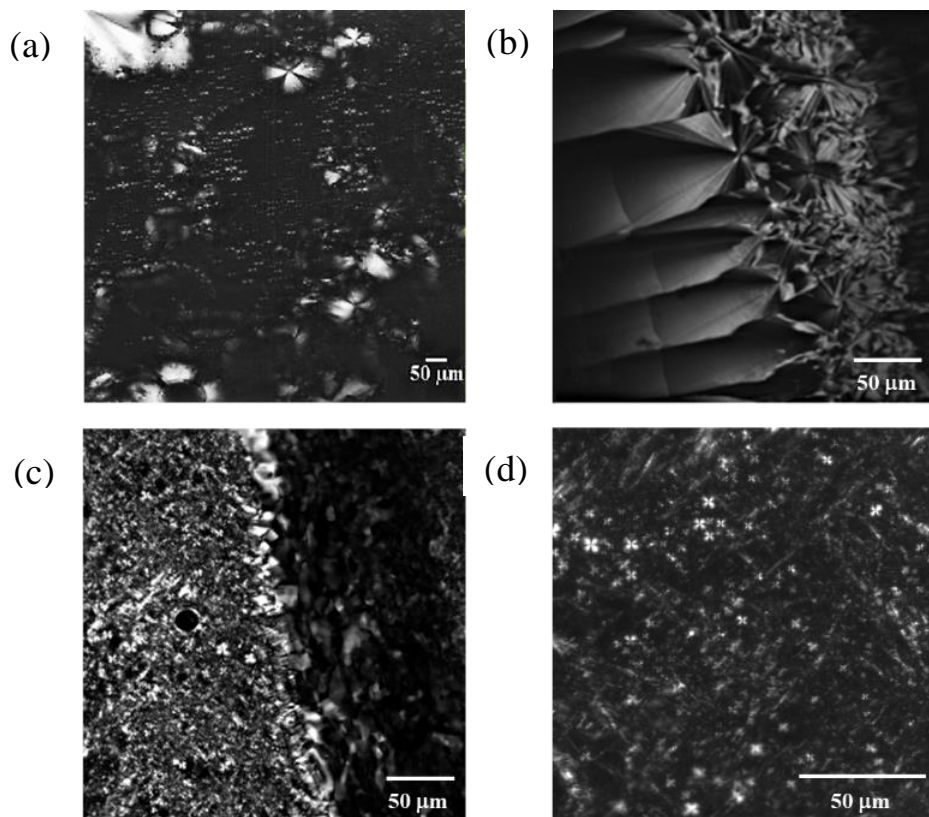
Figure 16. Optical microscopy images corresponding to the systems: (a) L_α lamellar phase of $C_{10}DAO$-branched at w_s=0.70; (b) H_1 hexagonal phase (fan-like texture) of $C_{10}DAO$-linear at w_s=0.40; (c) H_1+L_α hexagonal and lamellar co-exsistence of $C_{10}DAO$-linear at w_s=0.51; (d) L_α Lamellar phase of $C_{10}DAO$-linear at w_s=0.70.

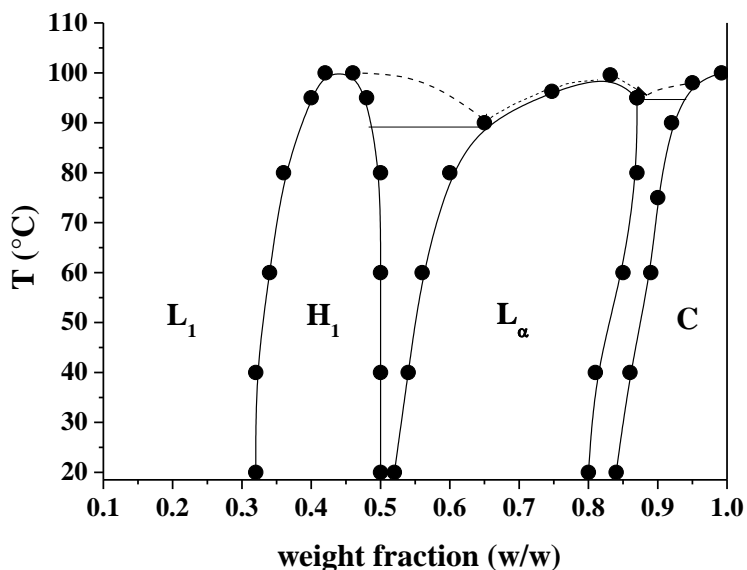The phase diagram of the ($C_{10}DAO$-linear)-water binary system is shown in Figure 17.

Figure 17. Phase diagram (weight fraction versus temperature) of C_{10}DAO-linear/water system. The following notation is used for the various region: L_1=isotropic phase, H_1=hexagonal LLC phase, L_α=lamellar LLC phase, C=crystalline phase.

In this case, four different phases were observed with increasing surfactant concentration. At low surfactant concentration, a L_1 phase (isotropic water-rich solution) is found. Above w_s=0.32, at 25 °C, samples were found viscous and birefringent. Particularly, in the composition range from w_s=0.32 to w_s=0.50 POM analysis revealed the typical fan-like texture of a direct hexagonal LLC phase (H_1, Figure 15 b). Such attribution was definitely confirmed by SAXS experiments (see below). By increasing the surfactant concentration, Maltese crosses start to appear in the POM micrographs. They coexist with the fan-like texture up to w_s=0.52, highlighting the existence of a narrow H_1+L_α biphasic region. Above this concentration threshold, only Maltese crosses were detectable. The L_α is stable in the w_s range 0.52-0.80. Upon further surfactant addition, hydrated solid crystals (C) started to form. A L_α+C biphasic region was initially found, which above w_s=0.84

turned to a C phase. The stability domains of all the LLC and solid phases are scarcely affected by temperature, being the phase boundaries almost vertical. Only at high temperature, above 100 °C, all of them melt to an isotropic liquid phase.

The slope of the phase boundaries depends on the driving forces of the phase transition: a negative slope indicates that the transition is driven by entropy, while a positive slope indicates that the driving force is of enthalpic nature [126]. Vertical phase boundaries mean that the driving forces are close to zero. The last is the case of the transition from L_1 to H_1 in the (C_{10}DAO-linear)-water diagram. In this transition, only a small curvature changes in going from finite C_{10}DAO-linear micelles to the infinite cylinders of the hexagonal phase occurs, resulting in a small increase of the entropy due to confinement of the hydrocarbon tails in a less restricted environment. This small entropy increase is balanced by the reduction of motional freedom of the cylinders in the hexagonal array with respect to freely diffusing micelles. From the enthalpic viewpoint, it is to be considered that many properties of the cylinders in the hexagonal and the micellar phases are very similar. On the other hand, the positive slope of the phase boundary between the L_α and C stability domains highlights that the dehydration-induced transition from C_{10}DAO-linear lamellae to the solid phase is driven by enthalpy, being crystallization exothermic. This evidences are similar to those found for the longer-chain alkyl amine oxide surfactant C_{12}DAO [126, 185].

Inspection of the (C_{10}DAO-linear)-water phase diagram reveals that the transition from H_1 to L_α also presents an almost vertical phase boundary. In the case of C_{12}DAO the boundaries between the stability domains of different LLC phases present a negative slope, indicating that the transitions from structures with higher curvature (such as hexagonally arrayed cylinders) to the phases with lower curvature (e.g., stacked lamellae) are driven by entropy, since the number of microstates available for the tails in a less confined structure increases. The almost vertical boundaries in the (C_{10}DAO-linear)-water phase diagram points to a reduction of this effect, which could be connected to the minor mobility freedom constraints in the aggregates

formed by the shorter surfactant. The reduction of the entropic driving force could be also the reason for the absence of the cubic phase interposing between the H_1 and the L_α stability domains, which is found for $C_{12}DAO$ [126, 185] and is not detected for the shorter analogue.

Some structural details of the LLC phases formed by $C_{10}DAO$-branched and $C_{10}DAO$-linear in aqueous mixtures were obtained by a SAXS investigation. For some SAXS diffractogram of the ($C_{10}DAO$-branched)-water binary sample acquired at 25 °C is characterized by a single, strong reflection at q=0.18 Å^{-1} (Figure 18 a).

Taking into account results from POM analysis, and recalling here that for diluted samples second (or higher) order Bragg peak of the L_α phase is not always detectable [185], this reflection without any doubt represents the first order Bragg peak of the L_α phase. Under this assumption, the diffractogram allows an estimation of the structural parameters, i.e. the lattice parameter (a_{lam}), the water layer thickness (d_W), and the bilayer thickness (d_L). The values of these parameters, estimated at various temperatures, are collected in Table 4. Upon increasing the temperature, the Bragg peak slightly shifts to high q values (see Figure 18), indicating a decrease of the lattice parameter, probably due to a dehydration of the surfactant headgroup. According to equations reported in the SAXS section, also d_L and d_W follow the same trend. As can be seen in Figure 18 a, the second order Bragg peak appears at 40 °C at the q value expected for a lamellar arrangement, corroborating the correct attribution of the single reflection observed at lower temperatures.
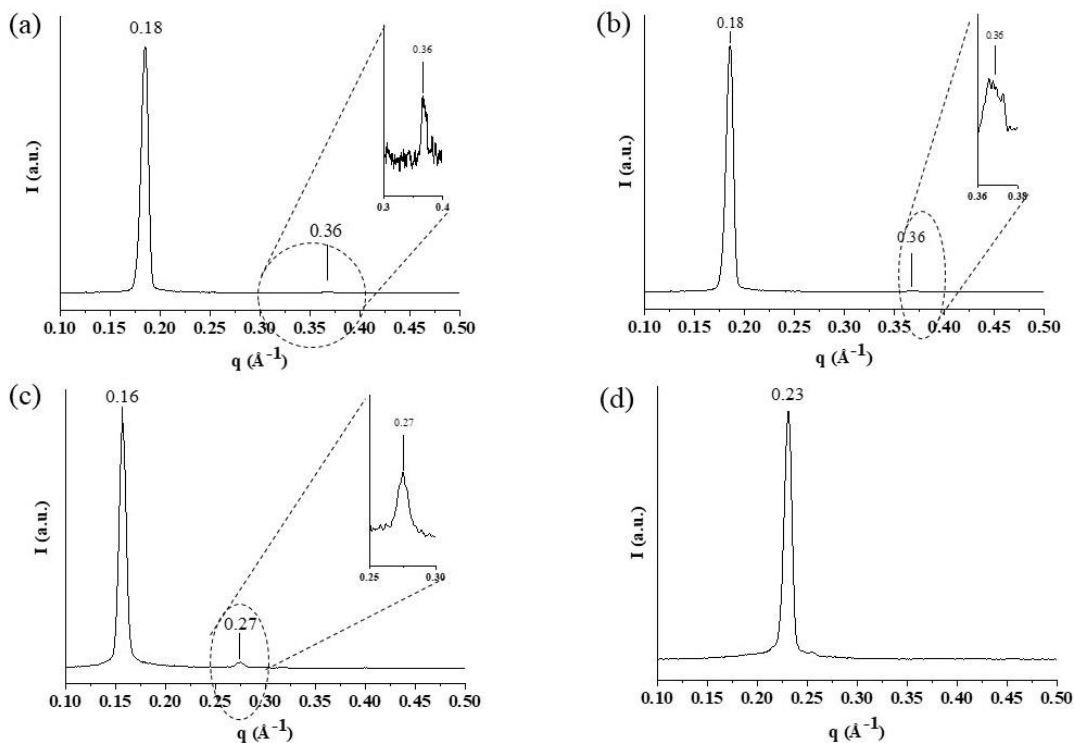
Figure 18. SAXS diffractogram of: (a) $C_{10}DAO$-branched/water w_s=0.70 at 40 °C and (c); $C_{10}DAO$-branched/water w_s=0.67 (b), $C_{10}DAO$-linear/water w_s=0.40 at 25 °C; $C_{10}DAO$-linear/water w_s=0.75 at 25 °C.

The SAXS diffractograms obtained for a more concentrated ($C_{10}DAO$-branched)-water binary sample (w_s=0.67) show a similar behavior (Figure 18 a): even in this case a single peak is observed at low temperature, the second order Bragg peak becoming detectable only at 35 °C (Figure 18 b). Structural parameters of this lamellar sample are reported in Table 1, and show an increment of d_L and a reduction of d_W, a reflection of the higher surfactant concentration in the mixture.

The SAXS analysis was also performed on the ($C_{10}DAO$-linear)-water binary samples at w_s equal to 0.40 and 0.75. The diffractogram obtained for the former sample at 25 °C, reported in Figure 18 c, shows two Bragg peaks in the ratio 1:√3 corresponding to the first (hk=10) and second (hk=11) order reflections. From these data a lattice parameter a_{hex}=46.3 Å was calculated.

The latter sample is in the lamellar phase. Similarly, to what observed for the lamellar (C_{10}DAO-branched)-water mixtures, a single peak can be observed at 25 °C. Analysis of the diffrattogram reveals that binary C_{10}DAO-linear lamellae are characterized by a lattice parameter smaller (Table 4) than that found for C_{10}DAO-branched.

C_{10}DAO-branched ($w_s = 0.67$)						
T (°C)	25	30	35	40	45	50
a (Å)	36.4	35.9	34.7	33.7	---	---
d_W (Å)	12.0	11.9	11.5	11.1	---	---
d_L(Å)	24.4	24.1	23.3	22.6	---	---
C_{10}DAO-branched ($w_s = 0.78$)						
T (°C)	25	30	35	40	45	50
a (Å)	35.9	35.7	34.0	---	---	---
d_W (Å)	7.9	7.9	7.5	---	---	---
d_L(Å)	28.0	27.9	26.5	---	---	---
C_{10}DAO-linear ($w_s = 0.75$)						
T (°C)	25	30	35	40	45	50
a (Å)	27.2	27.1	26.9	26.7	26.6	26.7
d_W (Å)	6.5	6.5	6.5	6.4	6.4	6.4
d_L(Å)	20.7	20.6	20.4	20.3	20.2	20.3

Table 4. Structural parameters at different temperature and w_s of C_{10}DAO-branched and C_{10}DAO-linear.

In addition, apart from a tiny shift of the Bragg peak to higher q values, such a lamellar phase remains nearly unaltered up to 35 °C (Figure 19), the highest temperature investigated by SAXS, indicating that the L_α phase obtained using the linear surfactant is more stable than the same LLC phase obtained using its branched isomer.
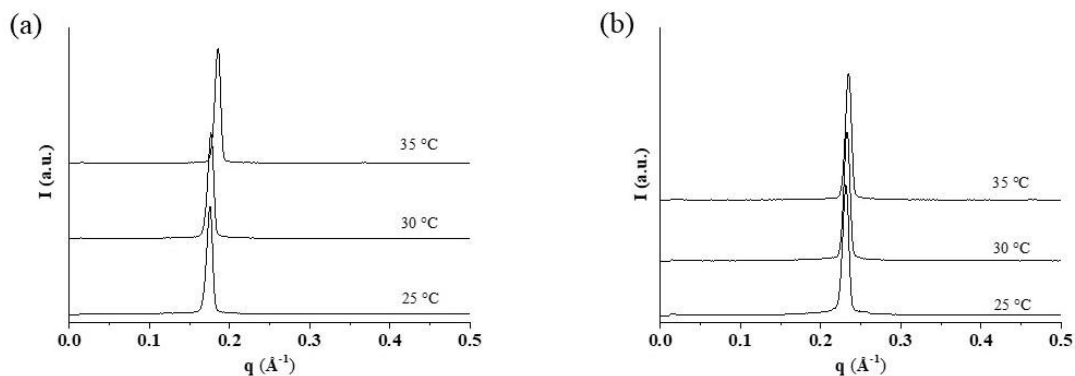
Figure 19. SAXS diffractogram versus T: (a) $C_{10}DAO$-branched $w_s=0.67$; (b) $C_{10}DAO$-branched $w_s=0.78$.

3.6) Phase behavior: validation of the HS QCM-D method

The determination of the phase behavior in aqueous mixtures is fundamental for the comprehension and, potentially, for the prediction of the functional properties of new surfactants. However, the experimental construction of phase diagrams is difficult, time-consuming, and costly. For these reasons new approaches, fast and reliable at the same time, are of great interest in formulation science and technology [186, 187]. Recently, HS QCM-D was shown to be a fast and easy technique able to detect surfactant or lipid phase transitions induced by hydration using a very low amount of substance [155, 188].

In the present study, HS QCM-D was used as an alternative method to investigate the phase behavior of both $C_{10}DAO$-branched and $C_{10}DAO$-linear in water. The measurements were performed as a function of time during continuous hydration at 25 °C (Figure S_4 a-b). The prominent changes in resonance frequency $\Delta f/n$ and dissipation $\Delta D/n$ were related to hydration-induced transitions between different LLC phases of the ($C_{10}DAO$-branched)-water and ($C_{10}DAO$-linear)-water binary systems. In general, experiments started by measuring the uncoated sensor in a dry N_2 atmosphere. Afterwards, the sensor was spin-coated with 20 μL of an aqueous surfactant solution with $w_s=0.05$, at rps=32 for 30 s. The coated sensor was then dried

in the oven for 10 min at 50 °C under a flow of N_2 gas, until a stable baseline of frequency was obtained. The film thickness was determined by comparing data obtained for uncoated and coated sensor, and was found to increase with the number of spin-coating depositions (Figure S_6). For the HS QCM-D measurements, the surfactant solution was deposited ten times, leading to a film thickness of 180 and 160 nm for $C_{10}DAO$-branched and $C_{10}DAO$-linear, respectively. Finally, the humidity scanning experiment was initiated with the same procedure used by Björklund and Kocherbitov [155].

In the QCM-D humidity module used for the measurements, the measurement chamber in which the sensor is located is separated from a flowing LiCl aqueous solution by a Gore® membrane. The membrane is permeable only to water vapor, which diffuses from the solution into the gas phase above the sensor and thus regulates the *RH* (Relative Humidity) above the film coated on the sensor. In equilibrium conditions, which are easily reached because of the small amount of sample used, the water chemical potential in the hydrated surfactant layers' equals that in the gas phase above the sensor, which in turn, equals that in the LiCl solution. Thus, the water activity in the LiCl solution (a_w) is directly proportional to *RH* (a_w=*RH*/100). The HS QCM-D experiment was carried out under controlled dilution of a saturated LiCl solution (a_w=0.12 [188]) to continuously regulate *RH* in the QCM-D chamber.

The $\Delta f/n$ and $\Delta D/n$ values for the different overtones were measured as a function of time during dilution of the LiCl solution flowing in the humidity module (Figure S_4). From the knowledge of the dilution ramp, time was converted to a_w [26]. Variations of $\Delta f/n$ and $\Delta D/n$ curve profiles of the initially dry $C_{10}DAO$-branched and $C_{10}DAO$-linear films were provoked by the continuous increase in *RH*, leading to the LLC phase transitions detected.

Figure 20 reports (a) $\Delta f/n$ and (b) $\Delta D/n$ as a function of a_w for the binary system ($C_{10}DAO$-branched)-water.
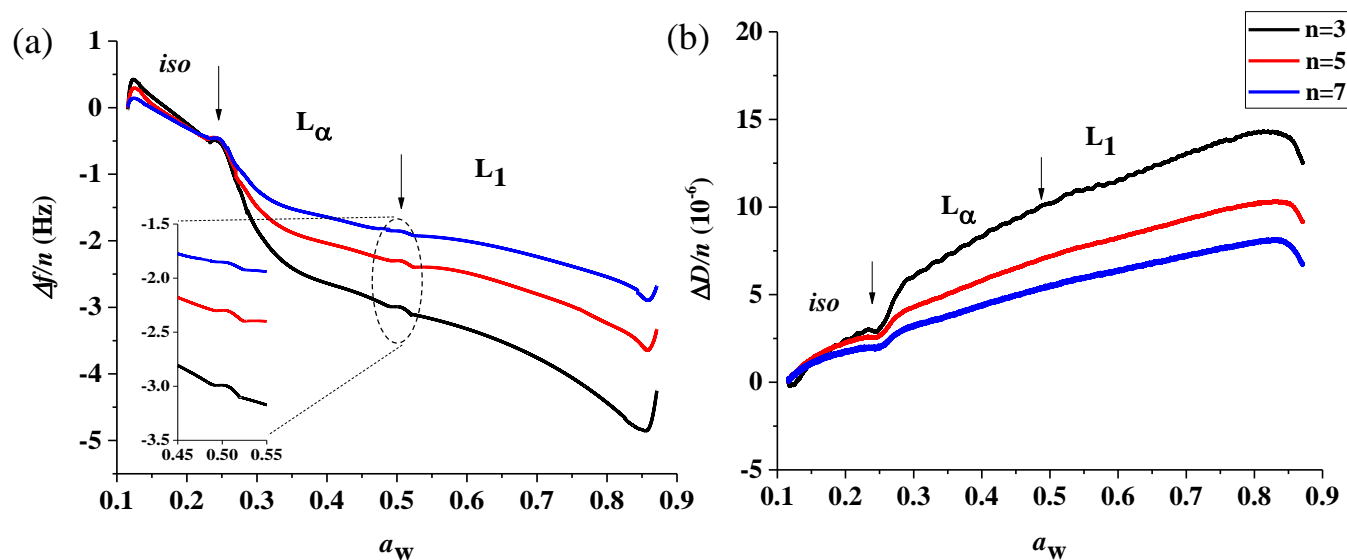
Figure 20. Frequency shift $\Delta f/n$ and dissipation $\Delta D/n$ as a function of water activity a_w (a and b) for C$_{10}$DAO-branched. Arrows indicate water activity levels where phase transition in $\Delta f/n$ and $\Delta D/n$ was detected as a result of hydration-induced phase transitions. Abbreviations: L$_1$=micellar phase; L$_\alpha$=lamellar phase.

It has to be stressed that, differently from all the other data reported in the literature, in this case measurements starts not from a solid but from a dry viscous liquid. With increasing a_w, $\Delta f/n$ smoothly decreases, indicating that the surfactant film absorbs water. As the water activity level reaches about $a_w \approx 0.25$, a phase transition from the viscous liquid to a LLC phase was clearly seen as an abrupt slope change. Above this a_w value, $\Delta f/n$ steeply decreases. From the comparison with the POM and SAXS data, these HS QCM-D results can be confidently interpreted in terms of the system transition to a L$_\alpha$ arrangement. Interestingly, in the viscous liquid phase the normalized frequency shifts are independent of overtone number, as predicted by the Sauerbrey model, while their absolute values decrease with increasing n in the lamellar phase. This behavior has been already reported for LLC phases and shows that they are plastic materials characterized by extensive energy dissipation. Consistently, the transition is also detected in the $\Delta D/n$ trend, which shows an initial increment indicating that the viscous liquid film becomes less rigid with increasing

75

the water content. A further increase is observed upon the transition to the L_α phase, deriving from the high relative mobility and deformability of locally stacked lamellae. Above $a_w \approx 0.25$, $\Delta D/n$ also decrease with increasing n, consistent with the $\Delta f/n$ results.

No evident discontinuity in both the $\Delta f/n$ and $\Delta D/n$ trends was found at higher a_w values, where the transition from the transition from L_α to the surfactant-water isotropic mixture was found to occur by POM data. A closer scrutiny of the curves reveals only a small peak at $a_w \approx 0.5$ (see the insets in Figure 19). Reasons for the poorly marked transition can be proposed to reside in the disordered and defective organization of the $C_{10}DAO$-branched molecules in the lamellae, which does not change much as micelles (see below) are formed.

Also the phase behavior of the ($C_{10}DAO$-linear)-water system was investigated by HS QCM-D, using the same procedure adopted for $C_{10}DAO$-branched. Results are reported in Figure 21.

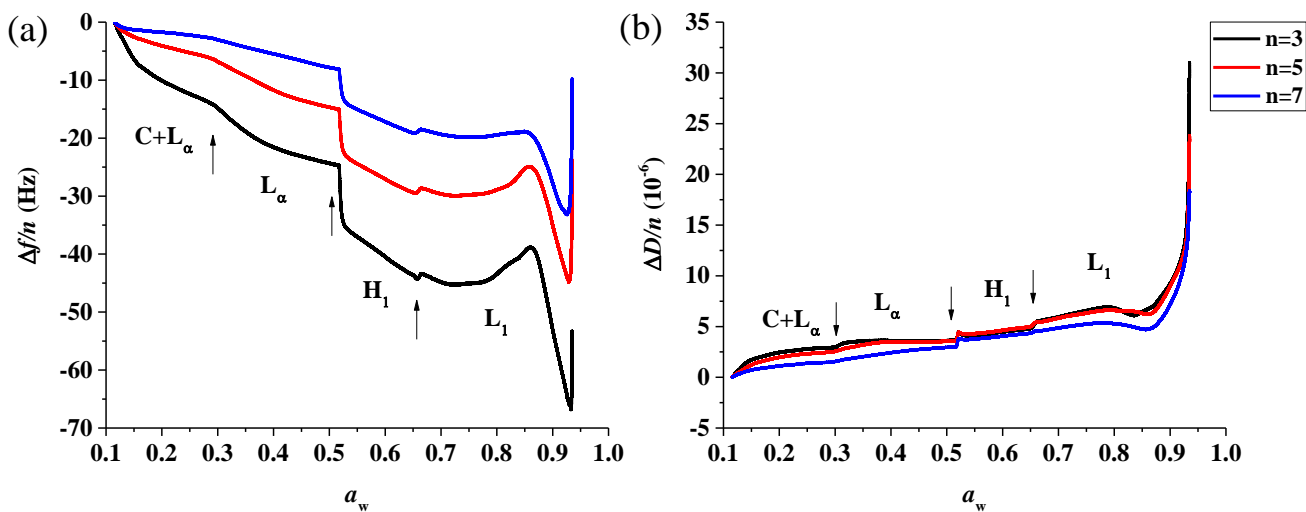
Figure 21. Frequency shift $\Delta f/n$ and dissipation $\Delta D/n$ as a function of water activity a_w (a and b) for $C_{10}DAO$-linear. Arrows indicate water activity levels where phase transition in $\Delta f/n$ and $\Delta D/n$ was detected as a result of hydration-induced phase transitions. Abbreviations: L_1=micellar phase; H_1=hexagonal phase; L_α=lamellar phase; L_α+C=lamellar and crystal phase; C=crystal phase.

The measurements start from a_w=0.12 which is the lowest value achievable using the LiCl solution. With increasing a_w, $\Delta f/n$ decreases, which is not expected for solid surfactants. This evidence suggests that measurements start from a sample in which C_{10}DAO-linear crystals already co-exist with a L_α phase. The presence of lamellae in the hydrated surfactant film is confirmed by the evidence that $\Delta f/n$ absolute value decreases with increasing n. A clear slope change is observed at $a_w \approx 0.3$; on the basis of the POM and SAXS results, this can be identified as the threshold above which only lamellae exist. At $a_w \approx 0.3$ an abrupt $\Delta f/n$ drop is observed, which is interpreted as the transition from the L_α to the H_1 phase. No evidence of cubic phase, whose stability region is generally delimited by evident peaks, is observed between the L_α to the H_1 phases, confirming the POM evidences. A small but well-detectable peak at $a_w \approx 0.65$ marks the transition from the H_1 phase to the isotropic L_1 mixture. The L_1 phase is expected to persist up to the highest a_w value examined; the maximum observed in the $\Delta f/n$ trend at $a_w \approx 0.65$, consequently, has not to be ascribed to a phase transition but rather could hypothetically derive from a morphological change of the surfactant aggregates in solution, or to a change in the inter-aggregate interactions. Further investigation is definitely needed to clarify this point.

The $\Delta D/n$ trends, show in Figure 20 b, show the same transitions observed in the $\Delta f/n$ graph. In the stability domain of the H_1 phase, $\Delta D/n$ does not depend on n. This indicates the hexagonal arrangement of surfactant cylinders to be more rigid and less able to dissipate energy than stacked lamellae.

Overall, the phase behaviors of C_{10}DAO-branched and C_{10}DAO-linear observed using POM and SAXS on the one hand and HS QCM-D on the other are remarkably consistent. This supports HS QCM-D as a fast method to obtain reliable information on surfactant phase diagrams. It clearly detects transitions between solid and a LLC phase as well as between different LLC phases. Transitions to isotropic mixtures are also detectable, even though less evident. As possible drawback, one could argue that HS QCM-D is not able to discriminate between different LLC phases, whose structure has to be identified by different techniques. For this reason, it can be

proposed a method for a fast screening of how the phase behavior of a certain surfactant, already known, is affected by the presence of other components (e.g., co-surfactants, polymers, additives). Under this viewpoint, HS QCM-D is a precious tool in surfactant formulation technology.

3.7) Isotropic surfactant aqueous solutions: SANS results.

**C$_{10}$DAO-linear micelles.** SANS curve profile reported in the figure 21 b clearly shows the presence of the peak in the $0.102<q<0.154$ due to electrostatic interparticle interaction. SANS from C$_{10}$DAO micelles in D$_2$O (w_s=0.15) was modeled with ellipsoid with mild polydispersity, following the with factor structure of Hayter and Penfold. The ellipsoid equation used to fit the experimental data is reported in supplementary material EqS$_1$ The remainder of the C$_{10}$H$_{21}$ tails and their terminal-CH$_3$ groups are placed inside of the ellipsoid. Fitting parameters, volume fraction, the charge aggregates. The radii of the ellipsoidal is R_a and R_b, typical of a prolate ellipsoid in Table 5 are reported. C$_{10}$DAO headgroup volume was taken from the partial-specific volume measurements of Benjamin [190] and was confirmed by reflectivity data at an air-water interface [191] Fitting the micellar SANS data as either monodisperse or polydisperse spheres would require core radii greater than the fully extended length of a surfactant tail, implying either a physically unreasonable "hole" at the center of the micelle, or that possibly wet headgroups are pulled into the micelle interior. In this latter case a spherical model simply does not fit.

C$_{10}$DAO-branched. SANS from C$_{10}$DAO micelles in D$_2$O (w_s=0.15) was modeled assuming monodisperse, hard sphere micelles following the methodology of Hayter and Penfold and reporte din the figure 22 a. Sphere micelle equation used to fit the experimental data is reported in the supplementary material EqS$_2$. SANS profile does not show the presence of a peak due to electrostatic interparticle interaction but with the Haythter and Penfold strcture factor the fitting was enhanced, this means that a

small but not high charge was considered. The contribution of a factor structure was taken into account, in addition to the form factor, to fit the data. The ellipsoidal model has been initially, tried to fit the experimental data unfortunately without success. Then, the experimental data has been fitted with the hard sphere model with Hayter and Penfold structure factor and the experimental data were perfectly fitted.

For what concern the $C_{10}DAO$-branched (w_s=0.40) was modeled assuming a mild polydisperse cylinder micelles with the factor structure of Hayter and Penfold and in the figure 22 c is reported. The equation used to fit the experimental data in the supplementary materiali s reported EqS_3. All features in Table 5 are reported. Particularly the SANS curve profile shows a presences of the peak due to an electrostatic interparticle interactions.

In the case of $C_{10}DAO$-branched a morphology transition from spherical to cylindrical micelles between $0.15<w_s<0.40$ was detected. Particularly, the cylinder micelles are not organized into a supramolecular structure to generate hexagonal phases as is possible to see from the rheology data (see figures below).
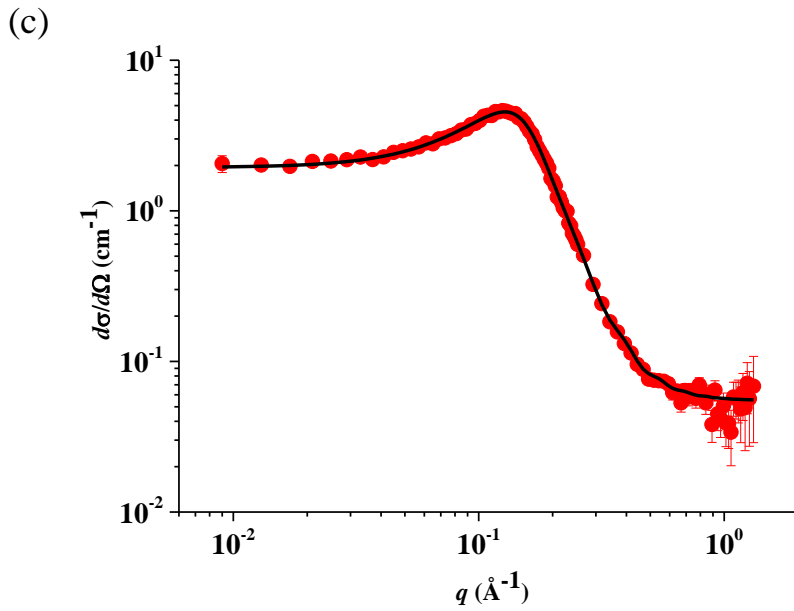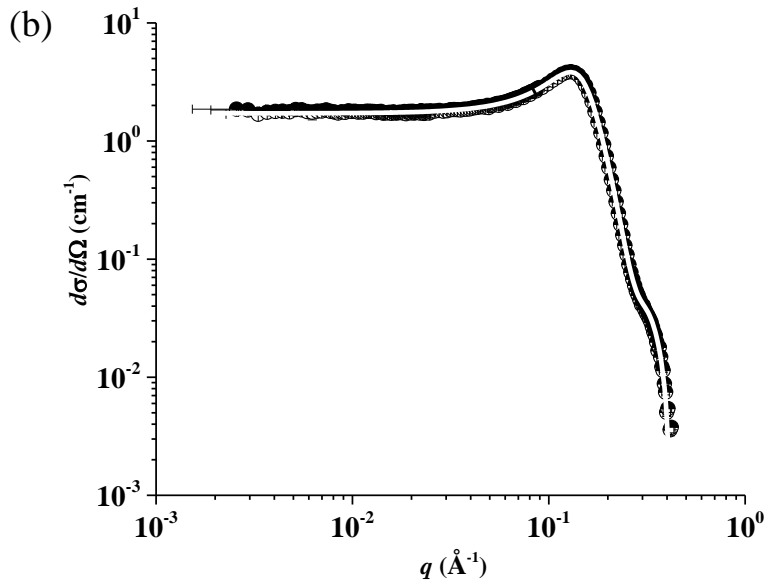
(b)

(c)
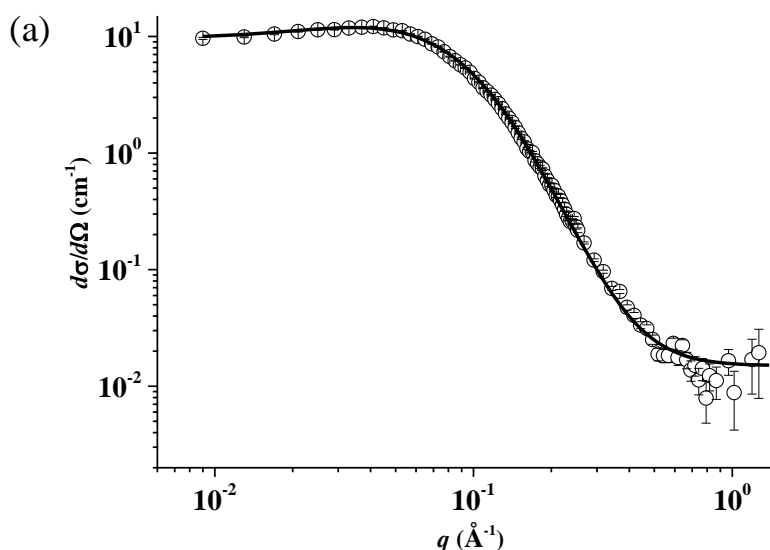
Figure 22. SANS curve profiles for (a) $C_{10}DAO$-branched/D_2O and (b) $C_{10}DAO$-linear/D_2O w_s=0.15 and $C_{10}DAO$-branched/D_2O w_s=0.40.

SANS parameters								
	SLDx10^6 [Å^2]	**Charge [e]**	**R[Å]**	**Vol [Å^3]**	**Radius_a**	**Radius_b**	**N_a**	**Length [Å]**
C$_{10}$-branched w_s**=0.15**	-0.145	1.39	13	416.49	/	/	22	/
C$_{10}$-linear w_s**=0.15**	-0. 155	9.27	/	389.49	13.85	20.29	61	/
C$_{10}$-branched w_s **=0.40**	-0.145	6.89	13	416.49	/	/	51	40

Table 5. SANS parameters for C$_{10}$DAO-branched/D$_2$O and C$_{10}$DAO-linear/D$_2$O systems.

From the aggregation numbers for C$_{10}$DAO-branched and C$_{10}$DAO-linear even at different concentrations it is clear that the branching generates the formation of more thick micelles with respect to the linear surfactant

3.8) Rheological behavior investigation

The viscoelastic properties of C$_{10}$DAO-branched and C$_{10}$DAO-linear aqueous mixtures were investigated by rheological measurements [192].
The viscosities of (C$_{10}$DAO-branched)-water samples with different surfactant content are reported in Figure 23 as a function of the shear rate at 25 °C.
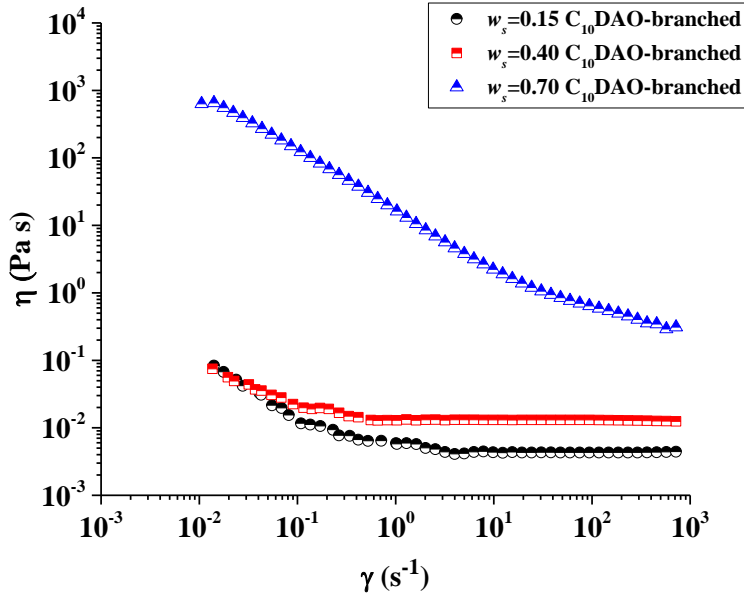
Figure 23. Viscosity versus shear rate diagram for the $C_{10}DAO$-branched/water system.

Viscosities of samples with w_s equal to 0.15 and 0.40 were very low and only weakly dependent on the shear rate. This behavior is expected for these L_1 samples, which contain spherical or cylindrical micelles, as demonstrated by SANS experiments. Viscosity increases with increasing surfactant concentration but remains, overall, quite low. The L_α sample with w_s=0.70 presents a much higher viscosity over the whole investigated shear rate range, and behaves as a shear-thinning fluid, whose viscosity decreases with increasing the shear rate.

The same procedures were than applied to investigate the rheological properties of $C_{10}DAO$-linear aqueous mixtures at the same concentration used for $C_{10}DAO$-branched. The viscosity versus shear rate data are shown in Figure 24.
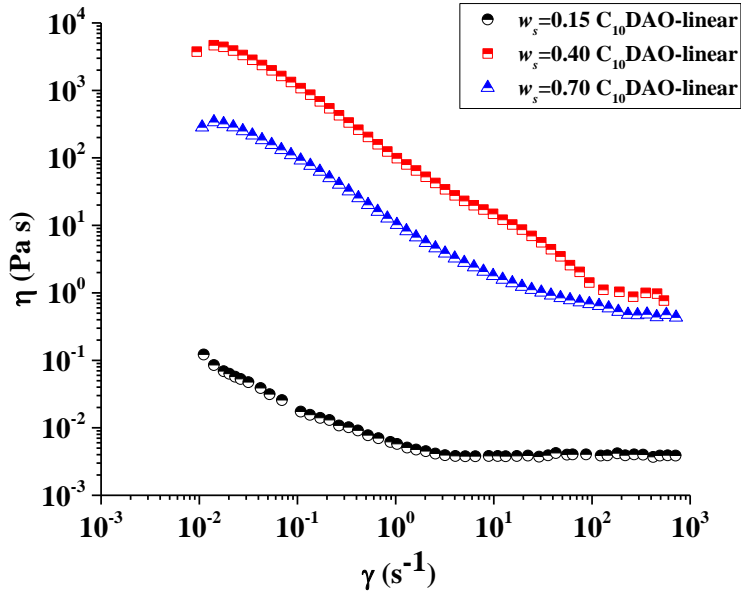
Figure 24. Viscosity versus shear rate diagram for the $C_{10}DAO$-linear/water system

The sample with w_s=0.15 presents a low viscosity which remains nearly constant at high shear rate. This is consistent with the SANS results indicating the sample to be a liquid solution containing small-size micellar aggregates (L_1 sample). Samples with w_s equal to 0.40 and 0.70 are much more viscous and present a shear-thinning behavior, an evidence of their liquid crystalline organization. Particularly, the sample with w_s = 0.70, which according to the SAXS results is in the L_α phase, shows a viscosity lower than the sample with w_s = 0.40, which is in the H_1 phase. Thus H_1 samples are macroscopically stiffer than L_α ones, suggesting the hexagonal arrays of long (infinite) cylinders to be microscopically less dynamic than stacked lamellae [84]. Thus, the viscosity results reflect strong interactions among rod-structured aggregates, favoring the formation of the compact rod-like network in the hexagonal phase [78]. On the other hand, the lamellar liquid crystals consist of surfactant bilayers, separated by an aqueous medium and for this reason the elastic and the viscous component are lower than the hexagonal liquid crystals [193].

The viscoelastic properties of the same samples were then checked by oscillatory experiments. The storage (or elastic) modulus, G', and the loss (or viscous) modulus, G'', are reported in Figure 25 as a function of the angular frequency, ω.
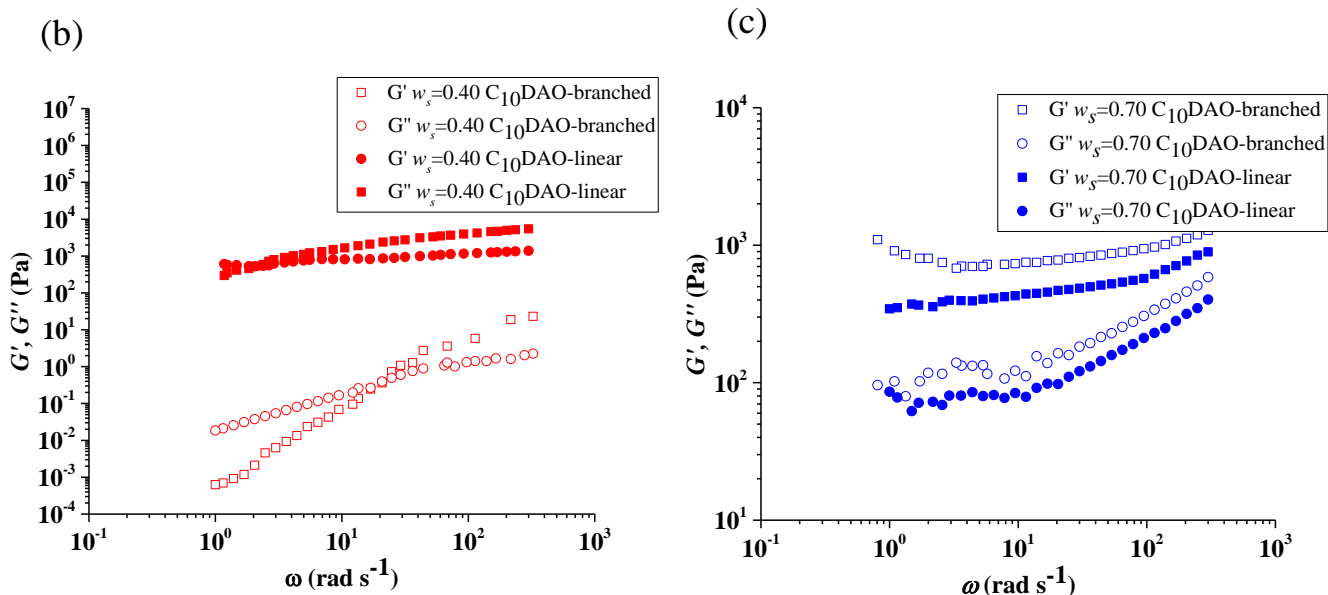
(a)

(b)   (c)
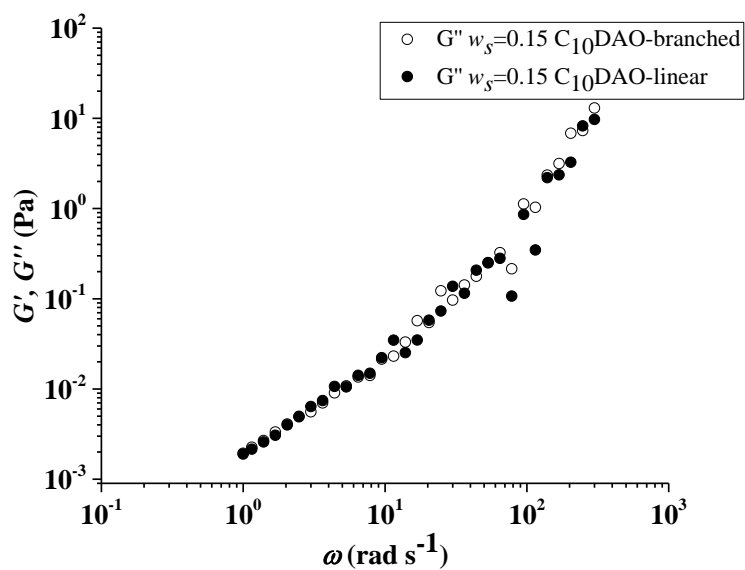
Figure 25. Storage modulus G' and loss modulus G'' versus angular frequency of the $C_{10}DAO$-branched/water and $C_{10}DAO$-linear/water systems at different w_s overlapped.

In the case of the sample with $w_s=0.15$, the oscillation experiment furnished negligible G' values as compared to G'', thus indicating that the L_1 sample containing spherical micelles presents a Newtonian behavior. A different viscoelastic behavior was observed for the sample with $w_s=0.40$, for which both G' and G'' were detectable and were found to increase with increasing ω. Particularly, at low frequency the viscous response dominates (G''>G'), a typical behavior for viscous fluid. As ω increases, G'' becomes approximately equal to G', and the so-called crossover frequency is detected. At high frequency, G'>G'' and a behavior similar to that of an elastic solid is observed. Thus, the change of the $C_{10}DAO$-branched micelle morphology from spherical to cylindrical, as highlighted by SANS measurements, along with the increased concentration which leads to increased interparticle interaction, convert the system rheology from that typical of a Newtonian fluid (at $w_s = 0.15$) to that expected for a pseudoplastic material (at $w_s=0.40$).

Figure 24 shows the G' and G'' trends upon ω variation at 25 °C for the $C_{10}DAO$-branched aqueous mixture with $w_s=0.70$, which presents a L_α structure. As can be seen, G' dominates and remains basically constant over a large frequency spectrum,

while G" smoothly increases. This behavior, typical on non-Newtonian fluids, [194] corresponds to a rubbery plateau.

The results of the oscillatory experiments for the same samples are shown in Figure 15. For the sample with w_s=0.15 only the loss modulus could be measured, similarly to what found for the branched surfactant. A close similarity between the two surfactants was also found for the sample with w_s=0.70, for which almost constant moduli (with G'>G") were found in the whole explored frequency range. These results are consistent with the dilute samples (w_s=0.15) being in the micellar L_1 phase and the concentrated ones (w_s=0.70) in the L_α phase for both the C_{10}DAO-branched and the C_{10}DAO-linear surfactants. The oscillatory experiments for the C_{10}DAO-linear sample with w_s=0.40, which is in the H_1 phase, show high values for both moduli, as expected for LLC phases. The values are even higher than those observed for the lamellar sample (w_s=0.70), supporting what inferred from shear viscosity experiments. G' is higher than G" for most of the explored frequencies. Interestingly, at low frequency a sort of crossover is observed, similar to that found for the (C_{10}DAO-branched)-water sample with the same concentration, which however is micellar solution of elongated micelles.

3.9) Phase behavior of the (C₁₀DAO-branched)-AES-water system: POM results.

The phase behavior of the (C_{10}DAO-branched)-AES-water system is presented in Figure 26.
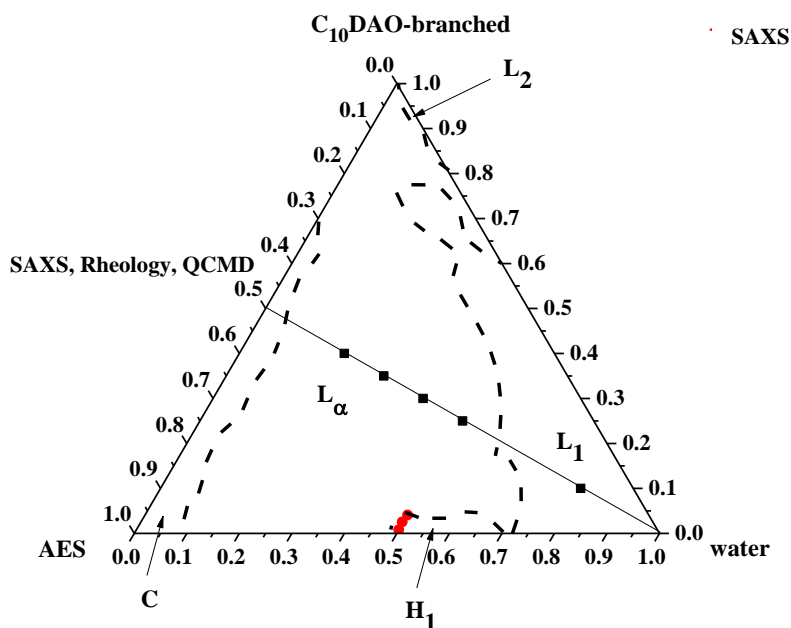
Figure 26. Phase diagram of the $C_{10}DAO$-branched/AES/H_2O. The following notation is used for the various regions: L_1 = isotropic water-rich solution phase, H_1 = Hexagonal LLC phase, L_α = Lamellar LLC phase.

Dashed lines indicate that the composition values delimiting two different phase regions. Five different phases were observed: two isotropic liquid mixtures (a water-rich solution, L_1, and a surfactant-rich solution, L_2), a hexagonal (H_1) and a lamellar LLC phases (L_α) and a crystalline solid (C). Identification of optically anisotropic samples was done by visual inspection through cross-polarizers, while the different liquid-crystalline supramolecular organizations where discriminated according to the texture shown by POM images (Figure 27).
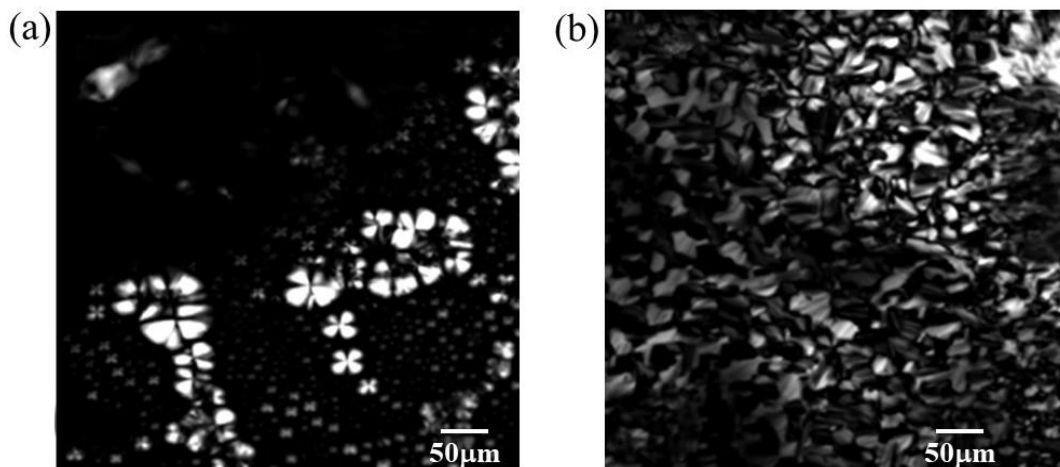
Figure 27. Photographs of the textures of different phases at different concentrations with crossed polarises at 25 °C. (a) Maltese crosses typical of the lamellar phase $w_{C_{10}DAO} = w_{AES} = 0.35$ $w_{water} = 0.30$; (b) fan-like texture typical of the hexagonal phase $w_{C_{10}DAO} = 0.015 w_{AES} = 0.50$ $w_{water} = 0.485$.

To present in a profitable way the results, it is worthy to start from the phase behavior of the two binary systems AES-water (reported on the horizontal axis) and (C$_{10}$DAO-branched)-water (reported on the right-hand side oblique axis). AES-water mixtures are isotropic water-rich solutions up to $w_{AES} = 0.27$. In the concentration range $0.27 < w_{AES} < 0.50$ hexagonal structures are detected. Above $w_{AES} = 0.27$ a wide stability range of lamellae is found, while in extremely concentrated mixtures ($w_{AES} > 0.90$) only hydrated surfactant crystals form. In the case of (C$_{10}$DAO-branched)-water mixtures the isotropic water-rich solution stability domain is much more extended (up to $w_{C_{10}DAO} = 0.60$). No hexagonal phase is detected the only LLC structure found is the lamellar one, which is stable for $0.60 < w_{C_{10}DAO} < 0.80$. More concentrated mixtures are surfactant-rich liquid solution (C$_{10}$DAO-branched itself, as pure substance, is a liquid).

Concerning the ternary system (C$_{10}$DAO-branched)-AES-water, inspection of Figure 26 shows that the isotropic L$_1$ solution is stable at low concentration of two

surfactants and extends at high surfactant concentration in mixtures in which $C_{10}DAO$-branched prevails. The H_1 phase is stable in a small domain along the Figure 26 AES-water binary axis. The L_α stability occupies most of phase diagram. In order to rationalize the behavior of the ($C_{10}DAO$-branched)-AES-water system, the phase stability moving from one surfactant-water axis to the other (at constant $w_s = w_{AES} + w_{C_{10}DAO}$, see the red line in Figure 27 can be analyzed. At $w_{AES} = 0.50$ a H_1 phase is stable; however, substitution of a small amount (less than 0.10) of AES with $C_{10}DAO$-branched converts the hexagonal structure to a lamellar one. This is connected with the low tendency of branched surfactants to form H_1 phase due to the relatively high critical packing parameter. With further increasing the $C_{10}DAO$-branched percent, the L_α phase remains stable up to almost 70%. Above this value, isotropic solutions form, favored by the branched surfactant, which disrupt the packing of the hydrophobic tails and reduce the attractive tail-tail interactions.

3.10) Phase behavior of the ($C_{10}DAO$-linear)-AES-water system: POM and SAXS results

The phase behavior of the ternary system ($C_{10}DAO$-linear)-AES-water was analyzed by the same procedure adopted for the system ($C_{10}DAO$-branched)-AES-water. The phase stability domains were identified by POM and SAXS experiments. The ternary phase diagram composed of ($C_{10}DAO$-linear)-AES-water in the figure 28 is reported.
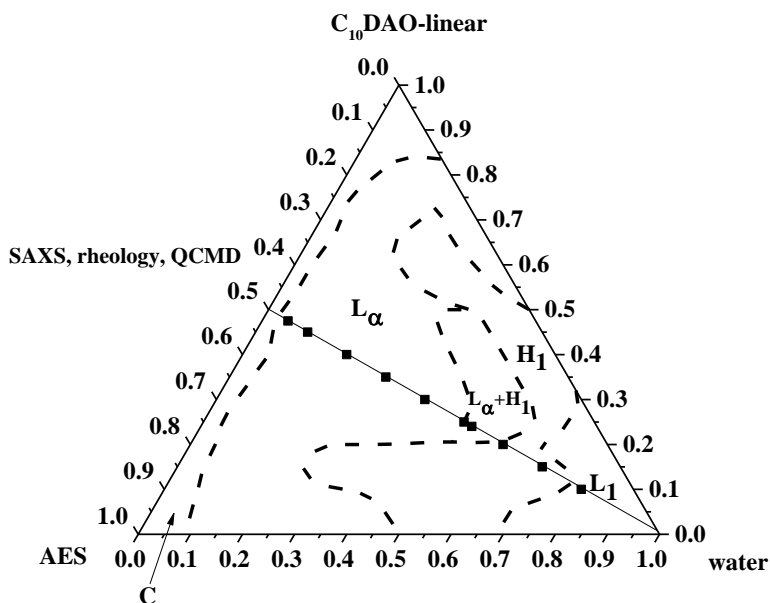
Figure 28. Phase diagram of the (C_{10}DAO-linear)-AES-H_2O. The following notation is used for the various regions: L_1 = isotropic water-rich solution phase, H_1 = Hexagonal LLC phase, H_1+L_α = Hexagonal+Lamellar phases; L_α = Lamellar LLC phase.

Four different phases were observed: L_1, H_1, L_α and C. The LLC phases made up most of the phase diagram. Differently from the other cases in which biphasic regions were too narrow to be detected, a wide domain of H_1+L_α co-existence was found. As examples, POM images collected in Figure 29 show the typical texture of hexagonal phases (Figure 29 a), the Maltese cross pattern typical of a lamellar phase (Figure 29 b), and the co-existence of Maltese crosses and non-geometric stripes structures indicating the presence of both hexagonal and lamellar structures (Figure 29 c).
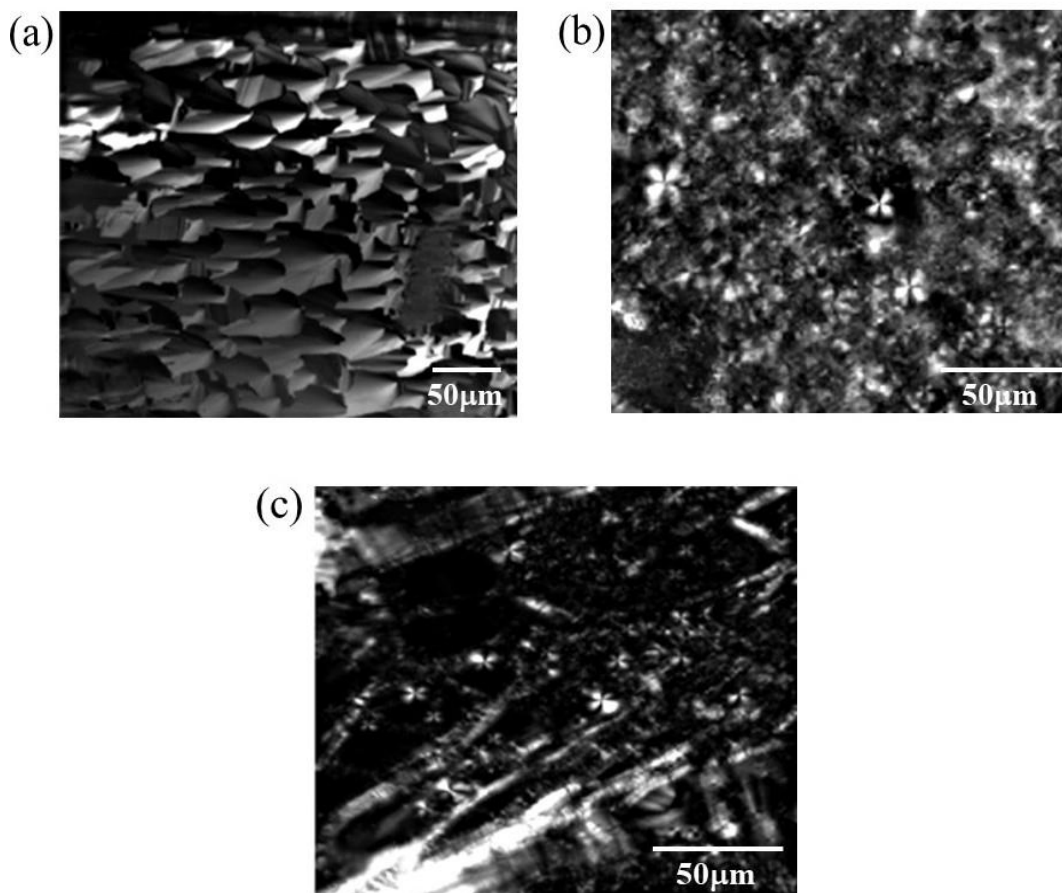
Figure 29. Photographs of the textures of different phases at different concentrations with crossed polarises at 25 °C.; (a) hexagonal phase $w_{C_{10}DAO} = w_{AES} = 0.15$ $w_{water} = 0.70$; (b) lamellar phase $w_{C_{10}DAO} = w_{AES} = 0.40$ $w_{water} = 0.20$; (c) hexagonal+lamellar phases $w_{C_{10}DAO} = w_{AES} = 0.25$ $w_{water} = 0.50$.

The phase behavior of the ($C_{10}DAO$-linear)-water system, shown on the right-hand side oblique axis, present a $L_1 \rightarrow H_1 \rightarrow L_\alpha \rightarrow C$ sequence identical to that of found for the AES-water binary system, the transition concentrations being almost identical. Thus, analysis of the ternary system behavior enhances synergism/antagonism between the two surfactant, straight phase boundaries parallel to the left-hand side oblique axis being expected for an ideal mixing. At low w_s, isotropic water-rich

solutions form, which convert in hexagonally structured samples with increasing total surfactant content. Surfactant mixing favors this transition: samples containing only AES or only C_{10}DAO-linear form H_1 LLCs at $w_s \approx 0.3$, while in mixtures containing the same weight fraction of the two surfactants (*i.e.*, along the black line in Figure 28), the same transition is observed at $w_s \approx 0.2$. The synergistic behavior between the two surfactants could be related to the fact that intercalation of C_{10}DAO-linear between AES molecules in the aggregates decreases the steric repulsion among the ethoxylic headgroups, while intercalation of AES between C_{10}DAO-linear molecules decreases the electrostatic repulsion among zwitterionic headgroups.

The $H_1 \rightarrow L_\alpha$ transition occurs at $w_s \approx 0.5$ in the two binary systems. In this case, mixtures with the same weight fraction of the two surfactants, present this transition at almost the same w_s. In samples in which both surfactants are present but one of the two prevails, the hexagonal structures are stable up to $w_s \approx 0.8$. In other words, the prevalence of the two surfactants destabilizes lamellar structure.

Comparison between (C_{10}DAO-branched)-AES-water and (C_{10}DAO-linear)-AES-water phase diagrams clearly shows the ability of the branched surfactant to destabilize LLC phases in favor of isotropic liquid mixtures. This feature was already found in the binary system (C_{10}DAO-branched)-water. The results reported in the present work demonstrate that this capability is maintained even in surfactant mixtures.

3.11) LLC phases analysis of the ternary C_{10}DAO-branched/AES/water and C_{10}DAO-linear/AES/water systems: SAXS results.

Structural details of the LLC phases formed by (C_{10}DAO-branched)-AES and (C_{10}DAO-linear)-AES mixtures in water at 25 °C were obtained by a SAXS investigation. The compositions of the analyzed samples are reported in table 1-2, together with the obtained parameters, while the most significant SAXS

diffractograms are shown in Figure 30. Concerning the (C_{10}DAO-branched)-AES-water system, the first four samples align along the diagram bisector (*i.e.*, $w_{C_{10}DAO} = w_{AES}$). The SAXS diffractogram of the sample with $w_{C_{10}DAO} = w_{AES} = 0.40$ and $w_{H_2O} = 0.20$ is characterized by two peaks, a strong reflection at q=0.14 $\mathring{A}^{-1}$ and a second small reflection at q=0.28 $\mathring{A}^{-1}$ (Figure 30 a); thus, Bragg peaks show the 1:2 ratio typical of L_α phases, allowing a lattice parameter $a_{lam} = 43.7$ to be estimated. In Table 6, the results obtained for the other samples analyzed along the same bisector; all of them clearly shows the features of the lamellar arrangement. The lattice parameter tends to increase with the amount of water, consistent with a swelling of the water layer between stacked lamellae. Only the datum with $w_{C_{10}DAO} = w_{AES} = 0.25$ shows remarkably lower lattice parameter. This evidence is not straightforward to be interpreted, but could be somehow related to the closeness of the sample composition to the phase transition from L_α to L_1.

The small portion of H_1 phase present in the (C_{10}DAO-branched)-AES-water phase diagram was also investigated. The diffractogram obtained for the sample with $w_{C_{10}DAO} = 0.015 w_{AES} = 0.50$ and $w_{H_2O} = 0.485$, shown in Figure 30 b, also presents two Bragg peaks. The first strong reflection is detected at q=0.16 $\mathring{A}^{-1}$, while the second small reflection is positioned at q=0.27 $\mathring{A}^{-1}$. These peaks show the ratio 1:√3 typical of hexagonal phases, and the lattice parameter a_{hex}=45.7 Å was calculated. Inspection of table 6 reveals that a reduction of the branched surfactant amount leads to a smaller lattice parameter.
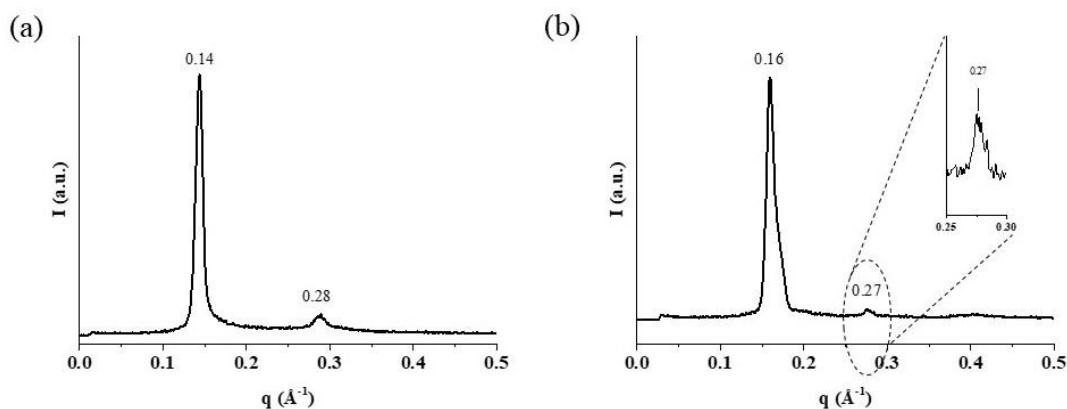
Figure 30. SAXS diffractogram of the ternary phase diagram system composed of $C_{10}DAO$-branched/AES/water at different w_s.

SAXS measurements on ($C_{10}DAO$-linear)-AES aqueous mixtures were performed according to the same protocol. A first group of analyzed samples presents the same amount of the two surfactants. The SAXS diffractogram of the sample with $w_{C_{10}DAO} = w_{AES} = 0.40$ $w_{H_2O} = 0.20$ is characterized by a two Bragg peaks at q=0.18 Å^{-1} and q=0.36 Å^{-1} (Figure 31 a). Thus, the peaks show the ratio 1:2 expected for a lamellar phase, and the lattice parameter was estimated to be a_{lam} =33.8 Å. Inspection of Table 7 shows that the lattice parameter of of lamellar samples increases close to the transition to the hexagonal phase.

For the sample with $w_{C_{10}DAO} = w_{AES} = 0.25$ $w_{H_2O} = 0.50$ the diffractogram, shown in Figure 31 b, presents two strong reflections at q=0.14 Å^{-1} and q=0.16 Å^{-1}, a third reflection at q=0.25 Å^{-1}, and a fourth small reflection at q=0.32 Å^{-1}. The first and third are related each other by the ratio 1:√3, and the second and fourth are related each other by the ratio 1:2, Thus, the results are consistent with the co-existence of hexagonal and lamellar structures (H_1+L_α). The lattice parameter for the hexagonal phase was estimated to be a_{hex} = 50.8 Å, while that for the lamellar phase was a_{lam}= 39.4 Å.

The diffractogram of the sample with $w_{C_{10}DAO} = w_{AES} = 0.15$ $w_{H_2O} = 0.70$, reported in Figure 31 c, is characterized by a two Bragg peaks, at q=0.17 $\mathring{A}^{-1}$ and q=0.29 $\mathring{A}^{-1}$, in the ratio expected for the hexagonal phase. From this data, and the lattice parameter $a_{hex} = 43.1$ $\mathring{A}$ was calculated.
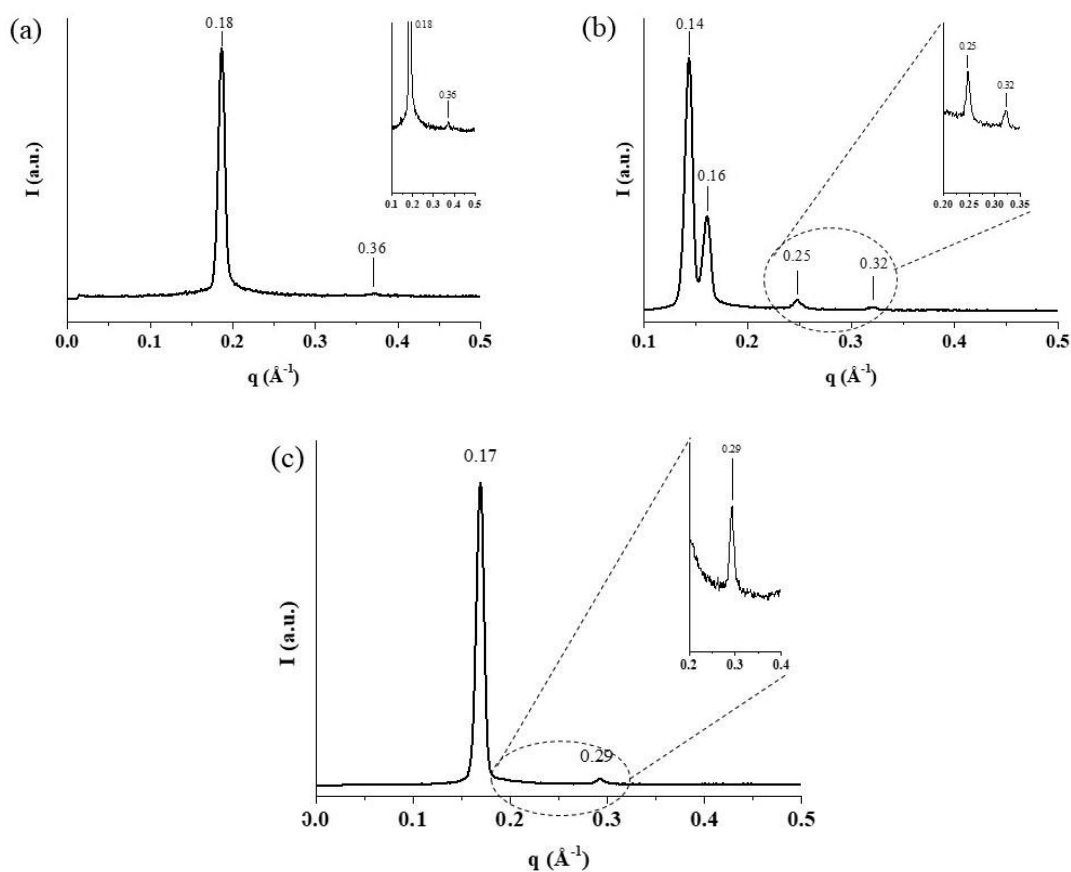
Figure 31. SAXS diffractogram of the ternary phase diagrm system composed of C_{10}DAO-branched/AES/water at different w_s.

SAXS PARAMETERS				
$w_{C_{10}DAO-branched}$	w_{AES}	w_{water}	Lattice parameter [$\mathring{A}$]	Phases
0.4	0.4	0.2	43.77	L_α
0.35	0.35	0.3	56.92	L_α
0.3	0.3	0.4	63.61	L_α
0.25	0.25	0.5	32.65	L_α

| 0.025 | 0.5 | 0.475 | 52.99 | H_1 |
| 0.015 | 0.5 | 0.485 | 45.78 | H_1 |

Table 6. Lattice parameters obtained by SAXS for the Compositions of $C_{10}DAO$-branched/AES/water system.

SAXS PARAMETERS				
$w_{C_{10}DAO-linear}$	w_{AES}	w_{water}	Lattice parameter [Å]	Phases
0.475	0.475	0.05	35.59	L_α
0.45	0.45	0.1	34.12	L_α
0.4	0.4	0.2	33.82	L_α
0.35	0.35	0.3	39.86	L_α
0.3	0.3	0.4	65.82	L_α
0.26	0.24	0.5	52.83+41.38	H_1+L_α
0.25	0.5	0.25	50.83+39.44	H_1+L_α
0.2	0.6	0.2	54.3+43.02	H_1+L_α
0.15	0.7	0.15	43.08	H_1

Table 7. Lattice parameters obtained by SAXS for the Compositions of $C_{10}DAO$-linear/AES/water system.

Overall, the SAXS investigation fully confirms the phase identification based on the POM images. Interestingly, abrupt variations of the lattice parameters are found close to phase boundaries.

3.12) A newly ternary phase behavior determination by HS QCMD

An alternative, inexpensive and fast method to investigate the surfactants phase behavior is the HS QCM-D, which is able to detect surfactant phase transitions induced by hydration using a very low amount of substance [26].

In the present study, HS QCM-D was used to investigate the phase behavior of ($C_{10}DAO$-branched)-AES and ($C_{10}DAO$-linear)-AES mixtures with the same amount of the two surfactants present in each mixture (i.e., along the black lines shown in Figure 25 and 27). The measurements were performed as a function of time during continuous hydration of the surfactants' mixture sample at 25 °C (Figures S_8).

The prominent changes in resonance frequency $\Delta f/n$ and dissipation $\Delta D/n$ were related to hydration-induced transitions between different structural organization of the surfactants in the sample. Experiments started by measuring the uncoated sensor in a dry N_2 atmosphere. Subsequently, the sensor was spin-coated with 20 μL of an aqueous surfactant solution with $w_s = 0.05$, at rps=32 for 30 s. The coated sensor was then dried in the oven for 10 min at 50 °C under a flow of N_2 gas, until a stable baseline of frequency was obtained. The film thickness was determined by analyzing data obtained for uncoated and coated sensor, obtaining a film thickness of 105 and 100 nm (Figures S_{13}-S_{14}) for the (C_{10}DAO-branched)-AES and (C_{10}DAO-linear)-AES mixtures, respectively.

The $\Delta f/n$ and $\Delta D/n$ values for the different overtones were measured as a function of time during dilution of the LiCl solution flowing in the humidity module (Figures S_8). Conversion from time to a_w was achieved by knowing the dilution time [155]. Variations of $\Delta f/n$ and $\Delta D/n$ curve profiles of the initially dry (C_{10}DAO-branched)-AES and (C_{10}DAO-linear)-AES films were generated by the continuous increase in *RH*, leading to the LLC phase transitions detected.

In the figure 32 the $\Delta f/n$ and $\Delta D/n$ as a function of a_w curves profiles for the diagonal of the ternary system (C_{10}DAO-branched)-AES-water containing an equal amount of the two surfactants are reported.
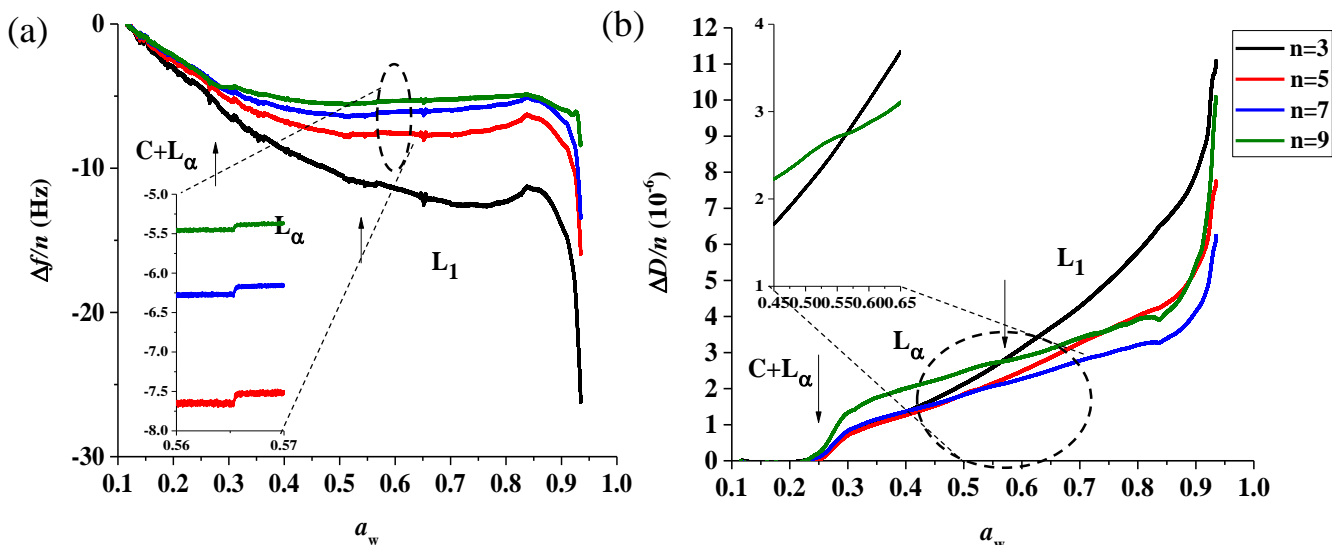
Figure 32. (a) Frequency shift Δ*f/n* and dissipation (b) Δ*D/n* as a function of water activity aw for
C_{10}DAO-branched/AES/water ($w_{C_{10}DAO} = w_{AES} = 0.50$). Arrows indicate water activity levels where

abrupt changes in Δ*f/n* and Δ*D/n* occur as a result of hydration-induced phase transitions.
Abbreviations: C+ L_{α}=crystal+lamellar phase; L_{α}=lamellar phase; L_1=micellar phase.

The measurements start from a_w=0.12. With increasing a_w, Δ*f/n* decreases, which is
not expected for solid surfactants. Moreover, the normalized frequency shifts are
independent of the overtone number. This behavior, predicted by the Sauerbrey
model, shows that the sample behave as plastic materials characterized by extensive
energy dissipation, as typical of LLC phases. This evidence suggests that
measurements start from a sample in which an LLC phase is present. In the same a_w
range, Δ*D/n* is constant, as expected for solids. Thus the measurement starts froma
sample in which the solid and an LLC phase co-exist. A first transition with
increasing surfactants hydration is observed at a_w≈0.25. From the comparison with
the POM and SAXS data, this transition detected by HS QCM-D can be confidently
interpreted in terms of the system changing from a C+L_{α} to a L_{α} stability range. This
phase transition is also detected in the Δ*D/n* trend, which shows an abrupt slope
change from the initial constant value to a steep increase.

With increasing water content along the black line in Figure 26, POM data show the
transition from L_{α} to a surfactant-water isotropic mixture, which occurs at w_s≈0.4.
However, no dramatic discontinuity in both the Δ*f/n* and Δ*D/n* trends was found for

98

a_w values higher than 0.25. Perusal of Figure 32 only reveals a small step in the $\Delta f/n$ graph and a broad shoulder in the $\Delta D/n$ graph at about $a_w \approx 0.55$ (see the insets in the figure), which could be probably ascribed at the L_α to L_1 transition. Indeed, HS QCM-D was already found to be poorly sensitive to transitions involving isotropic liquid phases.

The ternary phase diagram (C_{10}DAO-linear)-AES-water was investigated along the bisector at equal amounts of the two surfactant by HS QCM-D, using the same procedure adopted for (C_{10}DAO-branched)-AES aqueous mixtures (see, the black line in Figure 28). Variations of $\Delta f/n$ and $\Delta D/n$ during sample hydration are reported in the Figure 33.
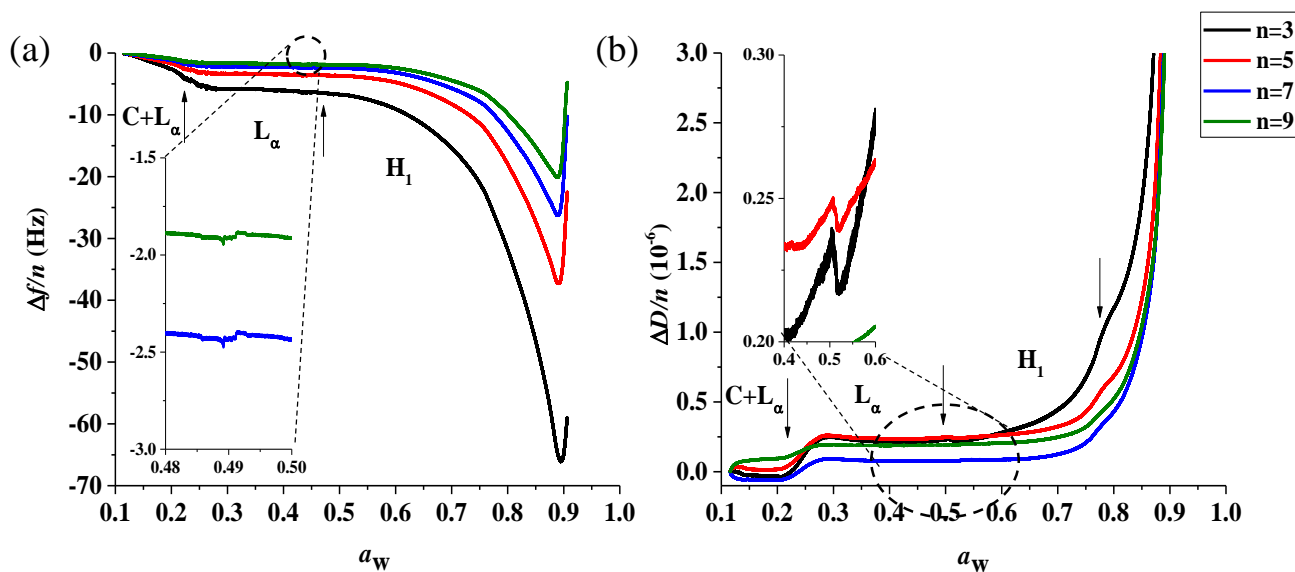
Figures 33. Frequency shift (a) $\Delta f/n$ and dissipation (b) $\Delta D/n$ as a function of water activity aw for C_{10}DAO-linear/AES/water ($w_{C_{10}DAO} = w_{AES} = 0.50$). Arrows indicate water activity levels where

abrupt changes in $\Delta f/n$ and $\Delta D/n$ occur as a result of hydration-induced phase transitions.
Abbreviations: $C+L_\alpha$=crystal+lamellar phase; L_α=lamellar phase; phase; H_1=hexagonal phase; L_1=micellar phase.

Even in this case the curves shows the C+L_α→L_α transition, corresponding to a clear slope change in both the $\Delta f/n$ and $\Delta D/n$ trends at a_w≈0.2. The presence of lamellae in the hydrated surfactant film is confirmed by the evidence that $\Delta f/n$ absolute value decreases with increasing n. A further slight, but still detectable, discontinuity is observed at a_w≈0.5 (see the insets in the figure 33 a). It is more evident in the $\Delta D/n$ trend in which a sharp peak is observed, than in the $\Delta f/n$ trend. On the basis of the POM and SAXS results, this can be identified as the transition from a lamellar to a hexagonal structure. At a_w≈0.8 a shoulder is detected in the $\Delta D/n$ trend, which could be ascribed to the H_1→L_1 transition. No evident discontinuity is observed in the $\Delta f/n$ trend, which confirms to be poorly sensitive to transitions involving isotropic liquid phases. The L_1 phase is expected to persist up to the highest a_w value examined.

Overall, the HS QCM-D results are in fair agreement with POM and SAXS data. This confirms that the HS QCM-D is a fast and inexpensive method to detect phase transitions in surfactant aqueous mixtures. However, since it does not allow an unequivocal and absolute assignment of the phase structure, it could be proposed as a method for a rapid screening of the effect of new components (e.g., co-surfactants, additives, a second surfactant) on the structural preferences of a surfactants whose phase behavior is already known. From this viewpoint, our results demonstrate, for the first time, HS QCM-D to be suitable to characterize the behavior of surfactant mixtures.

3.13) Rheological behavior investigation of the C_{10}DAO-branched/AES/water and C_{10}DAO-linear/AES/water systems.

The viscoelastic properties of the (C_{10}DAO-branched)-AES-water and (C_{10}DAO-linear)-AES-water aqueous mixtures were investigated by rheological measurements [12]. For both systems, samples containing the same amount of C_{10}DAO-branched (or C_{10}DAO-linear) and AES were considered.

First, the viscosities were measured as a function of the shear rate at 25 °C, see Figures 33 a and b for samples including the branched and the linear amine-oxide, respectively.
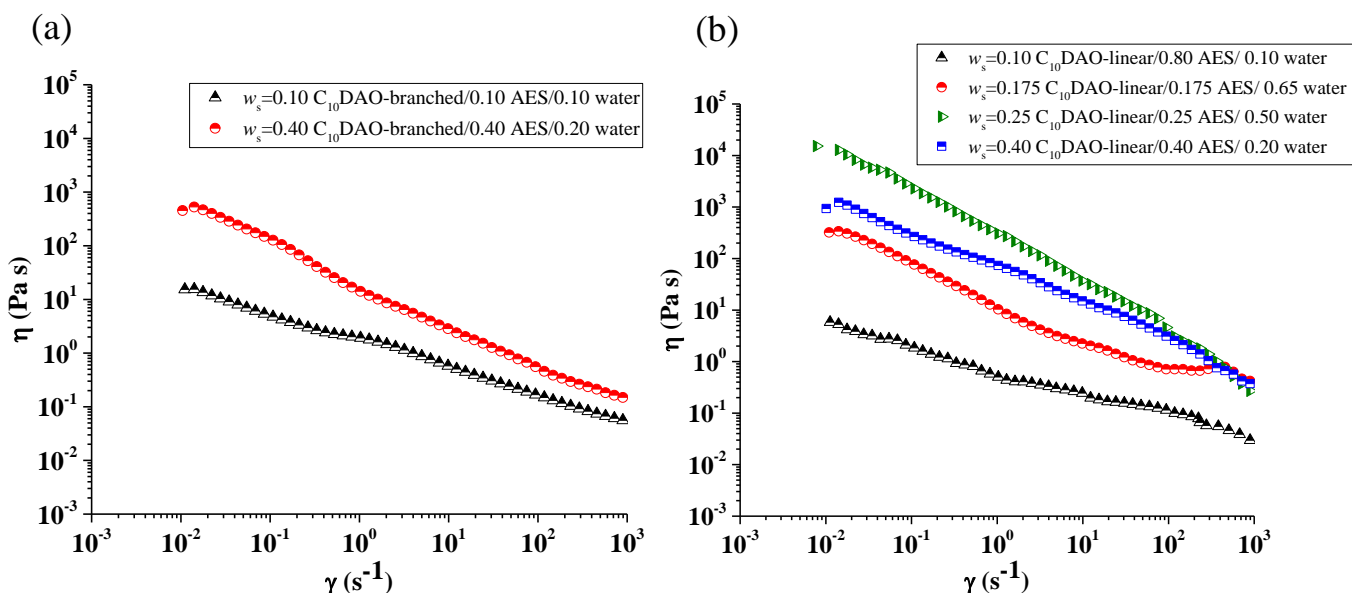
Figure 32. Viscosity versus shear rate diagram for the (a) C_{10}DAO-branched/AES/ water and (b) C_{10}DAO-linear/AES/ water systems.

The viscosity of the (C_{10}DAO-branched)-AES aqueous mixture with w_s=0.2 ($w_{C_{10}DAO} = w_{AES} = 0.20$) and $w_{water} = 0.80$ is low and weakly dependent on the shear rate, the sample behaving as a shear-thinning fluid, whose viscosity decreases with increasing the shear rate. Interestingly, at the same surfactant concentration the binary (C_{10}DAO-branched)-water mixture, which contains almost spherical micellar aggregates, presents a much lower and shear-independent viscosity. Thus, different behavior shown in Figure 32 indicates that in the ternary the L_1 phase contains different aggregates, presumably worm-like micelles [195].

The L$_\alpha$ sample with $w_{C_{10}DAO} = w_{AES} = 0.40$ and $w_{water} = 0.20$ presents a higher viscosity than the L$_1$ samples; moreover, the shear-thinning behavior is more marked.

Concerning the (C$_{10}$DAO-linear)-AES aqueous mixtures, the sample with $w_{C_{10}DAO} = w_{AES} = 0.20$ and $w_{water} = 0.80$ presents a typical shear-thinning behavior similar to that observed for the (C$_{10}$DAO-branched)-AES mixture at the same concentration. Thus, the sample is likely to contain worm-like micelles [195], whose formation can be concluded to be induced by the surfactant mixing, quite independently of the branching of the tails.

The L$_\alpha$ sample with $w_{C_{10}DAO} = w_{AES} = 0.40$ and $w_{water} = 0.20$ also behaves as a shear-thinning fluid, but presents a viscosity higher than L$_1$ samples and very close to that observed for the (C$_{10}$DAO-branched)-AES mixture at the same concentration. Thus, the viscosity of the lamellar phase seems to be poorly affected by the surfactant branching.

The sample with $w_{C_{10}DAO} = w_{AES} = 0.20$ and $w_{water} = 0.60$, and that $w_{C_{10}DAO} = w_{AES} = 0.25$ and $w_{water} = 0.50$ are much more viscous, an evidence of their different liquid crystalline organization. Particularly, the sample with $w_{C_{10}DAO} = w_{AES} = 0.25$, which according to the SAXS is the H$_1$+L$_\alpha$ biphasic domain, shows a viscosity lower than the sample with $w_{C_{10}DAO} = w_{AES} = 0.20$, which is in the H$_1$ phase. Thus, H$_1$+L$_\alpha$ samples are less rigid than H$_1$, suggesting that the co-existing LLC phases create a network of entangled structures, giving a higher microscopic dynamism than the hexagonal structures.

Thus, the viscosity results reflect for the H$_1$ phase a strong interaction among rod-structured aggregates, generating a compact rod-like network formation [78]. At the same time, the lamellar liquid crystals are composed of a surfactant bilayer, separated by an aqueous medium and this gives higher dynamism than the hexagonal liquid crystals [193].

The viscoelastic properties of the same samples were then investigated by oscillatory experiments. The storage (or elastic) modulus, G', and the loss (or viscous) modulus, G'', are reported as a function of the angular frequency, ω. In the figure 34 (a) the results obtained for the samples with $w_{C_{10}DAO} = w_{AES} = 0.10$ in the (C_{10}DAO-branched)-AES and in the (C_{10}DAO-linear)-AES aqueous mixtures are compared; figure 34 (b) shows the same comparison for the samples with $w_{C_{10}DAO} = w_{AES} = 0.40$.
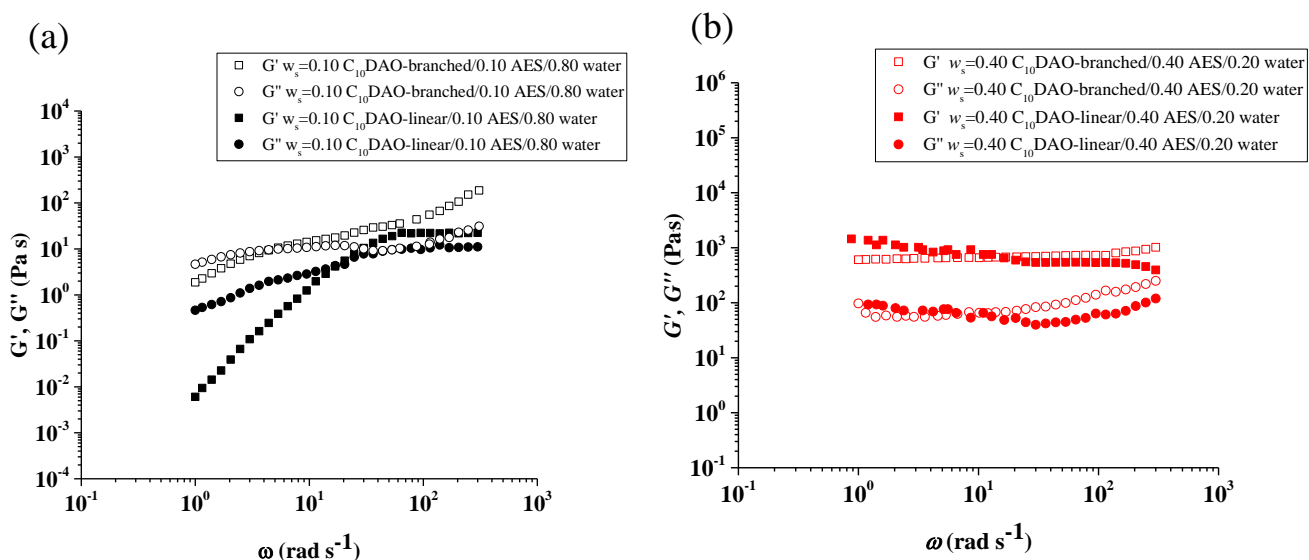
Figure 34. Storage modulus G' and loss modulus G'' versus angular frequency of C_{10}DAO-branched/AES and C_{10}DAO-linear/AES at equal w_s; (a) L_1 phase; (b) L_α phase.

In the case of dilute samples, G' and G'' values were found to increase with ω. Particularly, at low frequency the viscous response dominates (G''>G'), a typical behavior of viscous fluid. As ω increases, G'' becomes equal to G', and the so-called crossover frequency is detected. At high frequency, G'>G'' and a behavior similar to that of an elastic solid is observed. This behavior indicates that the L_1 samples present a non-Newtonian behavior, thus supporting the hypothesis that these samples contain elongated surfactant aggregates (probably worm-like micelles) able to overlap and

103

form entangled structures [194]. The comparison between the two dilute samples shows that the sample containing C_{10}DAO-branched presents a higher elasticity and viscosity than that containing C_{10}DAO-linear in the whole ω range.

For what concern the samples with $w_{C_{10}DAO} = w_{AES} = 0.40$, which present a L$\alpha$ structure, both G' and G'' remain basically constant over a large frequency spectrum, the elastic modulus dominating with respect to the viscous one. This behavior, typical on non-Newtonian fluids, [194] corresponds to a gel-like behavior.

In Figure 35 (a and b) the G' and G'' of (C_{10}DAO-linear)-AES-water samples with $w_{C_{10}DAO} = w_{AES} = 0.25$ and $w_{C_{10}DAO} = w_{AES} = 0.175$, which are in the H$_1$ and H$_1$+Lα stability domains, respectively, are shown.

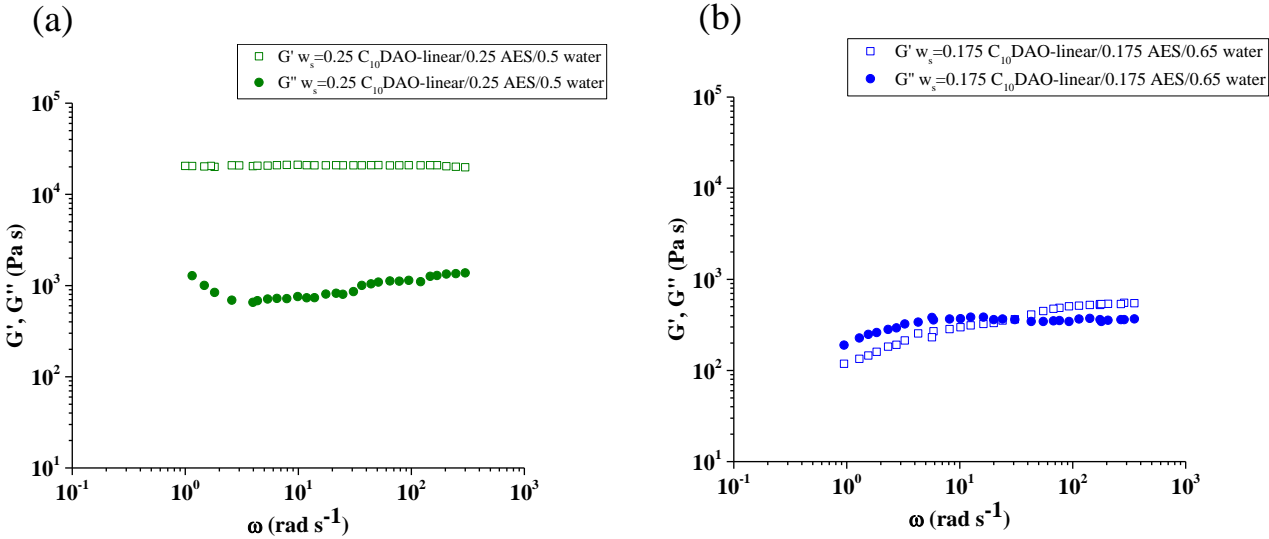

Figure 35. Storage modulus G' and loss modulus G'' versus angular frequency of C_{10}DAO-linear/AES at different w_s; (a) H$_1$ phase; (b) H$_{1+}$Lα phase.

For the former sample, the two moduli present very similar values, perusal of the figure reveals that at low frequency the viscous response dominates (G''>G'), a

104

typical behavior of viscous fluid. As ω increases, above the so-called crossover frequency, G'>G" and a behavior similar to that of an elastic solid is observed.

For what concern the sample with $w_{C_{10}DAO} = w_{AES} = 0.25$, which presents a $H_1 + L_\alpha$ structure, Figure 35 b shows that G' dominates and remains basically constant over a large frequency spectrum, while G" smoothly increases. This behavior is typical of gel-like samples, and is similar to that observed for the lamellar samples.

3.14) Effect of the amine oxide architecture in the ternary phase diagram systems

The comparison between the properties of the ternary systems ($C_{10}DAO$-branched)-AES-water and ($C_{10}DAO$-linear)-AES-water allows the effect of the tail branching on the mixed surfactants' self-aggregation to be studied. The phase diagram of the ternary system including the linear surfactant is dominated by hexagonal and lamellar LLC phases, while the isotropic micellar phase presents only a small stability domain. The highly viscous hexagonal phase could compromise the processability of a formulation based on this surfactant mixture. For this reason, a very effective strategy aimed at enlarging the stability domain of isotropic liquid mixtures and at reducing the hexagonal phase region, is based on the surfactant architecture [196, 197]. The tail branching is able to interrupt the intermolecular interaction and the effective packaging of the aliphatic tails, influencing the tendency to aggregate and the surfactants supramolecular organization [198-200]. Indeed, the phase diagram of the ternary system including $C_{10}DAO$-branched presents a large isotropic liquid region; the rest of the diagram is dominated by an extended lamellar region. Thus tail branching causes an almost complete destabilization of the hexagonal phases.

4) Conclusions

The molecular design of new surfactants offers the opportunity for the fine tuning of their aggregation properties, which reflects in their functional behavior. In this thesis, a new dimethylalkylamine oxide surfactant presenting a branched alkyl chain, C_{10}DAO-branched, was successfully synthetized and purified using simple and easily scalable procedures. The alkyl chain branching does not affect the protonation equilibrium of the amino-oxide headgroup. Thus, the protonated cationic form of C_{10}DAO-branched is present at acidic pH, while the zwitterionic form dominates in basic solutions. However, the aggregation behavior of the surfactant is much less pH-sensitive, with respect to the analogue bearing a linear alkyl chain, C_{10}DAO-linear. Micellization of the branched surfactant occurs at higher concentration and larger micellar aggregates form. C_{10}DAO-branched micellar solutions present lower surface tension than C_{10}DAO-linear ones. This clearly reflects in a higher foamability (particularly in the zwitterionic form) and in a longer foam stability (particularly in the cationic form).

The self-assembly behavior in water of the two amine oxide surfactant isomers, C_{10}DAO-branched and C_{10}DAO-linear, has been explored over the whole concentration range and for temperature ranging between 20 and 70 °C for C_{10}DAO-branched and between 20 and 110 °C for C_{10}DAO-linear. Investigation at higher temperature was hampered by the amine oxide degradation, with formation of an alkene and of hydroxylamine. From this viewpoint, the branched surfactant is weaker, because to lower energy required to form a bi-substituted alkene promotes the chemical degradation at a lower temperature than that required for the linear isomer. However, since the temperature in use for most of home-care formulations varies in the 15-50 °C range, the chemical instability seems a minor drawback of C_{10}DAO-branched, not precluding its application for practical purposes.

In aqueous mixtures, the two surfactants present a different phase behavior: $C_{10}DAO$-branched does not form any LLC structures below $w_s=0.62$; in contrast, the isotropic domain is limited to $w_s=0.32$ in the case of $C_{10}DAO$-linear. The LLC phases formed of $C_{10}DAO$-branched and $C_{10}DAO$-linear have been investigated by POM, SAXS, HS QCMD and rheology. Experimental results show that the formation of LLC phases is poorly affected by the temperature, but strongly depends on the surfactant molecular architecture.

The isotropic liquid phases formed by $C_{10}DAO$-branched at low concentration in aqueous mixture ($w_s=0.15$ and $w_s=0.40$) were studied by SANS, highlighting a morphological transition from ellipsoid to rod-like micelles. In contrast, $C_{10}DAO$-linear only forms spherical aggregates. The isotropic liquid phase formed by $C_{10}DAO$-branched at high concentration ($w_s=0.15$, 0.40) was supported by rheology measurements.

POM and SAXS results on LLC phases show that branching totally removes the hexagonal phase, just leaving a small stability domain on a lamellar phase. Rheological investigation demonstrates that the latter is much less viscous than the former one, indicating that hexagonally arrayed cylinders are more tightly and rigidly packed than stacked lamellae. These results support the hypothesis that the use of branched surfactants is a suitable strategy to increase the active (surfactant) concentration in detergent formulations

Industrial formulations are usually based on surfactant mixtures; for this reason, to validate the application of branched surfactants, in this thesis the phase behavior of the ternary systems ($C_{10}DAO$-branched)-AES-water and ($C_{10}DAO$-linear)-AES-water have been built by the same procedure used for the binary phase diagrams and investigated over the whole surfactant concentration range 25 °C. AES (alkyl ethoxy sulphate) is an anionic surfactant widely used in house-hold detergent formulations. The different architecture between $C_{10}DAO$-branched and $C_{10}DAO$-linear lead to the

formation of the different LLC phases in AES-containing aqueous mixtures. Concerning the mixture containing the branched surfactant five different liquid crystalline phases (L_1, H_1, $L\alpha$, C, L_2) were observed. The L_1 and $L\alpha$ phases cover most of the phase diagram. The domain of the H_1, C, L_2, phases are much narrower. The mixtures containing C_{10}DAO-linear four different liquid crystalline phases (L_1, H_1, $L\alpha$, C,) and one biphasic domain (H_1+$L\alpha$) were observed. The $L\alpha$, H_1 and C phases cover most of the phase diagram, while the L_1 region is relatively small.

Thus, experimental results showed that, even in the presence of the AES, the phase behaviour is strongly affected by the C_{10}DAO molecular architecture. As discussed for the binary systems, the hexagonal phase, whose stability domain is quite extended in the (C_{10}DAO-linear)-AES-water ternary system, could compromise the processability of a formulation based on this surfactant mixture. From this viewpoint tail branching appears to be a very effective modification aimed at increasing the micellar phases, reducing at the same time the hexagonal phase. Indeed, in the ternary phase diagram of the system (C_{10}DAO-branched)-AES-water the hexagonal phase is almost abolished and the stability domain of isotropic liquid mixture is much wider.

Form a molecular viewpoint, the results reported in this thesis show that the branching is able to interrupt the interaction and the effective packaging of the aliphatic tails, influencing the tendency to aggregate and the surfactants supramolecular organization. Therefore, the branching in the alkyl chain represent a possible strategy for altering the aggregation properties of the amino oxides surfactant both in the binary system and in the ternary system. Indeed, the branching effect alters the surfactant-surfactant and water-surfactant interaction, favoring the formation of concentrated isotropic micellar phases with low viscosity and disfavoring the formation of high viscosity lyotropic liquid crystalline phases.

To summarize, our results point to alkyl chain branching as a successful strategy to regulate the surfactant aggregation and functional behavior. Specifically, branched *N,N*-dimethylalkylamino oxide can be proposed in applications based on surfactant mixtures (e.g., in the formulation of wetting agents and/or foam booster).

5) *Bibliography*

[1] K. Mahajan, An overview of the global and european consumption of surfactants in household, industrial, and institutional cleaning applications, Household and Personal Care Today, 11(5) (2016), 24–26.

[2] C. Edser, Surfactant innovations push the boundaries in home care formulations, Focus on Surfactants, 11 (2014) 1–3.

[3] D. J. Wildemuth, J. F. Omnitz, N. L. Arledge, P. K. Stenger, S. W Capeci. (2018). Concentrated Surfactant composition. US Patent No. 2,160,029. Cincinnati, Ohio, U. S. United States Patent, Procter and Gamble Co.

[4] J. W. Holder, F. Thomas, G. M. Frankenbach, S. J. Hodson, D. E. O. Vanhoutte, G. T. Waning. (2017). Concentrated surfactant composition. US Patent No. 9,840,681. Cincinnati, Ohio, U.S. United States Patent, Procter and Gamble Co.

[5] M. W. Hamersky, J. W. Semmel III, M. R. Sivik, P. R. Mort III (2018). Concentrated surfactant composition. US Patent No. 2,160,37. Cincinnati, Ohio, U. S. United States Patent, Procter and Gamble Co.

[6] A. Koehler, C. Wildbolz, Comparing the environmental footprints of home-care and personal-hygiene products: The relevance of different life-cycle phases, Environmental Science & Technology, 43(22) (2009) 8643–8651.

[7] N. Calero, J. Santos, J. Muñoz, Methodology to estimate the yeld stress applied to ultraconcentrated detergents as model system, Chemical Engineering Science 166 (2017) 115–121.

[8] Y. Li, H. Zhang, M. Bao, Q. Chen, Aggregation behavior of surfactants with different molecular structures in aqueous solution: DPD simulation study. Journal of Dispersion Science and Technology, 33 (2012) 1437–1443.

[9] D. Wells, C. Fong, I. Krodkiewska, C. J. Drummond, Nonionic urea surfactants: Influence of hydrocarbon chain length and positional isomerism on the thermotropic and lyotropic phase behavior, Journal Physical Chemistry B 110(10) (2006) 5112–5119.

[10] J. G. Ma, B. J. Boyd, C. J. Drummond, Positional isomers of linear sodium dodecyl benzene sulfonate: Solubility, self-assembly, and air/water interfacial activity, Langmuir 22 (2006) 8646–8654.

[11] Y. J. Zhang, Y. L. Li, Y.B. Song, J. Li, Synthesis and aggregation behaviors of tail-branched surfactant Guerbet-cetyl trimethyl ammonium chloride, Colloid and Polymer Science 294(2) (2016) 271−279.

[12] I. Nainggolan, S. Radiman, A. S. Hamzah, R. Hashim, The effects of branched-tail structure of surfactant on the phase behaviour of alkylglucoside/water/n-octane ternary system, Applied Mechanics and Materials 754-755 (2015) 944−949.

[13] S. Alexander, G. N. Smith, C. James, S. E. Rogers, F. Guittard, M. Sagisaka, J. Eastoe, Low-Surface Energy Surfactants with Branched Hydrocarbon Architectures, Langmuir 30(12) (2014) 3413-3421.

[14] N. A. Nabila Saari, A. A. Mislan, R. Hashim, N. I. Zahid, Self-Assembly, Thermotropic, and Lyotropic Phase Behavior of Guerbet Branched-Chain Maltosides, Langmuir 34 (2018) 8962−8974

[15] F. Nilsson, O. Söderman, I. Johansson, Physical-chemical properties of some branched alkyl glucosides, Langmuir 13 (1997) 3349−3354.

[16] B. J. Boyd, C. J. Drummond, I. Krodkiewska, A. Weerawardena, D. N. Furlong, F. Grieser, Alkyl chain positional isomers of dodecyl α-D-glucoside: Thermotropic and lyotropic phase behavior and detergency, Langmuir 17 (2001) 6100−6107.

[17] J. M. Walsh, G. J. T. Tiddy, Liquid crystal phase behavior of branched poly(oxyethylene) surfactants, Langmuir 19(14) (2003) 5586-5594.

[18] C. Frank, H. Frielinghaus, J. Allgaier, Nonionic surfactants with linear and branched hydrocarbon tails: Compositional analysis, phase behavior, and film properties in bicontinuous microemulsions. Langmuir 23 (2007) 6526–6535.

[19] N. A. Lockwood, J. J. de Pablo, N. L. Abbott, Influence of surfactant tail branching and organization on the orientation of liquid crystals at aqueous-liquid crystal interfaces. Langmuir 21(15) (2005) 6805–6814.

[20] K. R. Wormuth, S. Zushma, Phase behavior of branched surfactants in oil and water. Langmuir 7 (1991) 2048–2053.

[21] R. Varadaraj, J. Bock, S. Zushma, N. Brons, T. Colletti. Effect of hydrocarbon chain branching on interfacial properties of monodisperse ethoxylated alcohol surfactants. Journal of Colloid and Interface Science, 147(2) (1991) 387–394.

[22] S. S. Adkins, X. Chen, Q. P. Nguyen, A.W. Sanders, K. P. Johnston, Effect of branching on the interfacial properties of nonionic hydrocarbon surfactants at the air-water and carbon dioxide-water interfaces, Journal of Colloid and Interface Science 346(2) (2010) 455–463.

[23] L. Ghaïcha, R. M. Leblanc, A. K. Chattopadhyay. Ellipsometric study of surfactants comprising linear and branched hydrocarbon chains at the air-water interface. Journal of Physical Chemistry 96 (1992) 10948–10953.

[24] K. Kratzat, H. Finkelmann, asymmetrically branched nonionic oligooxyethylene V_a-surfactants: Effect of molecular geometry on liquid-crystalline phase behavior, 5. Journal of Colloid and Interface Science 181(2) (1996) 542–550.

[25] L. Rekvig, M. Kranenburg, B. Hafskjold, B. Smit, Effect of surfactant structure on interfacial properties, Europhysics Letters, 63(6) (2003) 902–907.

[26] S. Björklund, V. Kocherbitov, Humidity scanning quartz crystal microbalance with dissipation monitoring setup for determination of sorption-desorption isotherms and rheological changes, Review of scientific instruments 86, 055105 (2015).

[27] C. Edser, Surfactant innovations push the boundaries in home care formulations, Focus on Surfactants, 11 (2014) 1-3.

[28] D. J. Wildemuth, J. F. Omnitz, N. L. Arledge, P. K. Stenger, S. W Capeci. (2018). Concentrated Surfactant composition. US Patent No. 2,160,029. Cincinnati, Ohio, U.S. United States Patent, Procter and Gamble Co.

[29] J. W. Holder, F. Thomas, G. M. Frankenbach, S. J. Hodson, D. E. O. Vanhoutte, G. T. Waning. (2017). Concentrated surfactant composition. US Patent No. 9,840,681. Cincinnati, Ohio, U.S. United States Patent, Procter and Gamble Co.

[30] M. W. Hamersky, J. W. Semmel III, M. R. Sivik, P. R. Mort III (2018). Concentrated surfactant composition. US Patent No. 2,160,37. Cincinnati, Ohio, U. S. United States Patent, Procter and Gamble Co.

[31] A. Koehler, C. Wildbolz, Comparing the environmental footprints of home-care and personal-hygiene products: The relevance of different life-cycle phases, Environmental Science & Technology, 43(22) (2009) 8643–8651.

[32] N. Calero, J. Santos, J. Muñoz, Methodology to estimate the yeld stress applied to ultraconcentrated detergents as model system, Chemical Engineering Science 166 (2017) 115-121.

[33] G. G. Ying, Fate, behavior and effects of surfactants and their degradation products in the environment, Environ Int 32(3) (2006) 417-431.

[34] I. Natali, E. Carretti, L. Angelova, P. Baglioni, R. G. Weiss, L. Dei. Structural and Mechanical Properties of "Peelable" Organoaqueous Dispersions with Partially Hydrolyzed Poly(vinyl acetate)-Borate Networks: Applications to Cleaning Painted Surfaces, Langmuir (2011), 27 (21), 13266-13235.

[35] M. J. Scott, M.N. Jones, The biodegradation of surfactants in the environment, Bba-Biomembranes 1508(1-2) (2000) 235-251.

[36] X. Maoa, R. Jianga, W. Xiaoa, J. Yubse of surfactants for the remediation of contaminated soils: A review, Journal of Hazardous Materials, 285 (2015) 419-435

[37] T. Cserhati, E. Forgacs, G. Oros, Biological activity and environmental impact of anionic surfactants, Environ Int 28(5) (2002) 337-348.

[38] A. Wibbertmann, I. Mangelsdorf, K. Gamon, R. Sedlak, Toxicological properties and risk assessment of the anionic surfactants category: Alkyl sulfates, primary alkane sulfonates, and α-olefin sulfonates, Ecotoxicology and Environmental Saftey, 74 (2011), 1089-1106.

[39] A. B. Caracciolo, M. Cardoni, T. Pescatore, L. Patrolecco, Characteristics and environmental fate of the anionic surfactant sodium lauryl ether sulphate (SLES) used as the main component in foaming agents for mechanized tunnelling, Environ Pollut 226 (2017) 94-103.

[40] S. A. Chegenizadeh Negin, Quan Xie, Most common surfactants employed in chemical enhanced oil recovery, Petroleum 3(2) (2017) 197-211.

[41] Z. Vinarov, V. Katev, D. Radeva, S. Tcholakova, N.D. Denkov, Micellar solubilization of poorly water-soluble drugs: effect of surfactant and solubilizate molecular structure, Drug Dev Ind Pharm 44(4) (2018) 677-686.

[42] M. S. Negahban-Azar, Sybil E., Potential Changes in Chemical Soil Quality Resulting from Graywater Recycling for Landscape Irrigation, Water Environment Federation 90(5) (2018) 452-464.

[43] R. P. Gullapalli, B.B. Sheth, Influence of an optimized non-ionic emulsifier blend on properties of oil-in-water emulsions, Eur J Pharm Biopharm 48(3) (1999) 233-238.

[44] Z. Vinarov, V. Katev, D. Radeva, S. Tcholakova, N.D. Denkov, Micellar solubilization of poorly water-soluble drugs: effect of surfactant and solubilizate molecular structure, Drug Dev Ind Pharm 44(4) (2018) 677-686.

[45] T. A. Cripe, K. O. Asante, (1994). Alkaline light duty dishwashing detergent composition containing an alkyl ethoxy carboxylate surfactant, magnesium ions, chelator and buffer. Us Patent No. 5,376,310. Cincinnati, Ohio, U.S. United States Patent, Procter and Gamble Co.

[46] M. S. Negahban-Azar, Sybil E., Potential Changes in Chemical Soil Quality Resulting from Graywater Recycling for Landscape Irrigation, Water Environment Federation 90(5) (2018) 452-464.

[47] D. Baderna, E. Lomazzi, A. Passoni, A. Pogliaghi, M.I. Petoumenou, R. Bagnati, M. Lodi, A. Viarengo, S. Sforzini, E. Benfenati, R. Fanelli, Chemical characterization and ecotoxicity of three soil foaming agents used in mechanized tunneling, J Hazard Mater 296 (2015) 210-220.

[48] K. Mohan, R. Gupta, K.K. Mohanty, Wettability Altering Secondary Oil Recovery in Carbonate Rocks, Energ Fuel 25(9) (2011) 3966-3973.

[49] J. Hibbs, Anionic Surfactants, Chemistry and Technology of Surfactants 4 (2006) 118-124.

[50] J. Steber, H. Berger, Biodegradability of anionic surfactants. 5, (1995) 134-182.

[51] Steber, J. and Wierich, P. (1987) The anaerobic degradation of detergent range fatty alcohol ethoxylates. Studies with ^{14}C-labelled model surfactants. Water Res.21, 661–667.

[52] Hales, G.S., Watson, G.K., Dodgson, K.S. and White, G.F. (1986) A comparative study of the biodegradation of the surfactant sodium dodecyltriethoxy sulfate by four detergent-degrading bacteria., J. Gen. Microbiol. 132, 953–961.

[53], R. D. Swisher (1987) *Surfactant Biodegradation* 2nd edition, revised and expanded. Marcel Dekker, New York and Basel.

[54] P. D. T. Huibers, Quantum-chemical calculations of the charge distribution in ionic surfactants, Langmuir 15(22) (1999) 7546-7550.

[55] I. Alkorta, J. Elguero, Theoretical study of strong hydrogen bonds between neutral molecules: The case of amine oxides and phosphine oxides as hydrogen bond acceptors, J Phys Chem A 103(2) (1999) 272-279.

[56] E. Lomax, Amphoteric Surfactants, Surfactant Science Series 59(Marcel Dekker) (1996) New York.

[57] V. M. Nace, Nonionic Surfactants: Polyoxyalkylene Block Copolymers, Surfactant Science Series 60(Marcel Dekker) (1996) New York.

[58] S. M. Blagojevic, N.D. Pejic, S.N. Blagojevic, Synergism and Physicochemical Properties of Anionic/Amphoteric Surfactant Mixtures with Nonionic Surfactant of Amine Oxide Type, Russ J Phys Chem A, 91(13) (2017) 2690-2695.

[59] Y. N. Y. Nagahara, M. Isoda, Y. Yamagata, N. Nishikawa, K. Takada, Structure and Performance of Cationic Assembly Dispersed in Amphoteric Surfactants Solution as a Shampoo for Hair Damaged by Coloring, Journal of Oleo Science 56(6) (2007) 289-295.

[60] S. M. Blagojevic, N. D. Pejic, S.N. Blagojevic, Synergism and Physicochemical Properties of Anionic/Amphoteric Surfactant Mixtures with Nonionic Surfactant of Amine Oxide Type, Russ J Phys Chem a+ 91(13) (2017) 2690-2695.

[61] Y. N. Y. Nagahara, M. Isoda, Y. Yamagata, N. Nishikawa, K. Takada , Structure and Performance of Cationic Assembly Dispersed in Amphoteric Surfactants Solution as a Shampoo for Hair Damaged by Coloring, Journal of Oleo Science 56(6) (2007) 289-295.

[62] T. P. Goloub, R. J. Pugh, B.V. Zhmud, Micellar interactions in nonionic/ionic mixed surfactant systems, J Colloid Interf Sci 229(1) (2000) 72-81.

[63] F. Li, G.Z. Li, J.B. Chen, Synergism in mixed zwitterionic-anionic surfactant solutions and the aggregation numbers of the mixed micelles, Colloid Surface A 145(1-3) (1998) 167-174.

[64] J. Yang, Viscoelastic wormlike micelles and their applications, Curr Opin Colloid In 7(5-6) (2002) 276-281.

[65] D. Bajpai, Laundry Detergents: An Overview, Journal of Oleo Science 7 (2007) 327-340.

[66] Y. X. Yu, J. Zhao, A.E. Bayly, Development of surfactants and builders in detergent formulations, Chinese J Chem Eng 16(4) (2008) 517-527.

[67] S.H. Im, Y.H. Jeong, J.J. Ryoo, Simultaneous analysis of anionic, amphoteric, nonionic and cationic surfactant mixtures in shampoo and hair conditioner by RP-HPLC/ELSD and LC/MS, Anal Chim Acta 619(1) (2008) 129-136.

[68] R. M. Trüeb, Shampoos: Ingredients, efficacy and adverse effects, Journal of the German Society of Dermatology 5(5) (2007) 256-265.

[69] A. Goldsipe, D. Blankschtein, Titration of mixed micelles containing a pH-sensitive surfactant and conventional (pH-insensitive) surfactants: A regular solution theory modeling approach, Langmuir 22(24) (2006) 9894-9904.

[70] J. Rodriguez-Hernandez, S. Lecommandoux, Reversible Inside−Out Micellization of pH-responsive and Water-Soluble Vesicles Based on Polypeptide Diblock Copolymers. Journal of the american chemical society, 127 (7) (2005) 2026-2027.

[71] Y. X. Li, K. Holmberg, R. Bordes, Micellization of true amphoteric surfactants, J Colloid Interf Sci 411 (2013) 47-52.

[72] W. N. Yu, D. H. N. Manik, C. J. Huang, L. K. Chau, Effect of elimination on antifouling and pH-responsive properties of carboxybetaine materials, Chemical Communications 53(65) (2017) 9143-9146.

[73] A. V. Lezov, P.S. Vlasov, A.A. Lezov, N.S. Domnina, G.E. Polushina, Molecular Properties of Poly(carboxybetaine) in Solutions with Different Ionic Strengths and pH Values, Polym Sci Ser a 53(11) (2011) 1012-1018.

[74] V. Lair, S. Bouguerra, M. Turmine, P. Letellier, Thermodynamic study of the protonation of dimethyldodecylamine N-oxide micelles in aqueous solution at 298 K. Establishment of a theoretical relationship linking critical micelle concentrations and pH, Langmuir 20(20) (2004) 8490-8495

[75] K. Aoki, M. Nakagawa, K. Ichimura, Self-assembly of amphoteric azopyridine carboxylic acids: Organized structures and macroscopic organized morphology influenced by heat, pH change, and light, J Am Chem Soc 122(44) (2000) 10997-11004.

[76] J. E. Klijn, M.C.A. Stuart, M. Scarzello, A. Wagenaar, J.B.F.N. Engberts, pH-dependent phase behavior of carbohydrate-based gemini surfactants. Effect of the length of the hydrophobic spacer, J Phys Chem B 110(43) (2006) 21694-21700.

[77] M. Johnsson, A. Wagenaar, M.C.A. Stuart, J.B.F.N. Engberts, Sugar-based gemini surfactants with pH-dependent aggregation behavior: Vesicle-to-micelle transition, critical micelle concentration, and vesicle surface charge reversal, Langmuir 19(11) (2003) 4609-4618.

[78] W. Wang, W. Lu, L. Jiang, Influence of pH on the aggregation morphology of a novel surfactant with single hydrocarbon chain and multi-amine headgroups, J Phys Chem B 112(5) (2008) 1409-1413.

[79] A. Goldsipe, D. Blankschtein, Molecular-thermodynamic theory of micellization of multicomponent surfactant mixtures: 2. pH-sensitive surfactants, Langmuir 23(11) (2007) 5953-5962.

[80] C. Carnero Ruiz, Thermodynamics of micellization of tetradecyltrimethylammonium bromide in ethylene glycol-water binary mixtures, Colloid and Polymer Science, 277 (7), (1999), 701-707.

[81] Z. Jiang, X.F. Li, G.F. Yang, L. Cheng, B. Cai, Y. Yang, J.F. Dong, pH-Responsive Surface Activity and Solubilization with Novel Pyrrolidone-Based Gemini Surfactants, Langmuir 28(18) (2012) 7174-7181.

[82] K. Ohki, F. Tokiwa, Potentiometric Titration of Amphoteric Surfactants in Micellar Solutions, The Journal of Physical Chemistry 71(6) (1966) 1824-1828.

[83] H. Katsuura, N. Takisawa, M. Manabe, H. Maeda, Effect of the protonation equilibrium on the interaction of mixed micelles with their counterions, Colloid Polym Sci 277(2-3) (1999) 261-264.

[84] H. Maeda, S. Muroi, M. Ishii, R. Kakehashi, H. Kaimoto, T. Nakahara, K. Motomura, Effects of Ionization on the Critical Micelle Concentration and the Surface Excess of Dodecyldimethylamine Oxide in Salt-Solutions, J Colloid Interf Sci 175(2) (1995) 497-505.

[85] H. Zhang, P.L. Dubin, J.I. Kaplan, Potentiometric and Dynamic Light-Scattering-Studies of Micelles of Dimethyldodecylamine Oxide, Langmuir 7(10) (1991) 2103-2107.

[86] Y. Imaishi, R. Kakehashi, T. Nezu, H. Maeda, Dodecyldimethylamine oxide micelles in solutions without added salt, J Colloid Interf Sci 197(2) (1998) 309-316.

[87] H. Maeda, Dodecyldimethylamine oxide micelles: Stability, aggregation number and titration properties, Colloid Surface A 109 (1996) 263-271.

[88] M. Scarzello, J.E. Klijn, A. Wagenaar, M.C.A. Stuart, R. Hulst, J.B.F.N. Engberts, pH-dependent aggregation properties of mixtures of sugar-based gemini surfactants with phospholipids and single-tailed surfactants, Langmuir 22(6) (2006) 2558-2568.

[89] A. W. M. Johnsson, J. B. F. N. Engberts, Sugar-Based Gemini Surfactant with a Vesicle-to-Micelle Transition at Acidic pH and a Reversible Vesicle Flocculation near Neutral pH, Journal of American Chemical Society 125 (2002) 757-760.

[90] H. Kaimoto, K. Shoho, S. Sasaki, H. Maeda, Aggregation Numbers of Dodecyldimethylamine Oxide Micelles in Salt-Solutions, J Phys Chem-Us 98(40) (1994) 10243-10248.

[91] D. X. Wang, S.Y. Li, Y. Ying, M.J. Wang, H.M. Xiao, Z.X. Chen, Theoretical and experimental studies of structure and inhibition efficiency of imidazoline derivatives, Corros Sci 41(10) (1999) 1911-1919.

[92] J. F. Rathman, J. G. Weers, F. U. Axe, C. A. Crichlow, L. D. Poland, D. R. Scheuing, R. J. Wiersema, A. G. Zielske, Effect of the Intramolecular Charge Separation Distance onthe Solution Properties of Betaines and Sulfobetaines, Langmuir 7 (1991) 854-567.

[93] T. T. L. Nguyen, A. Edelen, B. Neighbors, D.A. Sabatini, Biocompatible lecithin-based microemulsions with rhamnolipid and sophorolipid biosurfactants: Formulation and potential applications, J Colloid Interf Sci 348(2) (2010) 498-504.

[94] D. Myers, Surfactant Science and Technology, Wiley-Interscience Third Edition (Hoboken, NewJersey) (2017).

[95] M. Mandado, C. Van Alsenoy, R.A. Mosquera, Joint QTAIM and Hirshfeld study of the sigma and pi charge distribution and electron delocalization in carbonyl compounds: A comparative study with the resonance model, J Phys Chem A 109(38) (2005) 8624-8631.

[96] S. N. Blagojevic, S.M. Blagojevic, N.D. Pejic, Performance and Efficiency of Anionic Dishwashing Liquids with Amphoteric and Nonionic Surfactants, J Surfactants Deterg 19(2) (2016) 363-372.

[97] T. Crutcher, K.R. Smith, J.E. Borland, J.D. Sauer, J.W. Perine, Alkydimethylamine Oxides as Synergistic Fabric Softeners, J Am Oil Chem Soc 69(7) (1992) 682-689.

[98] J. H. Miller, D.A. Quebedeaux, J.D. Sauer, Amine Oxide/Alcohol Ethoxylate Blends Zero-Phosphate, High-Performance, Hard-Surface Cleaners, J Am Oil Chem Soc 72(7) (1995) 857-859.

[99] A. M. Corner, M.M. Dolan, S.L. Yankell, D. Malamud, C31g, a New Agent for Oral Use with Potent Antimicrobial and Antiadherence Properties, Antimicrob Agents Ch 32(3) (1988) 350-353.

[100] H. Maeda, R. Kakehashi, Effects of protonation on the thermodynamic properties of alkyl dimethylamine oxides, Adv Colloid Interfac 88(1-2) (2000) 275-293.

[101] S. Soontravanich, S. Walsh, J.F. Scamehorn, J.H. Harwell, D.A. Sabatini, Interaction Between an Anionic and an Amphoteric Surfactant. Part II: Precipitation, J Surfactants Deterg 12(2) (2009) 145-154.

[102] G. D'Errico, O. Ortona, L. Paduano, A. Tedeschi, V. Vitagliano, Mixed micellar aggregates of cationic and nonionic surfactants with short hydrophobic tails. An intradiffusion study, Phys Chem Chem Phys 4(21) (2002) 5317-5324.

[103] M. T. Garcia, E. Campos, I. Ribosa, Biodegradability and ecotoxicity of amine oxide based surfactants, Chemosphere 69(10) (2007) 1574-1578.

[104] F. Rios, M. Lechuga, M. Fernandez-Serrano, A. Fernandez-Arteaga, Aerobic biodegradation of amphoteric amine-oxide-based surfactants: Effect of molecular structure, initial surfactant concentration and pH, Chemosphere 171 (2017) 324-331.

[105] F. Rios, M. Lechuga, A. Fernandez-Arteaga, E. Jurado, M. Fernandez-Serrano, Anaerobic digestion of amine-oxide-based surfactants: biodegradation kinetics and inhibitory effects, Biodegradation 28(4) (2017) 303-312.

[106] S. E. Belanger, J. L. Brill, J.M. Rawlings, K.M. McDonough, A.C. Zoller, K.R. Wehmeyer, Aquatic toxicity structure-activity relationships for the zwitterionic surfactant alkyl dimethyl amine oxide to several aquatic species and a resulting species sensitivity distribution, Ecotox Environ Safe 134 (2016) 95-105.

[107] J. Lim, D. Han, Synthesis of dialkylamidoamine oxide surfactant and characterization of its dual function of detergency and softness, Colloid Surface A 389(1-3) (2011) 166-174.

[108] M. Baglioni, Y. J. Benavides, D. Berti, R. Giorgi, U. Keiderling, P. Baglioni, An amine-oxide surfactant-based microemulsion for the cleaning of works of art, J Colloid Interf Sci 440 (2015) 204-210.

[109] R. T. Wang, Y. L. Li, Q.X. Li, Synthesis and Properties of Dodecyldiethoxylamine Oxide, J Surfactants Deterg 16(4) (2013) 509-514.

[110] D. O.Barlow. G. L. K. Hoh, A. F. Chadwick, D. B. Lake, S. R. Sheeran, Hydrogen peroxide oxidation of tertiary amines, Journal of the American Oil Chemists' Society 40(7) (1963) 268-271.

[111] R. Lindigkeit, A. Biller, M. Buch, H. M. Schibel, M, Bopprè, T. Hartmann, The two Faces of Pyrrolizidine Alkaloids: the Role of the Tertiary Amine and its *N* Oxide in Chemical Defense of Insects with Acquired Plant Alkaloids, The FEBS Journal, 245 (1997), 626-636.

[112] K. Bergstad, J. E. Backvall, Mild and efficient flavin-catalyzed H2O2 oxidation of tertiary amines to amine N-oxides, J Org Chem 63(19) (1998) 6650-6655.

[113] K. K. M. Fleischmann, D. Pletcher, the kinetics and mechanism of the oxidation of amines and alcohols at oxide-covered nickel, silver, copper, and cobalt electrodes, Journal of Chemical Society 2 (1972) 1396-1403.

[114] C. J. Toney, F. E. Friedli, P. J. Frank, Kinetics and Preparation of Amine Oxides, J Am Oil Chem Soc 71(7) (1994) 793-794.

[115] L.W. Burnette, Miscellaneous Nonionic Surfactants, in Nonionic Surfactants, Surfactant Science Series 1 (1966) 403-410.

[116] Y. Hayashi, F. Shirai, T. Shimizu, Y. Nagano, K. Teramura, Synthesis and Properties of 2-Alkoxy-N, N-Dimethylethylamine N-Oxides, J Am Oil Chem Soc 62(3) (1985) 555-557.

[117] W. N. Marmer, W. M. Linfield, Soap Based Detergent Formulations: XVII. Synthesis and Surface Active Properties of Alkyl Benzene Derived Amine Oxides, Journal of american Oil Chemical Society 53 (1976) 73-76.

[118] P. R. Kust, J.F. Rathman, Synthesis of Surfactants by Micellar Autocatalysis - *N,N*-Dimethyldodecylamine N-Oxide, Langmuir 11(8) (1995) 3007-3012.

[119] S. K. Singh, M. Banjpai, V. K. Tyagi, Amine Oxide: A Review, Journal of Oleo Science 55(3) (2006) 99–119.

[120] A. P. Gerola, P. F. A. Costa, F. Nome, F. Quina, Micellization and adsorption of zwitterionic surfactants at the air/water interface, Current Opinion in Colloid & Interface Science, 32 (2017) 48-56.

[121] T. Imae, R. Kamiya, S. Ikeda. Electron Microscopic Observation of Rod-Like Micelles of Dimethyloleylamine Oxide Regenerated from Its Aqueous Solutions J Colloid Interf Sci 99 (1984) 300-301.

[122] R. Kakehashi, S. Yamamura, N. Tokai, T. Takeda, K. Kaneda, K. Yoshinaga, H. Maeda, Hydrogen ion titration of long alkyl chain amine oxide micelles, J Colloid Interf Sci 243(1) (2001) 233-240

[123] S. Ikaeda, M. A. Tsunoda, H. Maeda, The effects of ionization on micelle size of dimethyldodecylamine oxide, Journal of Colloid and Interface Science, 70 (3) 1979, 448-455.

[124] K. Fukada, M. Kawasaki, T. Kato, H. Maeda, Structure of lyotropic liquid crystals of the dodecyldimethylamine oxide-HCl-water system, Langmuir 16(6) (2000) 2495-2501

[125] P. W. Atkins. *Physical Chemistry*. W. H. Freeman & Company, New York: 1994.

[126] V. Kocherbitov, O. Söderman, Hydration of Dimethyldodecylamine-*N*-oxide: Enthalpy and Entropy Driven Processes, *J. Phys. Chem. B* 2006**,** *110,* 13649-13655.

[127] C. R. Birnie, D. Malamud, R. L. Schnaare, Antimicrobial evaluation of *N*-alkyl betaines and *N*-alkyl-*N,N*-dimethyl-1-amine oxides with variations in chain length, Antimicrob Agents Ch 44(9) (2000) 2514-2517.

[128] D. M. Lugo, J. Oberdisse, A. Lapp, G. H. Findenegg, Effect of Nanoparticle Size on the Morphology of Adsorbed Surfactant Layers, The Journal of Physical Chemistry B, 114 (12), 2010, 4183-4191.

[129] D. J. Barlow, M. J. Lawrence, T. Zuberi, S. Zuberi, R. K. Heenan, Small-angle neutron-scattering studies on the nature of the incorporation of polar oils into aggregates of *N,N*-dimethyldodecylamine-N-oxide, Langmuir 16(26) (2000) 10398-10403.

[130] H. Kawasaki, A. Sasaki, T. Kawashima, S. Sasaki. R. Kakeashi, I. Yamashita, K. Fukada, T. Kato, H. Maeda, Protonation-Induced Structural Change of Lyotropic

Liquid Crystals in Oley- and Alkyldimethylamine Oxides/ Water Systems, *Langmuir* 2005**,** *21,* 5731-5737

[131] R. Hao, R. Xing, Z. Xu, Y. Hou, S. Gao, S. Sun, Synthesis, Functionalization, and Biomedical Applications of Multifunctional Magnetic Nanoparticles, Advanced Material, 2010, 22, 2729-2742.

[132] H. Q. Liu, G.Y. Shi, B.C. Xu, S.Y. Chen, G.J. Zhang, Synthesis, Characterization and Properties of N-Alkyl-*N,N*-di(2-hydroxyethyl) Amine Oxides, J Surfactants Deterg 20(1) (2017) 129-136.

[133] B. Sansoni, SDA Research Demonstrates Safety of Amine Oxides, J Surfactants Deterg 7 (2004) 347.

[134] C. L. Roggenkamp, (1976). Acidic emollient liquid detergent composition. US Patent No. 3,943,234. Cincinnati, Ohio, U.S. United States Patent, Procter and Gamble Co.

[135] T. Gerstein, (1977). Non-irritating shampoo compositions containing stearyl amine oxide. US Patent No 4,033,895 Cincinnati, Ohio, U.S. United States Patent, Procter and Gamble Co.

[136] C. C. Kwok, M. S. Wong, Investigation of multifunctional, light-emitting dendrimers: effect of dendritic wedge, Thin Solid Films 417(1-2) (2002) 136-142.

[137] C. L. Burnett, Amended final report of the safety assessment of Drometrizole as used in cosmetics, Int J Toxicol 27 (2008) 63-75.

[138] R. Mena-Brito, (2012). Cleaning composition, U. S. Patent Application No. 14/649,852, Cincinnati, Ohio, U.S. United States Patent, Procter and Gamble Co.

[139] S. W. S. Frantz, (2005). New branched sulfates for use in personal care formulations, US Patent App. (10,896,464). Cincinnati, Ohio, U.S. United States Patent, Procter and Gamble Co.

[140] B. Wiegland, L. McCulloch, E. Lukenbach, (2002). Personal care formulations, US Patent App. (003, 44, 89). Cincinnati, Ohio, U.S. United States Patent, Procter and Gamble Co.

[141] P. C. Hu, R. J. Corona. (1996). Formulated branched chain alcohol ether sulfate compounds, US Patent App. (5,562,866,). Cincinnati, Ohio, U.S. United States Patent, Procter and Gamble Co.

[142] J. Bock, P. L. Valint Jr, M. W. Kim, M. L. Robbins, P. Steyn, S. Zushma, Krafft points and microemulsion phase behavior of some alkylarenesulfonates, Journal of Colloids and Surfaces 26 (1987) 191-203.

[143] Y. B. A. Garciaa, M. El-Emary, L. Fortney, R. S. Schechter, S. Yiv, W. H. Wade, HLB, CMC, and phase behavior as related to hydrophobe branching, J Colloid Interf Sci 89(1) (1982) 209-216.

[144] O. Dusart. M. P. Lascaux, R. Granet, S. Piekarki, Propribtes superficielles d'hexadecylbenzene sulfonates de sodium ramifies à l'interface eau-air, J Chem Phys 80(7-8) (1983) 5-10.

[145] C. Frank, H. Frielinghaus, J. Allgaier, H. Prast, Nonionic surfactants with linear and branched hydrocarbon tails: Compositional analysis, phase behavior, and film properties in bicontinuous microemulsions, Langmuir 23(12) (2007) 6526-6535.

[146] R. Varadaraj, P. Valint, S. Zushma, R. Thomas, Fundamental Interfacial Properties of Alkyl-Branched Sulfate and Ethoxy Sulfate Surfactants Derived from

Guerbet Alcohols. 1. Surface and Instantaneous Interfaclal Tensions, J Phys Chem-Us 95 (1990) 1671-1676.

[147] M. A. Hashim, J. Kulandai, R. S. Hassan, Biodegradability of branched alkylbenzene sulphonates, Journal of Chemical Technology and Biotechnology, 54 (3), 1992, 207-214.

[148] G. H. Sayed, F. M. Ghuiba, M. I. Abdou, E. A. A. Badr, S. M. Tawfik, N. A. M. Negm, Synthesis, surface and thermodynamic parameters of some biodegradable nonionic surfactants derived from tannic acid, 393, 2012, 96-104

[149] M. T. Garcia, E. Campos, J. Sanchez-Leal, I. Ribosa, Anaerobic degradation and toxicity of commercial cationicsurfactants in anaerobic screening tests, Chemosphere, 41, 2000, 705-710.

[150] S. M. Tawfik, Synthesis, surface, biological activity and mixed micellar phase properties of some biodegradable gemini cationic surfactants containing oxycarbonyl groups in the lipophilic part, Journal of Industrial and Engineering Chemistry, 28, 2015, 171-183.

[151] M. T. Garcia, E. Campos a, I. Ribosa a, A. Latorre b, J. Sanchez-Leala, Anaerobic digestion of linear alkyl benzene sulfonates: Biodegradation kinetics and metabolite analysis, Chemosphere 60 (2005) 1636–1643.

[152] P. F. Souter, A. T. Brooker, L. S. Bewick, C. Ure. (2017). Automatic dishwashing detergent composition. US Patent No. 03,62,538. Cincinnati, Ohio, US, United States Patent.

[153] S. Alexander, J. Eastoe, A. M. Lord, F. Guittard, A. R. Barron, Branched Hydrocarbon Low Surface Energy Materials for Superhydrophobic Nanoparticle Derived Surfaces, Applied Material and Interfacs, 2016,8, 660-666

[154] J. Lu, J. Liyanage, S. Solairaj, S. Adkins, G. P. Arachchilage, D. H. Kim, C. Britton, U. Weerasooriya, G. A. Pope, New surfactant developments for chemical

enhanced oil recovery, Journal of Petroleum Science and Engineering, Journal of Petroleum Science and Engineering, 120, (2014), 94–101

[155] S. Björklund, V. Kocherbitov, Hydration-Induced Phase Transitions in Surfactant and Lipid Films, Langmuir, 32, 2016, 5223-5232.

[156] P. C. Jocelyn, N. Polgar, 26. Methyl-substituted αβ-unsaturated acids. Part I, Journal of Chemical Society (Resume) (0) (1953) 132-135.

[157] P. Pillai, N. Pal, A. Mandal, Synthesis, Characterization, Surface Properties and Micellization Behaviour of Imidazolium-based Ionic Liquids, J Surfactants Deterg 20(6) (2017) 1321-1335.

[158] I. Ali, M.R. Shah, M. Imran, Shafiullah, Synthesis of Sulfur-Based Biocompatible Nonionic Surfactants and Their Nano-Vesicle Drug Delivery, J Surfactants Deterg 20(6) (2017) 1367-1375.

[159] A. L. Barran-Berdon, S.K. Misra, S. Datta, M. Munoz-Ubeda, P. Kondaiah, E. Junquera, S. Bhattacharya, E. Aicart, Cationic gemini lipids containing polyoxyethylene spacers as improved transfecting agents of plasmid DNA in cancer cells, J Mater Chem B 2(29) (2014) 4640-4652.

[160] F. J. Rossotti, The Determination of Stability Constants and Other Equilibrium Constants in Solution, McGraw-Hill Book Company, Inc New York, Toronto, London (1961).

[161] O. Ortona, G. D'Errico, L. Paduano, V. Vitagliano, Interaction between cationic, anionic, and non-ionic surfactants with ABA block copolymer Pluronic PE6200 and with BAB reverse block copolymer Pluronic 25R4, J Colloid Interf Sci 301(1) (2006) 63-77.

[162] A. Lomakin, D. B. Teplow, G.B. Benedek, Quasi elastic light scattering for protein assembly studies, in: E.M. Sigurdsson (Ed.), Amyloid Proteins: Methods and Protocols, 299 Humana Press, Totowa, New Jersey., (2005).

[163] H. X. Zhang, O. Annunziata, Effect of macromolecular polydispersity on diffusion coefficients measured by Rayleigh interferometry, J Phys Chem B 112(12) (2008) 3633-3643.

[164] I. Russo Krauss, R. Imperatore, A. De Santis, A. Luchini, L. Paduano, G. D'Errico, Structure and dynamics of cetyltrimethylammonium chloride-sodium dodecylsulfate (CTAC-SDS) catanionic vesicles: High-value nano-vehicles from low-cost surfactants, J Colloid Interf Sci 501 (2017) 112-122.

[165] A. F. Dexter, A.S. Malcolm, A.P.J. Middelberg, Reversible active switching of the mechanical properties of a peptide film at a fluid-fluid interface, Nat Mater 5(6) (2006) 502-506.

[166] P. Bartlett, R.H. Ottewill, A neutron scattering study of the structure of a bimodal colloidal crystal, J. Chem. Phys. 96 (1992) 3306–3318.

[167] T. P. Russell, J.S. Lin, S. Spooner, G.D. Wignall, Intercalibration of small-angle X-ray and neutron scattering data, J. Appl. Crystallogr. 21 (1988) 629–638.

[168] Ornstein, L. S.; Zernike, F. Proceedings of the Section of Sciences. Koninklijke Akademie Van Wetenschappen te Amsterdam (1914), *17*, 793.

[169] Hayter, J. B.; Penfold, An analytic structure factor for macroion solutionsJ. Mol. Phys. (1981), 42, 109.

[170] Hayter, J. B.; Penfold, A rescaled MSA structure factor for dilute charged colloidal dispersions, J. J. Chem. Soc., Faraday Trans. 1 (1981), 77, 1851.

[171] Hansen, J. P.; Hayter, Concentrated colloidal dispersions viewed as **one**-component macrofluids, J. B. Mol. Phys. (1983), 46, 651.

[172] S. Björklund, V. Kocherbitov, Humidity scanning quartz crystal microbalance with dissipation monitoring setup for determination of sorption-desorption isotherms and rheological changes, Review of Scientific Instruments 86(5) (2015) 055105.

[173] M. W. Ferry, (1981). Detergent compositions containing amine oxide and non-ionic surfactants and polyethykene glycol US Patent No (4,276,205). Cincinnati, Ohio, U.S. United States Patent, Procter and Gamble Co.

[174] K. M. Mullen, J. Mercurio, C.J. Serpell, P.D. Beer, Exploiting the 1,2,3-Triazolium Motif in Anion-Templated Formation of a Bromide-Selective Rotaxane Host Assembly, Angew Chem Int Edit 48(26) (2009) 4781-4784.

[175] K. Bergstad, J.E. Backvall, Mild and efficient flavin-catalyzed H_2O_2 oxidation of tertiary amines to amine N-oxides, J Org Chem 63(19) (1998) 6650-6655.

[176] A. C. Cope, E. R. Trumbull, Olefins from amines, the Hofmann elimination reaction and amine oxide pyrolysis, Organic reactions 5 (1960) 317-387.

[177] A. Laezza, A. Casillo, S. Cosconati, C.I. Biggs, A. Fabozzi, L. Paduano, A. Iadonisi, E. Novellino, M.I. Gibson, A. Randazzo, M.M. Corsaro, E. Bedini, Decoration of Chondroitin Polysaccharide with Threonine: Synthesis, Conformational Study, and Ice-Recrystallization Inhibition Activity, Biomacromolecules 18(8) (2017) 2267-2276.

[178] L. Goracci, R. Germani, J.F. Rathman, G. Savelli, Anomalous behavior of amine oxide surfactants at the air/water interface, Langmuir 23(21) (2007) 10525-10532.

 [179] F. Tokiwa, K. Ohki, potentiometric titration of nonionic-cationic surfactants, The Journal of Phyirical Chemistry 70 (1966) 3437-3441.

[180] V. Lair, S. Bouguerra, M. Turmine, P. Letellier, Thermodynamic study of the protonation of dimethyldodecylamine N-oxide micelles in aqueous solution at 298 K. Establishment of a theoretical relationship linking critical micelle concentrations and pH, Langmuir 20(20) (2004) 8490-8495.

[181] A. A-J. L. Martínez-Balbuena, Ernesto Hernández-Zapata, C. Márquez-Beltránd., Applicability of the Gibbs Adsorption Isotherm to the analysis of

experimental surface-tension data for ionic and nonionic surfactants, Adv Colloid Interfac 274 (2017) 178-184.

[182] S. R. Green, T.J. Su, J.R. Lu, J. Penfold, The monolayer structure of the branched nonyl phenol oxyethylene glycols at the air-water interface, J Phys Chem B 104(7) (2000) 1507-1515.

[183] J. L. Wang, A.V. Nguyen, S. Farrokhpay, A critical review of the growth, drainage and collapse of foams, Adv Colloid Interfac 228 (2016) 55-70.

[184] Y. Wang, X.C. Liu, Y.W. Zhou, J.P. Niu, Influence of Hydrocarbon Chain Branching on Foam Properties of Olefin Sulfonate with FoamScan, J Surfactants Deterg 19(6) (2016) 1215-1221.

[185] L. Mol, B. Bergenstahl, P. M. Claesson, Forces in dimethyldodecylamine oxide- and dimethyldodecylphosphine oxide-water systems measured with an osmotic stress technique, Langmuir 9 (1993) 2926–2932.

[186] N. A. Blumenschein, D. Han, M. Caggioni, A. J. Steckl, Magnetic particles as liquid carriers in the microfluidic lab-in-tube approach to detect phase change. ACS Applied Materials & Interfaces 6 (2014) 8066−8072.

[187] J. Lee, A. Bose, A. Tripathi, Rapid exploration of phase behavior in surfactant systems using flow in microchannels. Langmuir, 22 (2006) 11412–11419.

[188] A. Peschel, A. Langhoff, E. Uhl, A. Dathathreyan, S. Haindl, D. Johannsmann, I. Reviakine, Lipid phase behavior studied with a quartz crystal microbalance: A technique for biophysical studies with applications in screening, Journal of Chemical Physics,145(20) (2016) 204904/1−204904/11.

[189] S. D. Zor, H. Cankurtaran, QCM humidity sensors based on organic/inorganic nanocomposites of water soluble-conductive poly(diphenylamine sulfonic acid), International Journal of Electrochemical Science 11(9) (2016) 7976–7989.

[190] L. Benjamin, Partial molal volume changes during micellization and solution of nonionic surfactants and perfluorocarboxylates using a magnetic density balance, *J. Phys. Chem.* (1966) *70*, 3790.

[191] Warisnoicharoen, W.; Barlow, D. J.; Lawrence, M. J.; Lu, J. R.; Muslim, A. M.; Penfold, J.; Su, T. J.; Webster, J. R. P.; Zuberi, T. *Langmuir*, submitted for publication, 2000.

[192] G. Montalvo, M. Valiente, E. Rodenas, Rheological properties of the L phase and the hexagonal, lamellar, and cubic liquid crystals of the CTAB/benzyl alcohol/water system, Langmuir 12(21) (1996) 5202–5208.

[193] S. V. Ahir, P.G. Petrov, E.M. Terentjev, Rheology at the phase transition boundary: 2. Hexagonal phase of Triton X100 surfactant solution, Langmuir 18(24) (2002) 9140-9148.

[194] D. Roux, F. Nallet, O. Diat, Rheology of Lyotropic Lamellar Phases, Europhys Lett 24(1) (1993) 53-58.

[195] C. A. Dreiss, Wormlike micelles: where do we stand? Recent developments, linear rheology and scattering techniques, Soft Matter, 3, (2007), 956-970.

[196] C. Richards, G.J.T. Tiddy, S. Casey, Liquid crystal and solution phases of sodium dodecyl-*p*-benzene sulfonate (LAS) and hexa-oxyethylene glycol dodecyl ether ($C_{12}E_6$); 1:1 mixture in water, Colloid. Surf. A 288 (2006) 103–112.

[197] C. Richards, M.S. Mohammadi, G.J.T. Tiddy, Colloid., Formulating liquid detergents with naturally derived Surfactants-Phase behaviour, crystallisation and rheo-stability of primary alkyl sulphates based on coconut oil Surf. A 338 (1-3) (2009) 119-128.

[198] A. Saupe, Textures, Deformations, and Structural Order of Liquid Crystals, Journal of Colloid Interface Science, 58 (1977) 549–558.

[199] A. N. Galatanu, I.S. Chronakis, F.A. Dan, A. Khan, Ternary Phase Diagram of the Triton X-100/Poly(acrylic acid)/Water System Langmuir 16 (2000) 4922–4928.

[200] F. B. Rosevear, Liquid Crystals: The Mesomorphic Phases of Surfactant Compositions, J. Soc. Cosmet. Chem. 19 (1968) 581–594.

6) Supplementary materials

1) Phase behaviour of $C_{10}DAO$-branched/water and $C_{10}DAO$-linear water systems.
In Figure 1-2 the surfactant composition prepared for ocular inspection and SANS (
⬤); POM and SAXS(△), HS QCM-D (⬤, △)and rheology for C_{10}DAO-branched/water and C_{10}DAO-linear water systems are reported, respectively.
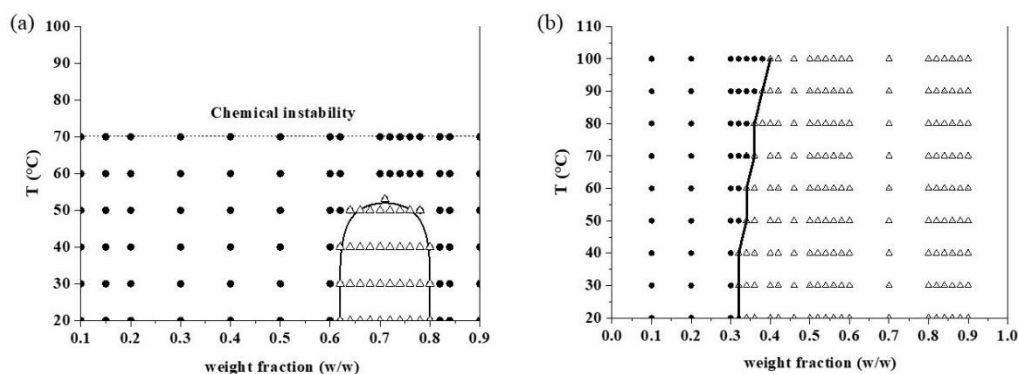
Figure S1. (A) Binary compositions prepared for ocular inspection, POM, SAXS, SANS, HS QCM-D and rheology analysis for C_{10}DAO-branched/water system; (B) Binary compositions prepared for ocular inspection, POM, SAXS, SANS, HS QCM-D and rheology analysis for C_{10}DAO-linear/water system.

2) Nuclear Magnetic Resonance (NMR) analysis
In Figure S2 the β-elimination mechanism of the *N,N*-dimethyl-2-propylheptan-1-amine oxide is reported. In general, at high temperature the linear amine oxide tends

to form an alkene and hydroxylamine [1]. The β-elimination mechanism is more favored for branched surfactants. Indeed, at high temperature (70 °C) the treatment of the *N,N*-dimethyl-2-propylheptan-1-amine oxide leads to the formation of a more stable alkene, 4-methylenenonane and *N,N*-dimethylhydroxylamine. In the figure S2 the ^{1}H NMR spectrum of the *N,N*-dimethyl-2-propylheptan-1-amine oxide, 4-methylenenonane and *N,N*-dimethylhydroxylamine is reported.
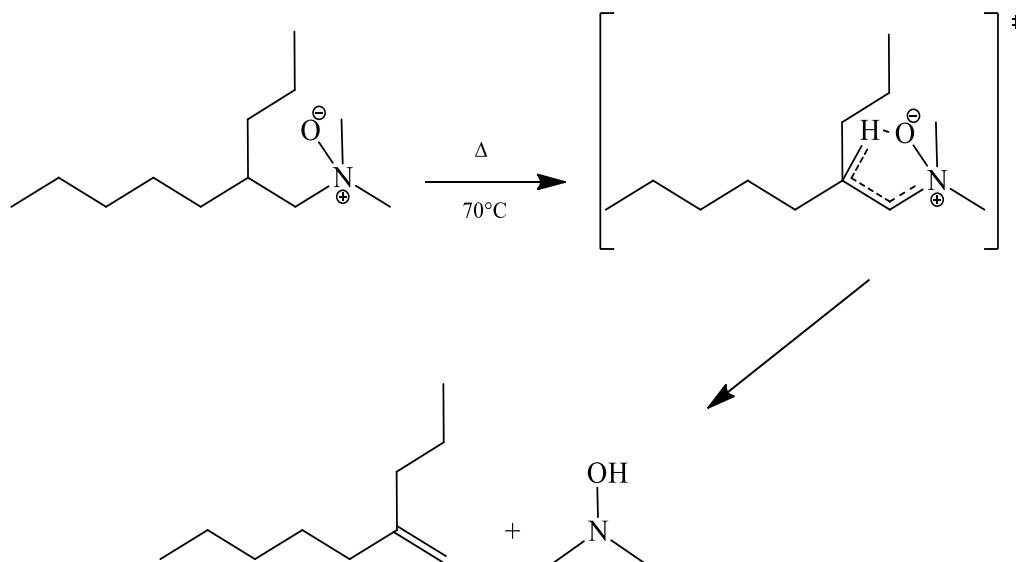
Scheme S$_2$. β-elimination mechanism of the *N,N*-dimethyl-2-propylheptan-1-amine oxide.

At δ=0.88-0.93 ppm, multiplet signals of terminal C$\underline{H}_3$ groups are registered. At δ=1.28-1.43 ppm, multiplet signals of C$\underline{H}_2$ groups are detected. At δ=1.96 ppm, singlet signal of terminal C$\underline{H}$ in β respect to the N$^+$O$^-$ group is registered. At δ=2.47 ppm, singlet signal of terminal C$\underline{H}_3$ groups of the *N,N*-dimethylhydroxylamine is registered. At δ=3.14-3.22 ppm, signals of C$\underline{H}_2$ in a to N$^+$O$^-$ group and C$\underline{H}_3$ bond to N$^+$O$^-$ group. At δ=4.68-5.10 ppm signals of the C$\underline{H}$ of the alkene are registered.
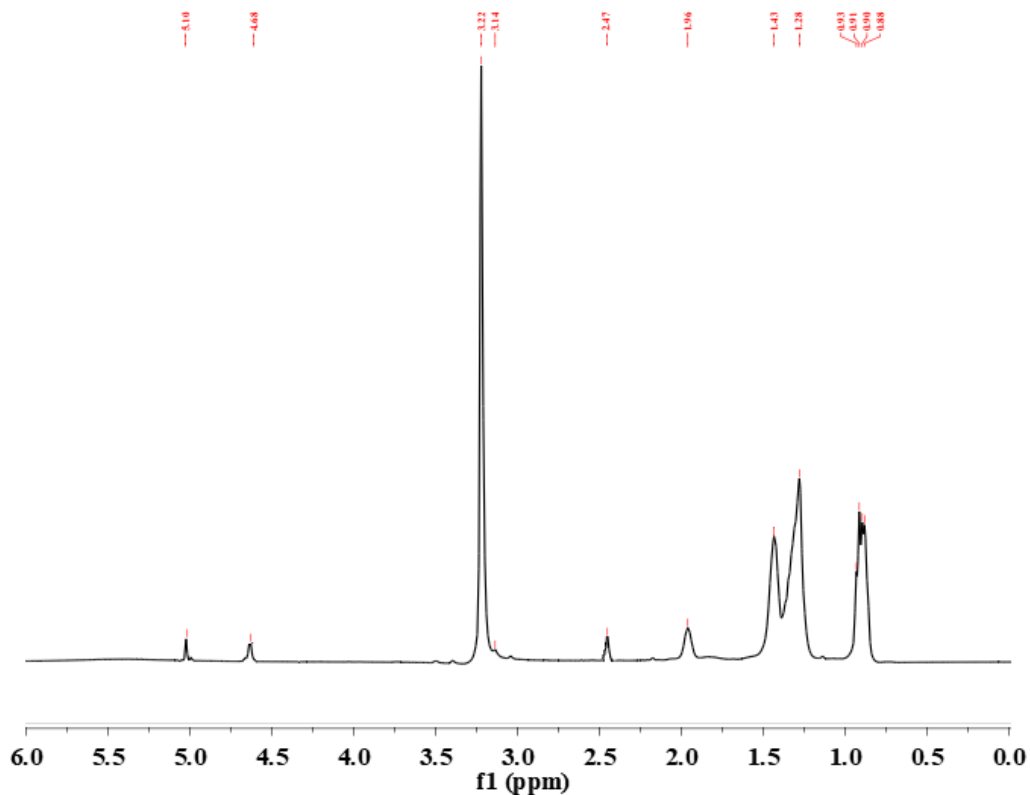
Figure S₂. ¹H NMR spectrum of *N,N*-dimethyl-2-propylheptan-1-amine β-elimination mechanism of in CDCl₃

3.2 Phase behavior: validation of the HS QCM-D method Δf/n and ΔD/n versus hydration time.

In the Figure S₄ the *Δf/n* and *ΔD/n* curve profiles as a function of time during continuous hydration at 25 °C for the system C₁₀DAO-branched/water and C₁₀DAO-linearwater are reported, respectively.
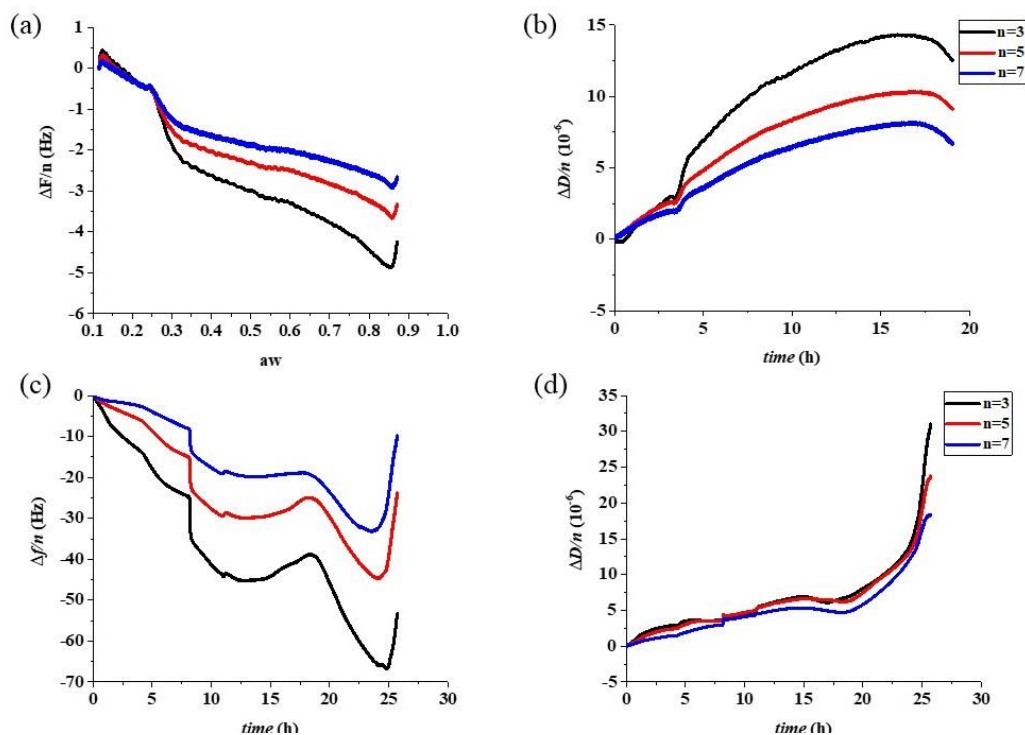
Figure S$_4$. (A)The $\Delta f/n$ and $\Delta D/n$ curve profiles for the system C$_{10}$DAO-branched/water as a function of time during continuous hydration at 25 °C. (B) The $\Delta f/n$ and $\Delta D/n$ curve profiles for the system C$_{10}$DAO-linear/water as a function of time during continuous hydration at 25 °C.

In the Figure S$_5$ the film thickness by comparing data obtained for uncoated and coated sensor was determined. For the HS QCM-D measurements, the surfactant solution was deposited ten times, leading to a film thickness of 180 and 160 nm for C$_{10}$DAO-branched and C$_{10}$DAO-linear, respectively.
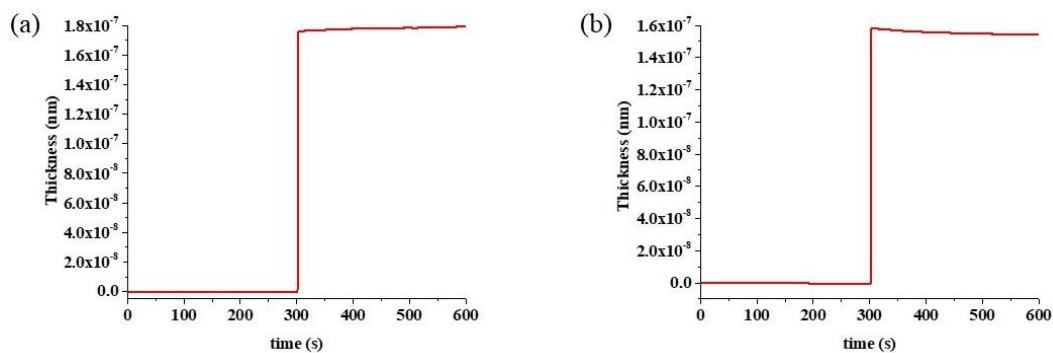

Figure S$_5$. The film thickness of 180 and 160 nm for (A) C$_{10}$DAO-branched and (B) C$_{10}$DAO-linear, was reported, respectively.

136

In the figure S_6 the film thickness, determined by comparing data obtained for uncoated and coated sensor was reported. Particularly, the film thickness was found to increase with the number of spin-coating deposition.
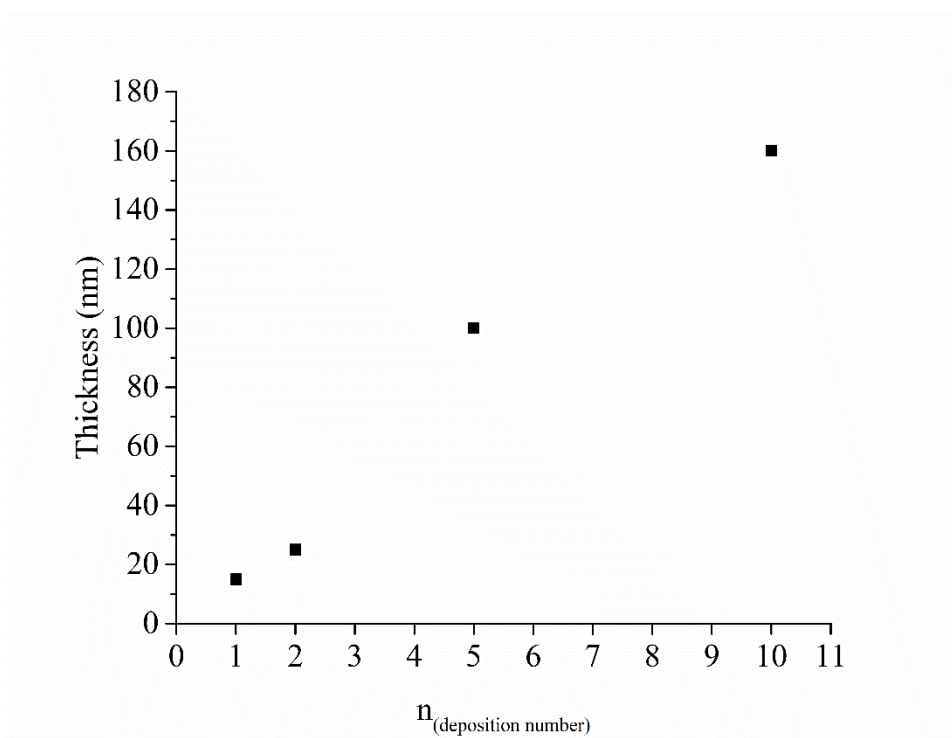

Figure S_6 the film thickness variation versus the deposition number

In the Figure S_7 the film thickness by comparing data obtained for uncoated and coated sensor was determined. For the HS QCM-D measurements, the surfactant solution was deposited ten times, leading to a film thickness of 105 and 100 nm for $C_{10}DAO$-branched/AES and $C_{10}DAO$-linear/AES, respectively.
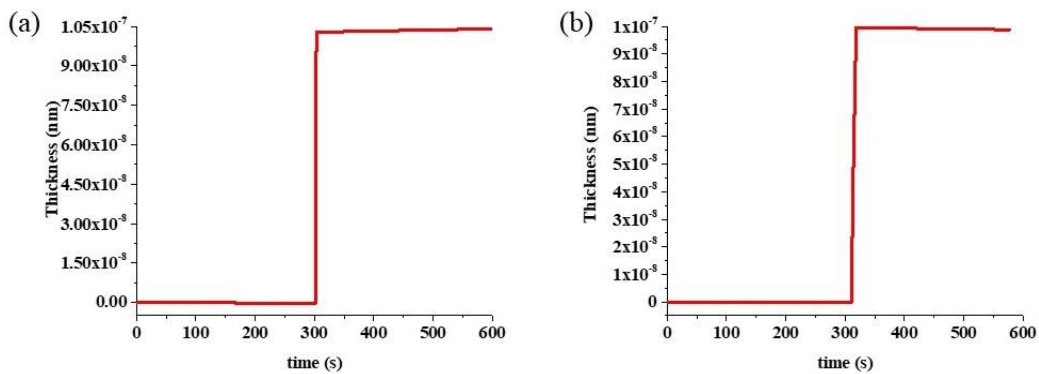
Figure S$_7$. The film thickness of 105 and 100 nm for (A) C$_{10}$DAO-branched/AES, (B) C$_{10}$DAO-linear/AES $w_{C_{10}DAO} = 0.50$ $w_{AES} = 0.50$ was reported, respectively.

In the Figure S$_4$ the Δ*f/n* and Δ*D/n* curve profiles as a function of time during continuous hydration at 25 °C for the system C$_{10}$DAO-branched/AES and C$_{10}$DAO-linear/AES are reported, respectively.
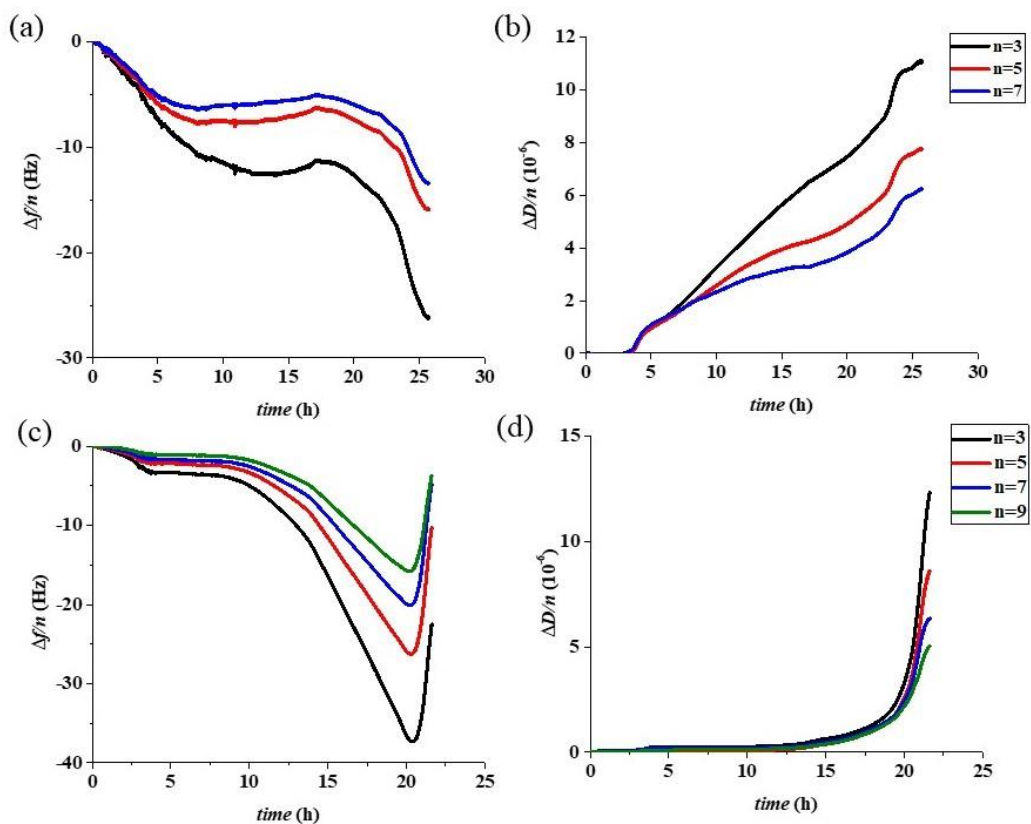
Figure S$_8$. (A)The $\Delta f/n$ and $\Delta D/n$ curve profiles for the system C$_{10}$DAO-branched/water as a function of time during continuous hydration at 25 °C. (B) The $\Delta f/n$ and $\Delta D/n$ curve profiles for the system C$_{10}$DAO-linear/water as a function of time during continuous hydration $w_{C_{10}DAO} = 0.50$ $w_{AES} = 0.50$ at 25 °C.
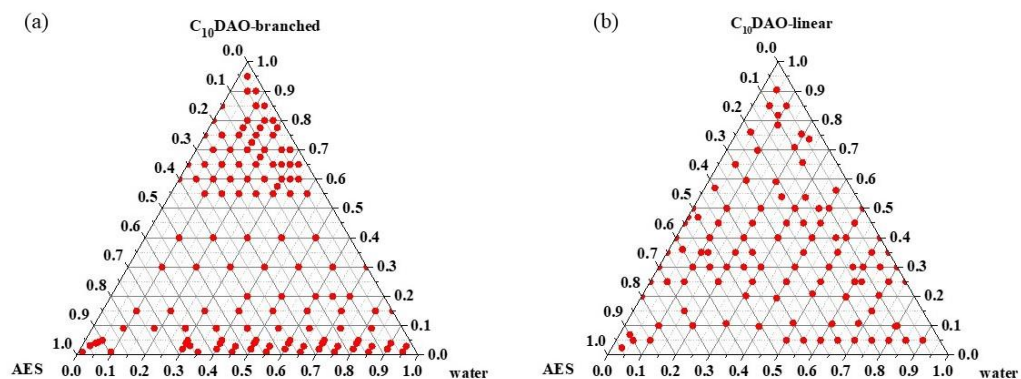
Figure S9. Ternary compositions of $C_{10}DAO$-branched/AES/water and $C_{10}DAO$-linearAES/water systems prepared for ocular inspection, POM, SAXS, Rheology analysis.

Equation EqS_1 used to fitt the SANS data of $C_{10}DAO$-linear w_s=0.15 with an ellipsoidal model.
The output of the 2D scattering intensity function for oriented ellipsoids is given by (Feigin, 1987)

$$P(q,\alpha) = \frac{\text{scale}}{V} F^2(q,\alpha) + \text{background}$$

Where

$$F(q,\alpha) = \frac{3\Delta\rho V(\sin[qr(R_p, R_e, \alpha)] - \cos[qr(R_p, R_e, \alpha)])}{[qr(R_p, R_e, \alpha)]^3}$$

And

$$r(R_p, R_e, \alpha) = \left[R_e^2 \sin^2\alpha + R_p^2 \cos^2\alpha\right]^{1/2}$$

α is the angle between the axis of the ellipsoid and $\vec{q}\rightarrow$, $V=(4/3)\pi R_p R_e^2$ is the volume of the ellipsoid , Rp is the polar radius along the rotational axis of the ellipsoid, Re is the equatorial radius perpendicular to the rotational axis of the ellipsoid and $\Delta\rho$ (contrast) is the scattering length density difference between the scatterer and the solvent.

Equation EqS_2 used to fitt the SANS data of $C_{10}DAO$-branched w_s=0.15 with an hardsphere model.

$$I(q) = \frac{\text{scale}}{V} \cdot \left[3V(\Delta\rho) \cdot \frac{\sin(qr) - qr\cos(qr)}{(qr)^3}\right]^2 + \text{background}$$

where *scale* is a volume fraction, V is the volume of the scatterer, rr is the radius of the sphere and *background* is the background level. *sld* and *sld_solvent* are the scattering length densities (SLDs) of the scatterer and the solvent respectively, whose difference is $\Delta\rho$.

Equation EqS_3 used to fitt the SANS data of $C_{10}DAO$-branched w_s=0.40 with an cylinder model.

$$P(q,\alpha) = \frac{\text{scale}}{V} F^2(q,\alpha).\,sin(\alpha) + \text{background}$$

Where

$$F(q,\alpha) = 2(\Delta\rho)V \frac{\sin\left(\frac{1}{2}qL\cos\alpha\right)}{\frac{1}{2}qL\cos\alpha} \frac{J_1\left(qR\sin\alpha\right)}{qR\sin\alpha}$$

and $\alpha\alpha$ is the angle between the axis of the cylinder and $\vec{q}$, $V=\pi R^2 L$ is the volume of the cylinder, L is the length of the cylinder, R is the radius of the cylinder, and $\Delta\rho$ (contrast) is the scattering length density difference between the scatterer and the solvent. J_1 is the first order Bessel function.

CURRICULUM VITAE ET STUDIORUM

INTERNATIONAL CONGRESS AND SCHOOLS PARTECIPATION

4/4-5/2016 Title:''Advanced training course on emerging biothecnologies for sustainable waste management and bioraffinery development''. Naples, (Italy).

6/12-20/2016 Title:''Introduction to neutronic techniques for the macroscopic study of matter, with application to physics, chemistry, biology and geology''. Valle Aurina (Italy) and Grenoble (France).

9/20-23/2016 ''Italian Chemistry Society XLIV Congress Physical Chemistry section''. Naples, (Italy).
Poster contribution Title: ''Physico-chemical characterization of the N,N-dimethylalkylamine-N-oxides micellization process''.

2016/10/4-8 Title: International Summer school 2016 ''Bio-Leaching and Metal Extraction Processes for Urban Mining: From Fundamental Principles to Practical Applications''. At Technische Universitat Dresden. Dresden, (Germany).

2016/12/16 Title: ''Bioinformatics and Computational Biology Conference''. Naples, (Italy).

6/19-22/2017 Title: ''16th European Student Colloid Conference (ESC)''. Florence (Italy).
Oral contribution Title: ''Salt-free catanionic surfactant mixtures: effect of the alkyl chain asymmetry on the self-aggregation processes''.

7/2-7/2017 Title: ''International School of Physical Chemistry. Materials for Biomedical Applications''. San Servolo, Venice (Italy).

9/4-7/2017 Title: ''9th International Symposium on Nano & Supramolecular Chemistry''. Naples, (Italy).
Poster contribution title: ''Polyfunctional ligands for supramolecular assemblies of Mn(II) catalysts in aqueous systems''.

6/25-28/2018 ''Italian Chemistry Society XLVI Congress Physical Chemistry section''. Bologna, (Italy).
Oral contribution Title: ''Salt-free catanionic surfactant mixtures: effect of the alkyl chain asymmetry on the self-aggregation processes''.
9/2-5/2018 ''Italian Chemistry Society XX Industrial Chemistry section''. Milan, (Italy).
Oral contribution Title:''Design, formulation and characterizationof anhydrous/highly concentrated surfactants mixtures''.

Publications

A. Laezza, A. Casillo, S. Cosconati, C. I. Biggs, A. Fabozzi, L. Paduano, A. Iadonisi, E. Novellino, M. I. Gibson, A. Randazzo, M, M. Corsaro. E. Bedini. Decoration of chondroitin polysaccharide with threonine: synthesis, conformational study and antifreeze activity, *Biomacromolecules* 2017, 18, 2267-2276

C. O. Rossi, P. Caputo, S. Ashimova, A. Fabozzi, G. D'Errico, R. Angelico. Effects of Natural Antioxidant Agents on the Bitumen: Aging Process: An EPR and Rheological Investigation. *Appl. Sci.* 2018, *8*(8), 1405.

M. Pallach, R. Marchetti, F. Di Lorenzo, A. Fabozzi, E. Giraud, D. Gully, L. Paduano, A. Molinaro, G. D'Errico, A. Silipo. Zymomonas mobilis exopolysaccharide structure and role in high ethanol tolerance. Carbohydrate Polymers. 201,2018, 293-299.

A. Fabozzi, R. Vitiello, I. Russo Krauss, M. Iuliano, G. De Tommaso, A. Amoresano, G. Pinto, L. Paduano, C. Jones, M. Di Serio, G. D'Errico. Synthesis, Surface Properties, and Self-Aggregation Behaviorof a Branched *N,N*-Dimethylalkylamine Oxide Surfactant. J Surfact Deterg (2018) DOI 10.1002/jsde.12205

Ph.D Courses

Organic Reaction in Biological system (20/9/2017) (Prof Alfonso Iadonisi)

Glycoscience (12/7/2016) (Dr. Emiliano Bedini)

Addressing renewable energy technologies with quantum chemistry (10/3/2017) (Prof Michele Pavone)

Small Angle Neutron Scattering snd Reflectometry for soft matter (13/11/2015) (Yuri Gerelli)

Tecniche di estrazione solido-liquido impiegate nella preparazione del campione per l'analisi chimica e nella produzione di estratti per usi industriali (3/3/16) (Dr. Daniele Naviglio).

Development of the FluidFM and its applications for 2D pattering as well as 3D microprinting (17/10/2016) (Dr. Zambelli)

Supramolecular chemistry of chiral callixarenes: interactions with protein and crystal surfaces. (13/10/2017) (Dr. Mauro Mocerino)